

Interactive comment on “Recent updates on the Copernicus Marine Service global ocean monitoring and forecasting real-time 1/12° high resolution system” by Jean-Michel Lellouche et al.

L. Vandenbulcke (Referee)

luc.vandenbulcke@ulg.ac.be

Received and published: 12 April 2018

The paper entitled “Recent updates on the Copernicus Marine Service global ocean monitoring and forecasting real-time 1/12° high resolution system” presents the innovations in the near-real time global PSY4V3 system simulating 2006-present, compared to the previous system. The paper then validates the innovations by looking at essential ocean variables. The discussion of the improvements is generally convincing. The model itself is actually very convincing, and some of the examined metrics are truly impressive with very low errors. The paper is also very well written and clear.

We thank Luc Vandenbulcke (Referee #1) for his careful reading of our manuscript and for his constructive remarks. Following his advices, we tried to make the manuscript clearer. All remarks detailed below by the referee were considered and/or discussed.

I have a small list of remarks / questions, in no particular order:

- to facilitate the reading of the paper, please make the names of the systems consistent through the whole text and figures (PSY4V3 or HRG-V2V3, etc).

Figure 1, Table 1 and Table 2 have been modified and the text has been changed accordingly.

- section 3.2 about correction of precipitation. It seems that figure 6 represents ECMWF (left panel), and ECMWF corrected by PMWC (right panel). In this case, of course in the right panel, the differences compared to PMWC are smaller than in the left panel. Thus Fig 6 is not very relevant and could be removed. On the contrary, Fig 7 shows the impact of the correction, and is very convincing.

We think that Figure 6 allows to locate the areas of low and strong correction of precipitations and therefore the areas that potentially will be the most impacted. For this reason, we would like to keep this figure. The maps of the Figure 6 have also been re-centered on Pacific at it was already the case for Figure 7.

- section 3.3 about assimilating climatological profiles at depth, starts by giving a list of possible causes for this drift. Could you expand this a little? One would like to understand why below 2000m, the model would drift and present larger and larger biases over time (such as written page 16 around line 21, and illustrated in Fig 11a); as this is kind of surprising and one wonders if there is something that can be done to the model itself?

Referee #2 has also mentioned this point. The text has been completed and the following reference has been added:

De Lavergne C., Madec, G., Le Sommer, J., Nurser, A. G., and Naveira-Garabato, A. C.: On the consumption of Antarctic Bottom Water in the abyssal ocean, *J. Phys. Oceanogr.*, 46, 635–651, doi:10.1175/JPO-D-14-0201.1, 2016.

- section 3.4, page 19 line 32, about the filtering of SLA anomalies, and the trapping of small structures, you say “this happens less” when filtering. Can you show this? It is also surprising that there seems to be no clear advantage of 10 or 300 passes of the filter. Does this tell something about the spatial scales?

We agree that the first version of the text was not very clear. Some sentences have been changed to clarify this point.

- section 3.5, page 20, lines 5-8: you say the “error increases” when TIW are marked, and this can be explained by cloudy images or by the model shift of TIW. This could be more clear. I don’t understand why images would be more clouded when TIW are more marked, is there any relation between these 2 processes (TIW and clouds). I agree with the second reason. In an ideal world, the error on model (resp. observations) would be determined without using the observations (resp. model); but the world is not ideal, and that the “Desroziers” method is effective and hence should indeed be used to improve the model. Therefore, if the model shifts structures (such as TIW), one indeed may need to modify the error affecting observations. If this is what you meant, maybe somewhere in the section you could write such an introduction.

We agree with all of that. We added in section 2.2 that “only one SST map is assimilated on the fifth day of the 7-day cycle” and that “cloudy regions are filled by the analysis performed in OSTIA”. We also added some supplementary explanations in section 3.5 making, we hope, the section clearer.

- for the whole of section 4, or maybe in section 1 or 2 already, you could specify clearly and once and for all if there are differences between the catch up period (2006-2016) and the operational period (2016-ongoing) ? I mean for atmospheric forcings, in situ observations reprocessing mode, etc. For example in section 4, at one point you say that in Jan 2014, you start using NRT observations (if I understood correctly)? Does that mean that before 2014, you used reprocessed observations?

The text has been completed in the introduction and in section 2.2 for all assimilated observations. For in situ temperature and salinity vertical profiles, it was already partially mentioned in the original manuscript page 9 (lines 7-14).

- section 4.2 in particular seems to indicate that the system relies a lot on data. But this feeling is present in the whole paper. Actually almost all of the improvements to the PSY4V3 system seem to be data-based, whether they concern data assimilation, error modelisation, atmospheric forcing data (precipitation)... This is not a criticism, just something that I notice. Maybe it becomes extremely difficult to improve the model itself any further, apart from forcing it with more and better data.

You are right. It is difficult to improve the model itself with the used version of NEMO.

We develop currently the next version of the global system, based on the version 3.6 of NEMO. Some new parameterizations present in this version will allow to improve the model itself (see first point in “Very general comments” part).

- page 25 lines 1-5, you talk about 3.2 mm/year. But I understand from the previous sections that the mean SSH is not allowed to evolve freely, but is forced to increase 2 mm/year. Can you clarify this?

The mean sea level time evolution is the result of an imposed trend for mass inputs (2.2 mm yr^{-1} , see section 2.1) together with a diagnostic steric effect re-computed from model temperature and salinity. Although the distribution between mass and steric diagnosed from the model is not yet fully satisfactory, the trend of the Global Mean Sea Level is consistent with the observations. This is already said in section 2.2 of the original manuscript.

The expected steric effect is about 1 mm yr^{-1} . The trend of the mean sea level corresponds to the sum of this steric effect and the trend of mass of 2.2 mm yr^{-1} .

Very general comments:

- Among the errors that you noticed in section 4, is it possible to identify some culprit processes, where the model leads to biases that could potentially be corrected by better algorithms? Maybe it's worth saying something about that in the paper.

You are right. We think also that some model biases could potentially be corrected by using better algorithms and more sophisticated parameterizations. Some of them are already available in NEMO 3.6 version. We added in the conclusion of the paper some sentences about the following algorithms/parameterizations we plan to use in the future system version:

- LIM3 multi-category ice model.
- Z^* vertical coordinate, which basically consists in changing the total ocean thickness and the sea level accordingly. This leads to the relaxation of the linear free surface assumption approximation and allows for exact global tracers conservation and the removal of unphysical surface salt fluxes.
- Split explicit free surface in place of the actual filtered free surface of Roulet and Madec 2000. Apart from the better representation of external gravity waves, this also provides a substantial CPU gain on massively parallel architectures.
- Vertical mixing (transition from a one equation TKE closure to a two-equations GLS scheme, Reffray et al., 2014).
- A third order horizontal advection scheme (UBS Upstream Bias auto diffusive Scheme – Shchepetkin et al., 2005), replacing the second order vector form differencing for momentum.

Reffray, G., Bourdalle-Badie, R., and Calone, C.: Modelling turbulent vertical mixing sensitivity using a 1-D version of NEMO, *Geosci. Model Dev. Discuss.*, 7, 5249-5293, <http://www.geosci-model-dev.net/8/69/2015/gmd-8-69-2015.html>, 2014.

Shchepetkin, A.F. and McWilliams, J.C.: The regional oceanic modeling system (ROMS): a split-explicit, free-surface, topography-following-coordinate oceanic model, *Ocean Modelling*, 9, 347-404, doi:10.1016/j.ocemod.2004.08.002, 2005.

- In the same line of ideas, it seems that the validation was done mostly on 2006-2016 (we don't see much about the NRT system, or maybe this is just a wrong impression I have). In particular, only for SLA do we see something about the lead time (1-7 days, so "3.5 days"). For other error metrics (SST RMS, etc), could it in the future be possible to assess the model as a function of lead time? For example, when you give the SST rms (0.1°C for example), and we speak about the NRT ("OPER") model, could you (a posteriori) compare observations with the forecast generated at day-1, day-2, ... , day-10, and give 10 values for the SST rms ?

You are right. We chose in this paper to show the impact of the many updates only on the hindcasts (catch up to real time which corresponds to the 2006-2016 period).

We performed also validation in NRT on forecasts and the performance of the daily 10-day forecasts has been checked. For instance, Figure A represents temperature RMS differences (model minus observation) for best analysis (hindcast) and for 1-day, 3-day, 5-day, 7-day and 9-day forecasts. As expected, the best analysis has the lower RMS and this RMS increases with the forecast length. Similar results are obtained for salinity, SLA and SST.

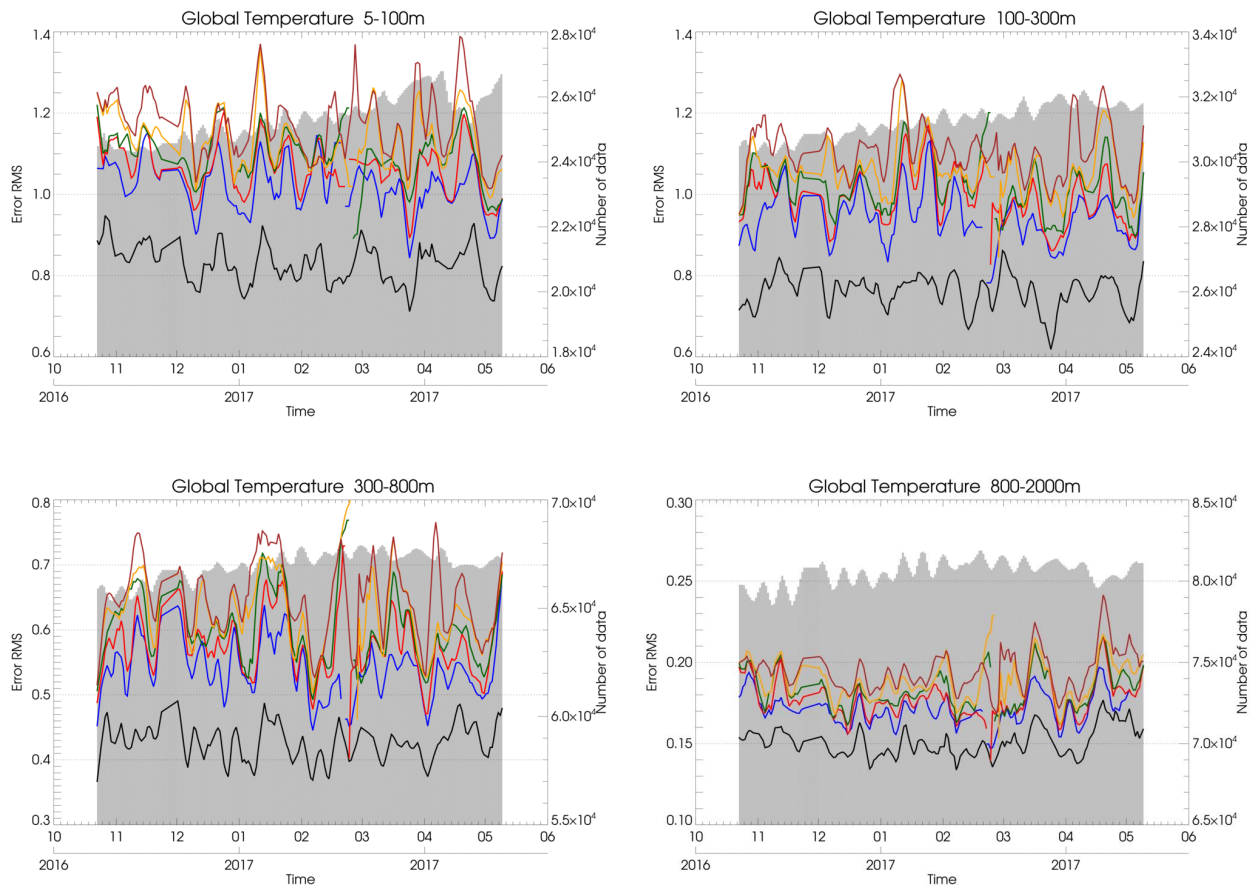


Figure A: Temperature ($^{\circ}\text{C}$) RMS differences (model minus observation) in the 5-100m, 100-300m, 300-800m and 800-2000m layers. Statistics are displayed for best analysis (black line) and for 1-day (blue line), 3-day (red line), 5-day (green), 7-day (orange line) and 9-day (brown line) forecasts. The number of available observations appears in grey in the background.

Typos, language errors, and minor remarks:

- in general, the paper mixes direct and indirect styles “we do this ...”, “this was done...”
- page 2 line 24: “an”
- page 21 L28 : missing “The”
- page 22 L 27 : “as” \rightarrow “such as”
- page 23 L18 : “worst” \rightarrow “worse”
- page 23 L23 : “after” \rightarrow “afterward”
- page 24 L18-20 : phrase is badly formulated

- page 25 : remove L20 (duplicates what's said just above)
- page 25 L 28: "solutionS"
- page 26 L5 : "from" → "for"
- all figures are too small when printed on paper.

All these "typos" errors have been corrected. Some sentences have been reformulated. The size of the figures has also been increased.

Interactive comment on “Recent updates on the Copernicus Marine Service global ocean monitoring and forecasting real-time 1/12° high resolution system” by Jean-Michel Lellouche et al.

Anonymous Referee #2

Received and published: 22 April 2018

General comments:

This Discussion paper discusses the main updates of the Mercator Ocean operational forecasting systems at 1/12 resolution, which is the highest resolution deterministic forecast product released by CMEMS. The manuscript is certainly interesting and deserves publication because documents the main changes and quality increase achievements of a state-of-the-art oceanographic analysis system. It can be useful for both developers and users.

We thank anonymous Referee #2 for his careful reading of our manuscript and for this comment.

However, in my opinion there are many scientific issues that are only empirically formulated, lack scientific justification and require a deeper explanation. In general, it is also not clear why some updates are discussed in details in section 3 and some others only mentioned in section 2: this seems quite arbitrary. I therefore recommend revising the manuscript to address the specific points below to help the readership to understand the motivation and justification of such changes, which will really help the usefulness of this work in the oceanographic community and the robustness of the paper.

The issues empirically formulated concern essentially the choice of the “threshold values”. For those involved in the quality controls QC1 and QC2, the justification and the criteria for choosing the value of these parameters have been added in the text.

For those involved in section 3.3, we followed the tunings used by Greiner et al., 2008 (internal report) and we checked that these values allow the method to work properly. We give to the Referee the access to this report: <https://cloud.mercator-ocean.fr/public.php?service=files&t=2f3c0f2d260b51aac32a4d03da71e2d3>.

We also described in details only some of the updates mentioned in section 2. The choice of updates separately illustrated and discussed in section 3 may seem arbitrary. It corresponds in fact to the updates that doesn't result from routine system improvements (bathymetry, runoffs, assimilated databases, Mean Dynamic Topography, etc.). This is mentioned in the manuscript.

I found the article well-written; it is a bit long, and I suggest the authors to consider removing some figures (29 figures are really too many in my opinion).

We agree that. We think also that the number of figures is large. We tried to reduce it before submitting but, on the other hand, we believe that all figures are beneficial to understanding the system. This manuscript describes a complex system with a lot of new ingredients. A solution would be to split the paper in two parts: description of the system and details of the main updates (sections 2 and 3), and scientific assessment (section 4). This has not been our final choice, also wanting to measure, in the same paper, the overall impact of the integration of all updates on the products quality.

We would like therefore to keep all the figures.

Specific comments:

Following constructive comments, we tried to make the manuscript clearer and more detailed. All remarks detailed below by the referee were considered and/or discussed.

Abstract L23: forecast error → background error.

The text has been modified overall the manuscript.

Introduction P1L16: I believe the fact that Mercator is entrusted by EC is not relevant: here it is relevant that Mercator Ocean is in charge of the global analysis and forecast system.

We agree that. Only the relevant part has been kept in the text.

P2L27: “four main areas”: I count 6 areas from the manuscript, moreover this number is subjective.

We added numbering of these four main areas (from (i) to (iv)) to better highlight them. This classification, and consequently the number of these main areas, is the one that appears in <http://marine.copernicus.eu/markets/use-cases>.

P3L5-10: seems a repetition and suggest to merge in P2L14-26.

We agree that. The text has been merged.

P3L27: “three twin ...” the number three appear evident only later in the paper, suggest dropping it.

We would like to maintain this paragraph in the introduction because we think that it is important to precise in the introduction that these three versions of system have been used to quantify the impact of the updates. We added some details about these simulations to clarify the paragraph.

P5L4-6: The point here is not that parameterizations in the version 3.1 of NEMO are still in the version 3.6, but how many new parameterizations and improvements of NEMO are you missing using version 3.1? In my opinion it should be discussed this way: although I perfectly understand that upgrading version is not easy for an operational system, and this is a justification for me, there are many years of ocean model developments not exploited here, which should be honestly mentioned.

We agree that. The text has been modified at the beginning of section 2.1: “The system PSY4V3 uses version 3.1 of the NEMO ocean model (Madec et al., 2008). This NEMO version is available since a few years and has been already used in the previous system PSY4V2. This was the available stable version of the code when we started the development of the system PSY4V3 a few years ago. Note that, using this version of the code, we do not access better algorithms and more sophisticated parameterizations present in the current NEMO 3.6 stable version that is now the standard version of the code.”

P6L8: maybe is good to say what are the problems coming from the use of z-coordinate you are referring to? Would it be better then to use sigma-coordinates? Or you mean something else?

The following sentence has been added: “z-coordinates, compared to sigma, isopycnal or hybrid coordinates, induce excessive numerical mixing over overflow sills (Winton et al., 1998). Mediterranean overflow, without any relaxation, would settle at an equilibrium depth of 800 m or so otherwise instead of 1100 m observed. Sigma coordinates could indeed improve the

representation of overflow processes but are likely to induce other problems elsewhere due to sigma gradient pressure error over steep topography or excessive diapycnal mixing in the interior (Marchesiello et al., 2009)”.

The two following references have been added:

Winton, M., R. Hallberg and A. Gnanadesikan, 1998: Simulation of Density-Driven Frictional Downslope Flow in Z-Coordinate Ocean Models. *J. Phys. Oceanogr.*, 28, 2163-2174.

Marchesiello, P., L. Debreu and X. Coulevar, 2009: Spurious diapycnal mixing in terrain-following coordinate models: The problem and a solution. *Ocean Modelling*, 26 (3-4), 156-169.

P6L22: it would be interesting to know what you found for 0, 50 and 100% of relative wind and which was the criteria to choose 50%.

We followed the results obtained by “Bidlot J.R., 2012: Use of MERCATOR surface currents in the ECMWF forecasting system: a follow-up study, Research Department Memorandum R60.9/JB/1228, Internal report available on request”.

In the conclusion of this report, it is written: “An impact study was performed with the ECMWF forecasting system in which surface currents from MERCATOR OCEAN were incorporated into the analysis as well as the forecast system. The data from MERCATOR were processed in such a way that only the slow varying features were retained. By prescribing surface current as part of the ocean surface boundary condition, it was demonstrated that both the surface stress and the surface wind profile above will adjust such that the effect on surface stress is **only about half** of what would have been intuitively obtained by subtracting the ocean current from the surface wind in which no account was taken of surface current.”

We followed also what it was said in the slide 13 (Figure A) of this presentation: http://cersat.ifremer.fr/templates/cersat/resources/meetingTalks/1505_Bidlot.pdf

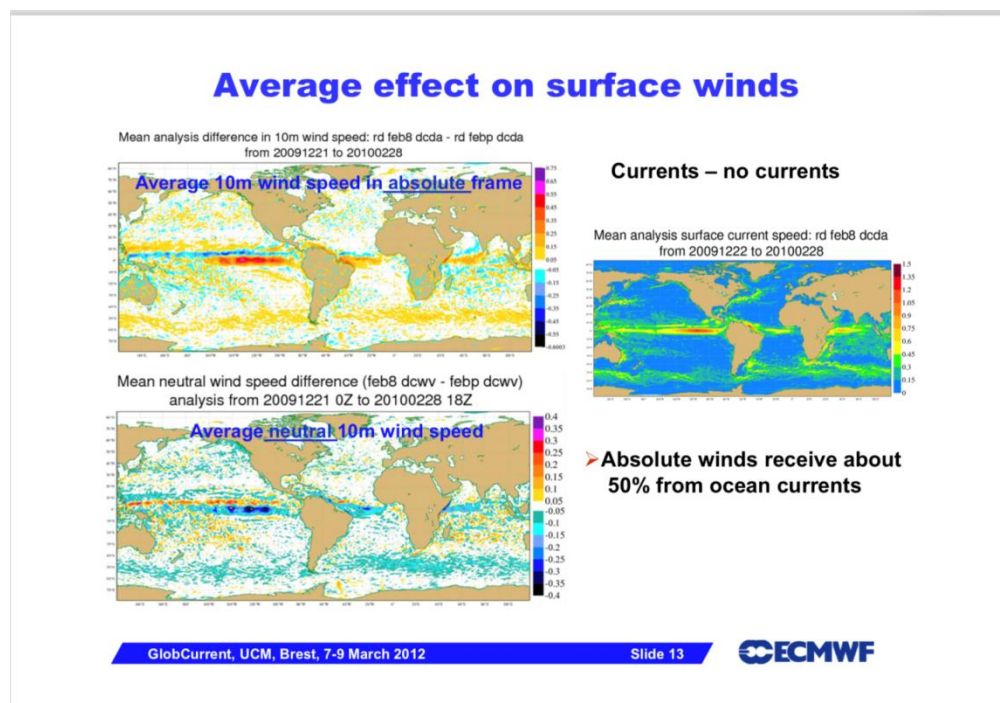


Figure A: Slide 13 of the presentation at Brest of Bidlot in 2012.

P7L1: negative gridded anomalies: maybe better to say negative variations of water masses estimated from GRACE (if I interpret correctly).

We agree that. The text has been modified following your suggestion. Moreover we have clarified the paragraph concerning the building of mean seasonal freshwater fluxes representing Greenland and Antarctica ice sheets and glaciers runoff melting.

P7L11: "...known..." suggest adding a reference.
References have been included.

P7L32: I assume covariances are static (seasonal) but do not vary inter-annually in the real-time system. It is better to state it explicitly.

The background error covariances in SAM rely on a fixed basis. They do not evolve in real-time but they contain the seasonal signal and the inter-annual signal from the 9-year simulation.

The following sentence has been added: "The background error covariances in SAM rely on a fixed basis, seasonally-variable ensemble of anomalies. They also contain the inter-annual signal from the 9-year simulation. This choice implies that, at each analysis step, a sub-set of anomalies is used to improve the dynamic dependency. A significant number of anomalies are kept from one analysis to the other (250 anomalies), thus ensuring error covariance continuity."

P9 paragraphs starting at L15 and L19 seem in contradiction: if the obs errors are adaptive, why do you need a retuning?

Adaptive tuning of errors has been implemented for satellite SLA and SST observations. The method has not been used for temperature and salinity vertical profiles because of the lack of in situ data. Three-dimensional fixed observation errors are then used for the assimilation of in situ temperature and salinity vertical profiles. It is mentioned in the paragraphs starting at L15 and L19 of the original manuscript and at the beginning of section 3.5.

P9L33: this requires a clarification on how you changed the formulation: from the anomaly dataset how do you define the SSH in the old and new system? Wind effect is also barotropic, i.e. is not clear what you actually changed.

You are right. We added some explanations in the text.

In the previous system PSY4V2, the SSH was split in barotropic and baroclinic components, as explained in Benkiran and Greiner, 2008 (page 2060). Moreover, in the system PSY4V2, barotropic height was computed without the wind effect.

The following reference has been added:

Benkiran, M. and Greiner, E.: Impact of the Incremental Analysis Updates on a Real-Time System of the North Atlantic Ocean, *J. Atmos. Ocean. Tech.*, 25, 2055-2073, 2008.

P10L12: suggest adding that the new approach is more consistent with what you actually do (using not a free run but a bias-corrected free run, which better mimics the operational system).

We added a sentence as suggested by the reviewer.

Section 2.3.1 & 2.3.2 It is not clear if these criteria are completely empirical or have some theoretical justification. If empirical as I guess, please discuss the criteria you used to obtain the values for the thresholds.

We agree that. At the beginning of section 2.3, we added some explanations about the criteria we used to obtain the values of the thresholds.

P12L11 it seems weird that there are more suspicious obs in 2012 and 2013. Any idea why?

We agree that. The CORA 4.1 CMEMS in situ database includes the years 2012 and 2013 and we expected a percentage of suspicious profiles relatively stable until 2013. It is almost the case for the temperature profiles but not for salinity. It can not be connected to a strong ENSO event that could explain that more suspicious salinity profiles than usual are detected for instance in the tropical Pacific. We tried to see if it was related to a network effect, but it is not the case. We asked also to the database producers and they have no explanation.

P13L1: how do you define the adjustment, achieved in 3 months?

We consider that an acceptable adjustment is achieved when between 80% and 90% of global energy is reached. To illustrate that, Figure B shows the evolution of the percentage of the three monthly quantities: turbulent kinetic energy (TKE), mean kinetic energy (MKE) and eddy kinetic energy (EKE). For all quantities, 90% of global energy is reached after 6 months. So we changed in the text “3 months” by “6 months”. It does not change the discussion.

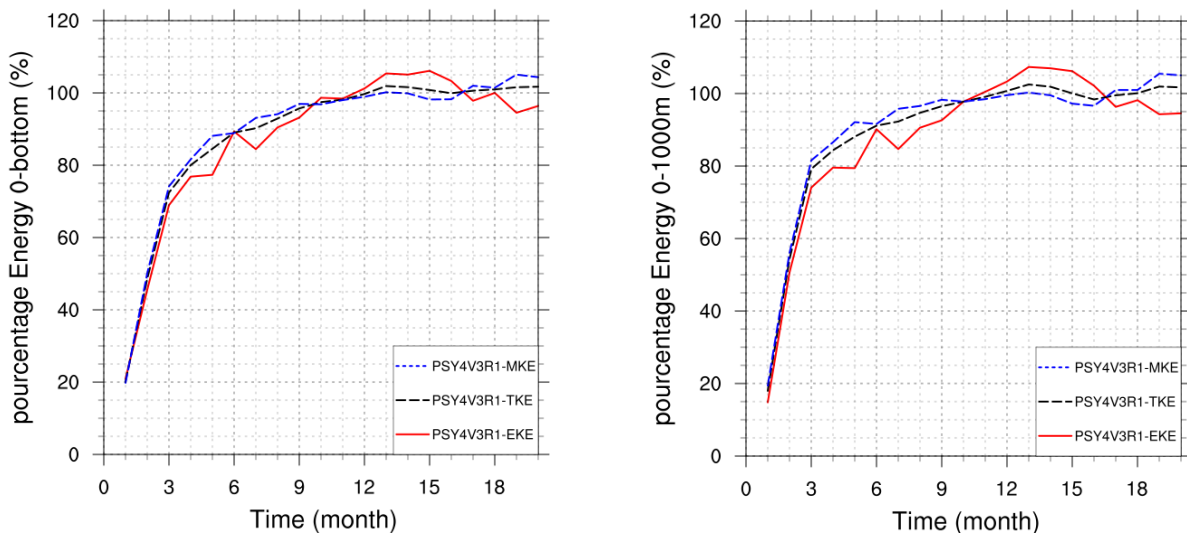


Figure B: Evolution of the percentage of the three monthly quantities: turbulent kinetic energy (TKE), mean kinetic energy (MKE) and eddy kinetic energy EKE. The 100% percentage corresponds to the mean of the months 9 to 20.

Figure 5 and discussion. It looks like the new initialization bears more subsurface biases, so that it is not really convincing that it is better than the old one. I think it deserves a better discussion.

The text has been modified.

Section 3.2: the discussion on the result (Figure 7) will benefit from a quantitative assessment (RMSE and bias reduction of the model vs salinity obs at global scale will be sufficient).

We agree that. The text has been completed.

Section 3.3: A reason for drift might be also inadequate background-error covariances that contain spurious correlations. This should be mentioned at the beginning. Again, the thresholds seem to be empirical and suggest writing the criteria for their adoption.

Referee #1 has also mentioned this point. The text has been modified.

Regarding the value of the thresholds, we followed the tunings used by Greiner et al., 2008 and we checked that these values allow the method to work properly for PSY4V3.

P18 Fig 12: It is weird that without the SEEK you have more variability than the observational product: I wonder whether the two datasets are really comparable, given that the 1/12 model may have a signal at higher resolution than the gridded altimeter product.

We try to make the two datasets comparable by subsampling the 1/12° model (1 point every 3) before doing the comparison with DUACS which is a product on a 1/4° regular horizontal grid. This has been clarified in the text.

Also here is an explanation regarding the excess of energy present in the BIAS simulation compared to the observational DUACS product. Figure C shows the mean currents on October-November-December 2013 with superimposed stream lines for the three simulations (FREE, BIAS, OPER) in the zoom (175° W – 125° W / 65° S – 20° S).

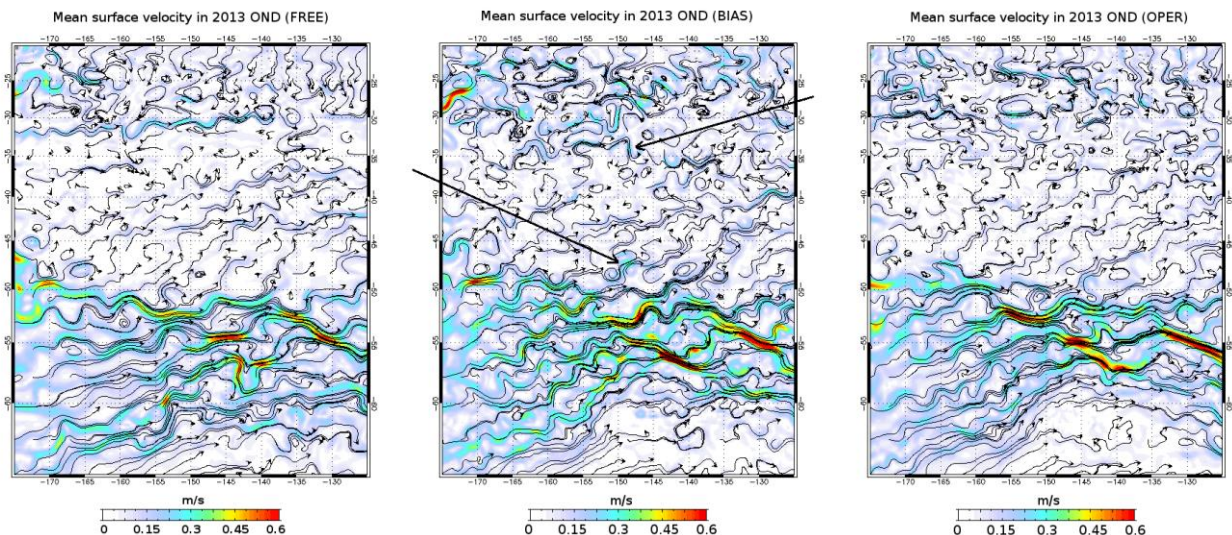


Figure C: Mean currents on October-November-December 2013 with superimposed stream lines for the three simulations (FREE, BIAS, OPER) in the zoom (175° W – 125° W / 65° S – 20° S).

South of 50° S, the Polar Front (PF) is more pronounced in BIAS and even more in OPER. On the other hand, between the East Australian Current (EAC) and the PF, the meridional gradient decreases in OPER. The gradient is not well maintained in BIAS north of the PF. The front leaks to the north in the less energetic zone where we thus find "spurious" meanders and eddies.

The average of the currents shows that the FREE has two very marked veins on the southern edges of the EAC and on the northern edge of the PF. This prevents the export of vorticity (which is advected zonally). In BIAS, the edges are less marked, and there are veins of current towards the less energetic zone. These veins disappear in OPER, especially south of the EAC. It can be noted that the BIAS shows PF connection at 150° W/48° S and EAC connection at 148° W / 35° S (black arrows).

To reduce that in the future, we plan to increase viscosity model coefficient or temperature and salinity in situ observations errors (or both) for the simulation using only temperature and salinity 3D-VAR large-scale biases correction.

Section 3.4.2: Suggest putting it more in the context. I assume that the filtering is applied to the anomaly from the BIAS experiment before covariance computation, and then these differently filtered covariances are used in single-track experiment. However, it is a deduction and recommend to begin the section explaining this.

We have switched the two subsections of section 3.4 to make it clearer. We have also better introduced these two subsections in the introduction of the section 3.4.

Section 3.5: This is the section that I found very hard to justify. I don't see a reasoning why observation errors are flow-dependent and should change so much with time, except the representativeness error component that might slightly change with season and/or particular events (eg presence of fronts, etc.). But this is less crucial than the background-errors that are certainly modulated by observation availability, large- and small scale processes, forcing, etc. This seems particularly true when looking at an observational dataset with nearly constant sampling (SST, Fig 18/19). I think the results improve not because observational errors really change with time, but because you are changing the ratio between background and observation errors, provided that background errors are of course flow-dependent as mentioned before. Moreover, the Desroziers method implies simultaneous tuning of background and observation errors. If the authors are able to provide a similar complementary retuning of background errors (I mean not with experiments but with diagnostics), it will really improve the robustness of the section. Otherwise a better discussion is needed, probably mentioning that what is actually done is to change the relative weight between background and observation errors, rather than changing observation error themselves.

We agree that. When we say "tuning of observations errors", we mean the sum of the instrumental and representativeness errors. It's true that the instrumental error doesn't change with time. On the contrary, the representativeness error is really flow-dependent.

We tried to apply the "Desroziers method" simultaneously on background and observation errors. But both errors tend to increase or decrease together. This evolution is slow but it is regular and

meaningless regarding the true errors. The ratio between background and observation errors remains constant. Moreover, in the OPER simulation and as mentioned in Lellouche et al. (2013) in the description of the data assimilation system SAM, an adaptive scheme corrects the background variance and gives an optimal background error variance based on a statistical test formulated by Talagrand (1998). This is why we let “Desroziers method” to adjust “instrumental + representativeness” error and “Talagrand method” to adjust the background error.

The text has been modified to make it clearer.

Figure 21: suggest better putting the figure and related discussion in context: the figure shows scores for assimilated vs non-assimilated (NOAA) datasets, so it is not clear the goal of the figure.

The text in section 4.1.1 has been completed.

Section 4.1.2 Title and text: as the SST source is similar between OSTIA and CATSAT (night time measurements from infrared sensors), I don't think the latter is really independent. I would define it “external” or similar.

We changed it.

Section 4.2 L21: 2005-2012 is not a decade; moreover, suggest trying the entire (inter-decadal) climatology to get rid of the weird increase of RMSE after 2012, probably due to the fact that the decadal mean is much too affected by the inter-annual variability therein.

“2005-2012 decade” has been changed to “2005-2012 truncated decade”. The five previous decades of WOA13v2 monthly climatology from 1955 and that can be found on the NODC website, properly represent 10-year periods.

It is true that the “2005-2012 truncated decade” contains strong La Niña event (2010-2011) and, as a consequence, is biased to cold. The previous decades (before 2005) are even colder and can no longer be used for recent dates. Moreover, 2005-2012 “truncated decade” doesn't contain the period of transition towards El Niño events and in particular the strong one occurring in 2015. This explains the increase of RMS difference between the WOA13v2 monthly climatology and the in situ observations after 2012. Using the entire (inter-decadal) climatology will globally increase this RMS from 2007 to 2012 but the “weird increase” after 2012 will be still present even if it will be a little reduced.

We clarified the text of section 4.2.

Section 4.3.1 Please clarify how you estimate 2 and 4 cm for instrumental and MDT errors; the MDT one seems in particular arbitrary; also, in the computation of the statistics, do you use any threshold to filter out certain misfits, in order to obtain that global value of RMS, or you use all observations?

The 2 cm is the instrumental prescribed error. It is the error value recommended by data centers.

We prescribe also in the system an a priori MDT error (Figure D), which is equal to 4 cm in average on the regions observed by altimetry.

The text has been modified.

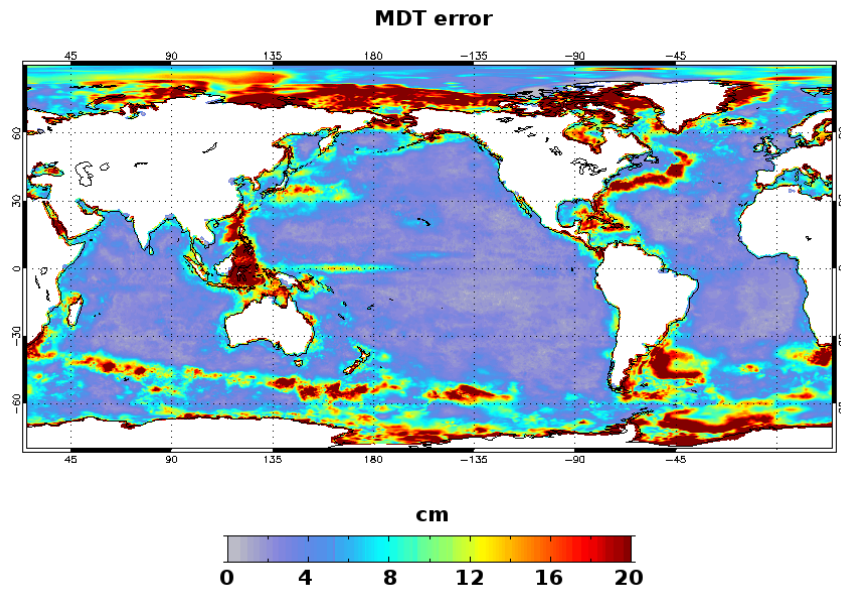


Figure D: MDT error a priori prescribed in the system PSY4V3.

Section 4.3.2. Please provide a reference for BADOMAR and GLOSS/CLIVAR. Also in section 4.4.1 and 4.5 there are products that are referred to only through links: is there any better way to refer to them?

References have been added for BADOMAR product and GLOSS tide gauge stations in section 4.3.2.

The link in section 4.5 has been replaced by a more classical reference. It concerns the Quality Information Document (QuID) for the product in question, which can be accessed via the CMEMS catalogue.

The link in section 4.4.1 has not been replaced because no evident classical reference has been found.

Recent updates on the Copernicus Marine Service global ocean monitoring and forecasting real-time 1/12° high resolution system

Jean-Michel Lellouche¹, Eric Greiner², Olivier Le Galloudec¹, Gilles Garric¹, Charly Regnier¹, Marie Drevillon¹, Mounir Benkiran¹, Charles-Emmanuel Testut¹, Romain Bourdalle-Badie¹, Florent Gasparin¹, Olga Hernandez¹, Bruno Levier¹, Yann Drillet¹, Elisabeth Remy¹, Pierre-Yves Le Traon^{1,3}

¹ Mercator Ocean, Ramonville Saint Agne, France

² Collecte Localisation Satellites, Ramonville Saint Agne, France

³ IFREMER, 29280, Plouzané, France

Correspondence to: Jean-Michel Lellouche (jllelouche@mercator-ocean.fr)

Abstract

Since October 19, 2016, and in the framework of Copernicus Marine Environment Monitoring Service (CMEMS), Mercator Ocean delivers in real-time daily services (weekly analyses and daily 10-day forecasts) with a new global 1/12° high resolution (eddy-resolving) monitoring and forecasting system. The model component is the NEMO platform driven at the surface by the IFS ECMWF atmospheric analyses and forecasts. Observations are assimilated by means of a reduced-order Kalman filter with a [three-dimensional3D](#) multivariate modal decomposition of the [backgroundforecast](#) error. Along track altimeter data, satellite sea surface temperature, sea ice concentration and in situ temperature and salinity vertical profiles are jointly assimilated to estimate the initial conditions for numerical ocean forecasting. A 3D-VAR scheme provides a correction for the slowly-evolving large-scale biases in temperature and salinity.

This paper describes the recent updates applied to the system and discusses the importance of fine tuning of an ocean monitoring and forecasting system. It details more particularly the impact of the initialization, the correction of precipitation, the assimilation of climatological temperature and salinity in the deep ocean, the construction of the [backgroundforecast](#) error

1 covariance and the adaptive tuning of observations error on increasing the realism of the
2 analysis and forecasts.

3 The scientific assessment of the ocean estimations are illustrated with diagnostics over some
4 particular years, assorted with time series over the time period 2007-2016. The overall impact
5 of the integration of all updates on the products quality is also discussed, highlighting a gain
6 in performance and reliability of the current global monitoring and forecasting system
7 compared to its previous version.

8

9 **1 Introduction**

10 Mercator Ocean monitoring and forecasting systems have been routinely operated in real-time
11 since early 2001. ~~They and~~ have been regularly upgraded by increasing complexity,
12 expanding the geographical coverage from regional to global and improving models and
13 assimilation schemes (Brasseur et al., 2006; Lellouche et al., 2013).

14 ~~After having successfully coordinated the European MyOcean and MyOcean2 projects~~
15 ~~(<http://www.myocean.eu>), Mercator Ocean was officially entrusted by the European~~
16 ~~Commission on November, 11, 2014 to implement and operate the Copernicus Marine~~
17 ~~Environment Monitoring Service (CMEMS), as part of the European Earth observation~~
18 ~~program Copernicus (<http://marine.copernicus.eu>). Since January 2009, Mercator Ocean,~~
19 which had primary responsibility for the global ocean forecasts of the MyOcean and
20 MyOcean2 projects since January 2009, developed several versions of its monitoring and
21 forecasting systems for the various milestones (from V0 to V4) of the MyOcean project, and
22 more recently, for milestones V1, V2 and V3 of the Copernicus Marine Environment
23 Monitoring Service (CMEMS), —as part of the European Earth observation program
24 Copernicus (<http://marine.copernicus.eu>) (see Fig. 1). Mercator Ocean opened the CMEMS in
25 May 2015 and is in charge of the global high resolution ocean analyses and forecasts. In this
26 context, Research and Development activities have been conducted these last years to
27 improve the real-time 1/12° high resolution (eddy-resolving) global analysis and forecasting
28 system. Since October 19, 2016, Mercator Ocean has delivered real-time daily services
29 (weekly analyses and daily 10-day forecasts) with a new global 1/12° system PSY4V3R1
30 (hereafter PSY4V3, see Fig. 1). Note that PSY4V3 will be the system for the CMEMS V4
31 milestone. —The main differences and links between the various versions of the Mercator
32 Ocean systems in the framework of past MyOcean project and current CMEMS are

1 | summarized in Table 1 and Table 2 for Intermediate Resolution $\frac{1}{4}^\circ$ Global configurations
2 | (hereafter IRG) and High Resolution $\frac{1}{12}^\circ$ Global configurations (hereafter HRG) systems
3 | respectively.

4 | These systems are intensively used in four main areas of application: (i) maritime safety, (ii)
5 | marine resources management, (iii) coastal and marine environment, and (iv) weather, climate
6 | and seasonal forecasting (<http://marine.copernicus.eu/markets/use-cases>). As described in
7 | Lellouche et al. (2013), the evaluation of such systems includes routine verification against
8 | assimilated and independent in situ and satellite observations, as well as a careful check of
9 | many physical processes (e.g. mixed layer depth evaluation as shown in Drillet et al. (2014)).
10 | Scientific studies brought precious additional evaluation feedbacks (Juza et al., 2015; Smith et
11 | al., 2016; Estournel et al., 2016). Finally, several studies showed the added value of surface
12 | currents analyses provided by these systems for drift applications (Scott et al., 2012; Drevillon
13 | et al., 2013).

14 | ~~Since May 2015, Mercator Ocean opened the CMEMS and has been in charge of the global~~
15 | ~~high resolution ocean analyses and forecasts. In this context, R&D activities have been~~
16 | ~~conducted these last years to improve the real time $\frac{1}{12}^\circ$ high resolution (eddy-resolving)~~
17 | ~~global analysis and forecasting system. Since October 19, 2016, Mercator Ocean delivers in~~
18 | ~~real time daily services (weekly analyses and daily 10 day forecasts) with a new global $\frac{1}{12}^\circ$~~
19 | ~~system PSY4V3R1 (hereafter PSY4V3, and corresponding to HRG_V2V3 in Fig. 1). Note~~
20 | ~~that PSY4V3 will be the system for the CMEMS V4 milestone.~~ In this system PSY4V3, the
21 | ocean/sea ice model and the assimilation scheme benefit ~~of~~ from the following main updates:
22 | atmospheric forcing fields are corrected at large-scale with satellite data; freshwater runoff
23 | from ice sheets melting is added to river runoffs; a time varying global average steric effect is
24 | added to the model sea level; the last version of GOCE geoid observations are taken into
25 | account in the Mean Dynamic Topography used for Sea Level Anomalies assimilation;
26 | adaptive tuning is used on some of the observational errors; a dynamic height criteria is added
27 | to the Quality Control of the assimilated temperature and salinity vertical profiles; satellite sea
28 | ice concentrations are assimilated; and climatological temperature and salinity in the deep
29 | ocean are assimilated below 2000 m to prevent drifts in those very sparsely observed depths.

30 | The impact of all these updates can be evaluated separately, thanks to an incremental
31 | implementation, taking advantage of Mercator Ocean's specific hierarchy of system
32 | configurations running with identical set up. To this aim, short simulations (from one year to a

1 few years) were performed by adding from one simulation to another one upgrade at a time,
2 using the IRG configuration or some high resolution-~~1/12°~~ regional configuration.

3 The system PSY4V3 was run over the October 2006 - October 2016 period to catch-up the
4 real-time assimilating the “reprocessed” databases available at that time, and the so-called
5 "near real-time" databases otherwise. Moreover, in the development phase of ~~an~~-the
6 operational system PSY4V3, it was decided to systematically perform ~~two other~~~~three~~ twin
7 numerical simulations over ~~a given~~the same time period, maintaining the same ocean model
8 tunings but varying the complexity and the level of data assimilation. ~~-The first one is a free~~
9 simulation (without any data assimilation) and the second one only benefits from temperature
10 and salinity large-scale biases correction using in situ observed temperature and salinity
11 vertical profiles. Inter-comparisons between the three simulations were then conducted in
12 order to better analyze and to try to quantify the impact of some component of the
13 assimilation system. These three versions of system have ~~also~~-been used to quantify the
14 impact of some updates.

15 In a previous paper (Lellouche et al., 2013), the main results of the scientific evaluation of
16 MyOcean global monitoring and forecasting systems at Mercator Ocean showed how
17 refinements or adjustments to the system impacted the quality of ocean analyses and
18 forecasts. The primary objective of this paper is to describe the recent updates applied to the
19 system PSY4V3 and ~~-The updates~~ showing the highest impact on the products quality.
20 Updates resulting from routine system improvements are not separately illustrated and
21 discussed (bathymetry, runoffs, assimilated databases, Mean Dynamic Topography, etc.). ~~-are~~
22 ~~separately illustrated and discussed~~So, , -with a particular focus was given to~~on~~ the
23 initialization, the correction of precipitation, the assimilation of climatological temperature
24 and salinity in the deep ocean, the construction of the ~~background~~~~forecast~~ error covariance
25 and the adaptive tuning of observations error. Another objective of this paper is to present a
26 first level evaluation of the system. The purpose here is not to perform an exhaustive
27 validation but only to check the global behavior of the system compared to assimilated
28 quantities or independent observations. Thus, an assessment of the hindcasts (2007-2016)
29 quality is conducted and improvements with respect to the previous system are highlighted in
30 order to show the level of performance and the reliability of the system PSY4V3. A
31 complementary study aimed at demonstrating the scientific value of PSY4V3 for resolving
32 oceanic variability at regional and global scale (Gasparin et al., 2018 – In revision in Journal
33 of Marine Systems). Lastly, several scientific studies have investigated local ocean processes

1 by comparing the PSY4V3 system with independent observations campaigns (Koenig et al.,
2 2017; Artana et al., 2018). This reinforces the system PSY4V3 evaluation effort.

3 This paper is organized as follows. The main characteristics of the system PSY4V3 and
4 details concerning the updates are described in Sect. 2. The impact of ~~the most~~some sensitive
5 upgrades is shown in Sect. 3. Results of the scientific evaluation, including some comparisons
6 with independent observations, are given in Sect. 4. Section 5 contains a summary of the
7 scientific assessment, as well as a discussion of the future improvements for the next version
8 of the global high resolution system.

9

10

11 **2 Description of the current global high resolution monitoring and** 12 **forecasting system PSY4V3**

13 This section contains the main characteristics of the CMEMS system PSY4V3 and details the
14 last updates to the system compared to the previous system PSY4V2R2 (hereafter PSY4V2,
15 see Fig. 1 and Table 2). A detailed description of ~~the main~~some sensitive updates is provided
16 in Sect. 3.

17 **2.1 Physical model and latest updates**

18 The system PSY4V3 uses version 3.1 of the NEMO ocean model (Madec et al., 2008). This
19 NEMO version is available since a few years and has been already used in the previous
20 system PSY4V2. ~~This was the available stable version of the code when we started the~~
21 ~~development of the system PSY4V3 a few years ago. Note that, using this version of the code,~~
22 ~~we do not access better algorithms and more sophisticated parameterizations present in the~~
23 ~~current NEMO 3.6 stable version that is now the standard version of the code. However, all~~
24 ~~the schemes and the parameterizations used in this version are still available in the current~~
25 ~~NEMO 3.6 stable version that is now the standard version of the code.~~ The physical
26 configuration is based on the tripolar ORCA12 grid type (Madec and Imbard, 1996) with a
27 horizontal resolution of 9 km at the equator, 7 km at Cape Hatteras (mid-latitudes) and 2 km
28 toward the Ross and Weddell seas. Z-coordinates are used on the vertical and ~~t~~The 50-level
29 vertical discretization retained for this system has a decreasing resolution from 1m at the
30 surface to 450 m at the bottom, and 22 levels within the upper 100 m. A “partial cells”
31 parameterization (Adcroft et al., 1997) is chosen for a better representation of the topographic

1 floor (Barnier et al., 2006) and the momentum advection term is computed with the energy
 2 and enstrophy conserving scheme proposed by Arakawa and Lamb (1981). The advection of
 3 the tracers (temperature and salinity) is computed with a total variance diminishing (TVD)
 4 advection scheme (Levy et al., 2001; Cravatte et al., 2007). We use a free surface formulation.
 5 External gravity waves are filtered out using the Roullet and Madec (2000) approach. A
 6 laplacian lateral isopycnal diffusion on tracers ($100 \text{ m}^2 \text{ s}^{-1}$) and a horizontal biharmonic
 7 viscosity for momentum ($-2e10 \text{ m}^4 \text{ s}^{-1}$) are used. In addition, the vertical mixing is
 8 parameterized according to a turbulent closure model (order 1.5) adapted by Blanke and
 9 Delecluse (1993), the lateral friction condition is a partial-slip condition with a regionalization
 10 of a no-slip condition (over the Mediterranean Sea) and the Elastic-Viscous-Plastic rheology
 11 formulation for the LIM2 ice model (Fichefet and Maqueda, 1997) has been activated (Hunke
 12 and Dukowicz, 1997). Instead of being constant, the depth of light extinction is separated in
 13 Red-Green-Blue bands depending on the chlorophyll data distribution from mean monthly
 14 SeaWIFS climatology (Lengaigne et al., 2007). The bathymetry used in the system is a
 15 combination of interpolated ETOPO1 (Amante and Eakins, 2009) and GEBCO8 (Becker et
 16 al., 2009) databases. ETOPO1 datasets are used in regions deeper than 300 m and GEBCO8 is
 17 used in regions shallower than 200 m with a linear interpolation in the 200 - 300 m layer.
 18 Internal-tide driven mixing is parameterized following Koch-Larrouy et al. (2008) for tidal
 19 mixing in the Indonesian Seas, as the system doesn't represent explicitly the tides. The
 20 atmospheric fields forcing the ocean model are taken from the ECMWF (European Centre for
 21 Medium-Range Weather Forecasts) IFS (Integrated Forecast System). A 3 h sampling is used
 22 to reproduce the diurnal cycle. Momentum and heat turbulent surface fluxes are computed
 23 from the Large and Yeager (2009) bulk formulae using the following set of atmospheric
 24 variables: surface air temperature and surface humidity at a height of 2 m, mean sea level
 25 pressure and wind at a height of 10 m. Downward longwave and shortwave radiative fluxes
 26 and rainfall (solid + liquid) fluxes are also used in the surface heat and freshwater budgets.
 27 Compared to the previous HRG system PSY4V2, the following updates were done on the
 28 model part (see Table 2):

- 29 - The bathymetry used in the system benefited from a specific correction in the Indonesian
 30 Sea inherited from the INDESO system (Tranchant et al., 2016).
- 31 - In order to solve numerical problems induced by the use of z-coordinates on the vertical
 32 (Willebrand et al., 2001), a relaxation toward the World Ocean Atlas 2013 (version 2)
 33 2005-2012 time period (hereafter WOA13v2,
 34 https://data.nodc.noaa.gov/woa/WOA13/DOC/woa13v2_changes.pdf) temperature

1 (Locarnini et al., 2013) and salinity (Zweng et al., 2013) climatology has been added at
2 Gibraltar and Bab-el-Mandeb straits. Indeed, z-coordinates, compared to sigma, isopycnal
3 or hybrid coordinates, induce excessive numerical mixing over overflow sills (Winton et
4 al., 1998). For instance, Mediterranean overflow, without any relaxation, would settle at
5 an equilibrium depth of 800 m or so otherwise instead of 1100 m observed. Sigma
6 coordinates could indeed improve the representation of overflow processes but are likely
7 to induce other problems elsewhere due to sigma gradient pressure error over steep
8 topography or excessive diapycnal mixing in the interior (Marchesiello et al., 2009). For
9 Gibraltar (respectively Bab-el-Mandeb), the relaxation area is centered at 8° W, 35° N
10 (respectively 46° E, 12° N). At the center the relaxation time is 10 days (respectively 50
11 days). This time is increased up to infinity 4° (respectively 5°) away from the center. The
12 relaxation is not constant over the vertical. It is only applied below 500 m and it is
13 increased linearly between 500 to 700 m. Between 700 m and the bottom of the ocean the
14 coefficient value is unchanged.

15 - Surface wind stress computation should in principle consider wind speed relative to the
16 surface ocean currents (Bidlot, 2012; Renault et al., 2016). However, this statement
17 applies to a fully coupled ocean/atmosphere system, which is not the case for the present
18 system PSY4V3. Based on sensitivity experiments and following the results obtained by
19 Bidlot (2002), we pragmatically consider only 50 % of the surface model currents in the
20 wind stress computation.

21 - The monthly runoff climatology is built with data on coastal runoffs and 100 major rivers
22 from the Dai et al. (2009) database (instead of Dai and Trenberth (2002) for the system
23 PSY4V2). This database uses new data, mostly from recent years, streamflow simulated
24 by the Community Land Model version 3 (CLM3) to fill the gaps, in all lands areas except
25 Antarctica and Greenland. In addition, we built mean seasonal freshwater fluxes
26 representing Greenland and Antarctica ice sheets and glaciers runoff melting. For this
27 purpose we have distributed the following mean values: 545 Gt yr⁻¹ for Greenland and
28 2400 Gt yr⁻¹ for Antarctic (corresponding to freshwater fluxes of 1.51 mm yr⁻¹ and 6.65
29 mm yr⁻¹ respectively). These values are in the range of estimations given by the IPCC-
30 AR13 (Church et al., 2013). They have been applied along Greenland and Antarctica
31 coastlines, and over an open ocean -mean values, 1.51 mm yr⁻¹ for Greenland and 6.65
32 mm yr⁻¹ for Antarctica, onto a domain varying seasonally and defined by the
33 climatological presence of icebergs observed by the Altiberg icebergs database project
34 (Tournadre et al., 2013). Domain covered by giant icebergs from Silva et al. (2006)

1 | comple~~ment~~~~st~~es southern most areas not covered by Altiberg data. One third of these
2 | quantities is applied off shore and two third along Greenland and Antarctic coastlines. We
3 | also used negative variations of water masses estimated from GRACE ~~negative-gridded~~
4 | ~~GRACE-anomalies~~ (Bruinsma et al., 2010) to distribute spatially these runoffs along
5 | coastlines.

- 6 | - As the Boussinesq approximation is applied to the model equations, conserving the ocean
7 | volume and varying its mass, the simulations do not properly directly represent the global
8 | mean steric effect on the sea level (Greatbatch, 1994). For improved consistency with
9 | assimilated satellite observations of sea level anomalies, which are unfiltered from the
10 | global mean steric component, a time-evolving global average steric effect is added to the
11 | sea level in the simulation. This global average steric effect has been computed as the
12 | difference between two successive daily global mean dynamic heights (vertical
13 | integration, from the surface to the bottom, of the specific volume anomaly).
- 14 | - Due to large known biases in precipitations (Stephens et al., 2010; Kidd et al., 2013), a
15 | satellite-based large-scale correction of precipitations has been performed, except at high
16 | latitudes (poleward of 65° N and 60° S). This is detailed in Sect. 3.
- 17 | - In order to avoid mean sea-surface-height drift due to the large uncertainties in the water
18 | budget closure, the following two treatments were applied:
 - 19 | o The surface freshwater global budget has been is-set to an imposed seasonal cycle
20 | (Chen et al., 2005). Only spatial departures from the mean global budget are kept
21 | from the forcing.
 - 22 | o A trend of 2.2 mm yr⁻¹ has been added to the surface mass budget in order to
23 | somewhat represent the recent estimate of the global mass addition to the ocean
24 | (from glaciers, land water storage changes, Greenland and Antarctica ice sheets
25 | mass loss) (Chambers et al., 2017). This term is implemented as a surface
26 | freshwater flux in the open ocean domain infested by observed icebergs.

27 | 2.2 Data assimilation and latest updates

28 | The data are assimilated by means of a reduced-order Kalman filter derived from a SEEK
29 | filter (Brasseur and Verron, 2006), with a three-dimensional 3D-multivariate modal
30 | decomposition of the backgroundforecast error and a 7-day assimilation cycle. It includes an
31 | adaptive-error estimate and a localization algorithm. This data assimilation system is called
32 | SAM (Système d'Assimilation Mercator). The backgroundforecast error covariance is based

1 on the statistics of a collection of ~~three-dimensional~~^{3D}-ocean state anomalies, ~~typically a~~
2 ~~few hundreds (250 anomalies for PSY4V3).~~ The anomalies are computed from a long
3 numerical experiment (9 years for PSY4V3) with respect to a running mean in order to
4 estimate the 7-day scale error on the ocean state at a given period of the year. A Hanning low-
5 pass filter is used to create the running mean with a cut-off frequency equal to 1/24 days⁻¹.
6 The background error covariances in SAM rely on a fixed basis, seasonally-variable ensemble
7 of anomalies. They also contain the inter-annual signal from the 9-year simulation. This
8 choice implies that, at each analysis step, a sub-set of anomalies (250 anomalies) is used to
9 improve the dynamic dependency. A significant number of anomalies are kept from one
10 analysis to the other, thus ensuring error covariance continuity. Altimeter data, in situ
11 temperature and salinity vertical profiles, and satellite sea surface temperature and sea ice
12 concentration are jointly assimilated to estimate the initial conditions for numerical ocean
13 forecasting. In addition, a 3D-VAR scheme provides a correction for the slowly-evolving
14 large-scale biases in temperature and salinity (Lellouche et al., 2013).

15 Compared to the previous HRG system PSY4V2, the following updates were done on the data
16 assimilation part (see Table 2):

- 17 - CMEMS satellite near real time sea ice concentration OSI SAF
18 ([http://marine.copernicus.eu/documents/QUID/CMEMS-OSI-QUID-011-001to007-](http://marine.copernicus.eu/documents/QUID/CMEMS-OSI-QUID-011-001to007-009to012.pdf)
19 [009to012.pdf](http://marine.copernicus.eu/documents/QUID/CMEMS-OSI-QUID-011-001to007-009to012.pdf)) is a new observation assimilated in the system PSY4V3. For this, a separate
20 monovariate/monodata analysis is carried out for the ice variables, in parallel to that for
21 the ocean. The two analyses are completely independent.
- 22 - CMEMS OSTIA SST (delayed time (reprocessed) until the end of 2006:
23 <http://marine.copernicus.eu/documents/QUID/CMEMS-OSI-QUID-010-011.pdf>, then
24 near real time: [http://marine.copernicus.eu/documents/QUID/CMEMS-OSI-QUID-010-](http://marine.copernicus.eu/documents/QUID/CMEMS-OSI-QUID-010-001.pdf)
25 [001.pdf](http://marine.copernicus.eu/documents/QUID/CMEMS-OSI-QUID-010-001.pdf)) is assimilated in the system PSY4V3, instead of near real time AVHRR SST
26 from NOAA in PSY4V2. A particular attention has been devoted to the computation of
27 the model equivalent. As OSTIA provides the foundation SST (considered nominally at
28 10 m depth), the SST model equivalent is performed by calculating the night-time average
29 of the first level of the model temperature. Moreover, only one SST map is assimilated on
30 the fifth day of the 7-day cycle. Cloudy regions are filled by the analysis performed in
31 OSTIA product.
- 32 - In addition to the quality control based on temperature and salinity innovation statistics
33 (detection of spikes, large biases), already present in the previous system, a second quality

- 1 control has been developed and is based on dynamic height innovation statistics (detection
2 of small vertically constant biases). This is detailed in Sect. 2.3.
- 3 - A new hybrid MDT, based on the “CNES-CLS13” MDT (Rio et al., 2014) with
4 adjustments made using the Mercator GLORYS2V3 (GLobal Ocean ReanalYsis and
5 Simulation – stream 2 – version 3) reanalysis and with an improved Post Glacial Rebound
6 (also called Glacial Isostatic Adjustment), has been used. This new hybrid MDT also takes
7 into account the last version of the GOCE geoid. This replaces the previous hybrid MDT
8 used in the previous system PSY4V2, which was based on the “CNES-CLS09” MDT
9 derived from observations (Rio et al., 2011). The new hybrid MDT significantly reduces
10 (not shown) sea level bias (more than 5 cm in some areas) and consequently temperature
11 and salinity in regions where the topography makes difficult the mean sea surface
12 estimation (e.g. Indonesia, Red Sea and Mediterranean Sea).
- 13 - A consistent along track SLA dataset
14 (<http://marine.copernicus.eu/documents/QUID/CMEMS-SL-QUID-008-032-051.pdf>),
15 with a 20-year altimeter reference period, is assimilated all along the simulation
16 performed with the system PSY4V3. Reprocessed observations are assimilated until the
17 end of August 2015. Near real time observations are assimilated afterward.
- 18 - The CORA 4.1 CMEMS in situ reprocessed database (Szekely et al., 2016;
19 <http://marine.copernicus.eu/documents/QUID/CMEMS-INS-QUID-013-001b.pdf>) has
20 been assimilated for the 2006-2013 period. In addition to Argo and other in situ data sets,
21 this database includes temperature and salinity vertical profiles from sea mammal
22 (elephant seals) database (Roquet et al., 2011) to compensate for the lack of such data at
23 high latitudes. From 2014 to present, the near-real time CMEMS product
24 (<http://marine.copernicus.eu/documents/QUID/CMEMS-INS-QUID-013-030-036.pdf>) is
25 assimilated.
- 26 - As the prescription of observation errors in the assimilation systems is not sufficiently
27 accurate, adaptive tuning of observation errors for the SLA and SST has been
28 implemented. The method has been adapted from diagnostics proposed by Desroziers et
29 al. (2005) and is detailed in Sect. 3.
- 30 - New three-dimensional observation errors files for the assimilation of in situ
31 temperature and salinity data have been re-computed from the MyOcean IRG system
32 PSY3V3R3 (see Fig. 1 and Table 1) using an offline version of the adaptive tuning
33 method mentioned above.

- 1 - A weak constraint towards the WOA13v2 climatology on temperature and salinity in the
2 deep ocean (below 2000 m) has been included in the two components (3D-VAR and
3 SEEK filter) of the assimilation scheme to prevent drifts in temperature and salinity and as
4 a consequence to obtain a better representation of the sea level trend at global scale in the
5 system. The method consists in assimilating vertical climatological profiles of temperature
6 and salinity at large scale and below 2000 m in regions drifting away from the
7 climatological values, using a non-Gaussian error at depth. This is detailed in Sect. 3.
- 8 - The time window for the 3D-VAR bias correction was reduced from 3 to 1 month to
9 obtain a correction that is more in line with the current physics, which is made possible by
10 the good spatial and temporal distribution of the Argo network from 2006.
- 11 - In the previous system PSY4V2, the SSH increment was the sum of barotropic and
12 baroclinic (dynamic) height increments as in Benkiran and Greiner, 2008. Dynamic height
13 increment was calculated from the temperature and salinity increments, while the
14 barotropic increment was an output of the analysis. Barotropic height was computed
15 without the wind effect. In the system PSY4V3, we directly use the total SSH increment
16 given by the analysis to take into account, among other things, the wind effect like the
17 hydraulic control near the straits (Song, 2006; Menemenlis et al., 2007).
- 18 - The uncertainties in the MDT estimate and the sparsity of the observation networks (both
19 altimetry and in situ profiles) on the 7-day assimilation window do not allow to accurately
20 estimate the observed global mean sea level. Moreover, the mean sea level time evolution
21 is the result of an imposed trend for mass inputs (2.2 mm yr^{-1} , see Sect. 2.1) together with
22 a diagnostic steric effect re-computed from model T and S. Therefore, the global mean
23 increment of the total sea surface height is set to zero and the mean sea level is not
24 controlled by data assimilation.
- 25 - The background error covariance matrices needed for data assimilation are defined using
26 anomalies of the different variables coming from a simulation in which only a 3D-VAR
27 large scale bias correction of T, S has been performed (instead of using a free run- as was
28 done in the previous system PSY4V2). This new approach is more consistent because it
29 better mimics the final operational system, which uses also the 3D-VAR bias correction.
30 Moreover, these anomalies are spatially filtered in order to retain only the effective model
31 resolution and in order to avoid injecting noise in the increments. This is detailed in Sect.
32 3.

1 2.3 Additional Quality Controls on in situ observations

2 To minimize the risk of erroneous observations being assimilated in the model, the system
3 PSY4V3 carries out two successive Quality Controls (QC1 and QC2) on the assimilated
4 temperature (T) and salinity (S) vertical profiles. These are done in addition to the quality
5 control procedures performed by the data producers. This observation screening is known as
6 background quality control. In both cases (QC1 and QC2), we estimate two parameters, which
7 are the mean and standard deviation of model innovations. These parameters are then used to
8 define space- and season-dependent threshold values which correspond to the mean plus N
9 times the standard deviation. The N parameter is chosen empirically to reach a compromise
10 between rejecting a lot of profiles (if the criterion is too strict) and rejecting in average no
11 more than 1 % of profiles which are contained in the tails of the probability density function
12 of the innovations.

13 2.3.1 Quality Control QC1

14 The first quality control QC1 has been already described in Lellouche et al. (2013) and can be
15 summarized as follows. An observation is considered suspicious if the two following
16 conditions are both satisfied:

$$17 \quad \begin{cases} |innovation| > threshold \\ |observation - climatology| > 0.5 * |innovation| \end{cases} \quad (1)$$

18
19 where the spatially and seasonally varying *threshold* value comes from statistics (mean,
20 standard deviation) computed with the very large number of temperature and salinity
21 innovations collected in the Mercator GLORYS2V1 (GLobal Ocean ReanalYsis and
22 Simulation – stream 2 – version 1) reanalysis (1993-2009). The first condition of equation (1)
23 is a test on the innovation. It determines whether the innovation is abnormally large which
24 would most likely be due to an erroneous observation. The second condition avoids rejecting
25 “good” observations (i.e. an observation close to the climatology) even if the innovation is
26 high due to the model background being biased. This first quality control QC allows ~~the~~
27 detection of spikes and large biases.

28 2.3.2 Quality Control QC2

29 The second quality control QC2 is based on dynamic height innovation (vertical integration
30 from the surface to the bottom) statistics and allows ~~detecting~~ detection of small biases which

1 | are present ~~in~~ the whole water column, and thus can induce large errors. It basically says
2 | that the thermal or haline component of dynamic height innovation ($hdyn(innov_T)$ or
3 | $hdyn(innov_S)$) cannot exceed some threshold in height ($threshold_T$ for thermal component or
4 | $threshold_S$ for haline component). It can be summarized as follows. A vertical profile is
5 | rejected if the following condition is satisfied:

$$6 \quad \left\{ \begin{array}{l} \text{For temperature : } \frac{|C*hdyn(innov_T)|}{\sum dz_T} > threshold_T \\ \text{For salinity : } \frac{|C*hdyn(innov_S)|}{\sum dz_S} > threshold_S \end{array} \right. \quad (2)$$

$$7 \quad \text{where } \left\{ \begin{array}{l} c = 200 / \sum dz \quad \text{if } 0 < \sum dz \leq 200 \\ c = 500 / \sum dz \quad \text{if } 200 < \sum dz \leq 500 \\ c = \sum dz \quad \text{if } \sum dz > 500 \end{array} \right. \quad (3)$$

8 | and dz_T is the model layer thickness corresponding to the temperature observation (same for
9 | dz_S and salinity). These last conditions (Eq. (3)) prevent the threshold from being reached too
10 | quickly in shallow areas.

11 | The average and standard deviation of the thermal or haline components of dynamical height
12 | innovation have been calculated from a global simulation at $1/4^\circ$, which is a twin simulation
13 | of the PSY4V3 one. Note that the simulation at $1/4^\circ$ also assimilates the CORA 4.1 CMEMS
14 | in situ database. The temperature and salinity threshold ~~two-dimensional2D~~ fields used by
15 | QC2 are then computed as the average plus six times the standard deviation of the dynamical
16 | height innovations (Fig. 2). With these temperature and salinity thresholds, the system will
17 | reject more easily biased salinity profiles in the tropics and biased temperature profiles in
18 | strong currents.
19 |
20 |

21 | It should also be noted that the QC2 quality control rejects the entire vertical profile while the
22 | QC1 quality control only rejects aberrant temperature and/or salinity values at some given
23 | depths on the vertical profile.

24 | Figure 3a shows an example of a “wrong” temperature profile detected by the QC2 (and not
25 | by the QC1) at the end of July 2008. In this case, $threshold_T$ is equal to 0.3 m (Fig. 3b). The
26 | first condition of Eq. (2) is satisfied and the profile is rejected. When this profile is
27 | assimilated (simulation without QC2), abnormal temperature RMS innovation values appear
28 | at the temporal position (July 2008) of this profile in the Azores region (Fig. 3c). Using QC2

1 quality control allows solving the problem for this particular profile but also for some others
2 profiles (see Fig. 3c).

3 Statistics of the QC1 and QC2 quality controls are summarized in Fig. 4, where the
4 percentage of suspicious temperature and salinity profiles is given as a function of the year
5 over the 2007-2016 period. This percentage is relatively stable for both temperature and
6 salinity profiles, with little year-to-year variability, except for the years 2012 and 2013 where
7 more suspicious temperature and salinity profiles than usual were detected. Nevertheless, this
8 percentage remains relatively low (less than 0.35 % for temperature and 3.5 % for salinity),
9 knowing that the number of temperature profiles available each year ranges between 1.1
10 million and 1.7 million and the number of salinity profiles between 150,000 and 600,000.

11

12 **3 Impact of some sensitivemajor updates**

13 Most of the deficiencies in the systems can be related to these main recurring problems:
14 initialization, atmospheric forcing biases, abyssal circulation and efficiency of the
15 assimilation schemes. The first three problems are related to uncertainties in poorly observed
16 areas or parameters (i.e. deep ocean, ice thickness) and to intrinsic errors of the atmospheric
17 forcing. The last problem is related to linearity and stationarity hypotheses in the assimilation
18 schemes. In this section, we detail ~~the-some~~ solutions adopted for the system PSY4V3,
19 reducing uncertainties in the thermohaline component and allowing flow dependence in our
20 assimilation scheme. These solutions correspond to a part of the updates mentioned in section
21 2 and that don't result from routine system improvements.

22

23 **3.1 Initialization of oceanic simulation**

24 One way to initialize physical ocean model simulations is by using climatological values of
25 temperature and salinity from databases and assuming the velocity field is zero at the start.
26 The model physics then spins up a velocity field in balance with the density field. Another
27 common way to initialize a model is with fields from a previous run of that model, or with the
28 results from another model.

29 Given that data assimilation of the current observation network rapidly (in about ~~63~~ months)
30 adjusts the model state in the first 1000 m, the first solution has been chosen to ~~avoid~~
31 minimize potential drifts occurring after some years of simulation. Compared with the

1 | previous system PSY4V2 starting in October 2012 from the WOA09 three-dimensional3D
2 | climatology (see Fig. 1), the PSY4V3 system starts in October 2006 using improved initial
3 | climatological conditions. For that, we chose to use ENACT-ENSEMBLES EN4 1° global
4 | product (Good et al., 2013) which consists in monthly objective analyses. The great interest of
5 | these monthly fields is that a three-dimensional3D observation weight (between 0 and 1)
6 | describes the influence of the observations for each field. This information helps to retain only
7 | the observed points and not the perpetual climatology. This allows the computation of
8 | validated trends for each month and of climatology for a particular date. For that, a pointwise
9 | linear regression and in particular the Kendall's robust line-fit method (Hoaglin et al., 1983) is
10 | used, allowing us to obtain an initial condition called "robust EN4" for any time based only
11 | on real observations.

12 | Two free simulations (without any data assimilation) have been performed with the system
13 | PSY4V3, using either WOA09 or robust EN4 as initial condition in October 2006. Figure 5
14 | shows the box-averaged innovations of temperature and salinity as a function of time and
15 | depth over the October 2006 - December 2007 period. The top left panel reveals that, using
16 | WOA09 as initial condition, a fresh bias appears in the first 100 meters of the innovation,
17 | particularly more pronounced at the surface. It is not anymore the case when using robust
18 | EN4 to initialize the model (top right panel). For temperature, the bottom left panel exhibits
19 | cold biases above 100 m and below 300 m that are considerably reduced by using robust EN4
20 | as initial condition (bottom right panel). The warm and salty bias between 200 m and 300 m is
21 | slightly reinforced. It mostly concerns the main thermocline whom motions are well
22 | correlated with the altimetry. but it concerns only the top 300 m and Tthis bias will be
23 | corrected by the assimilation of altimetry and Argo profiles. Deeper biases are reduced with
24 | this new initialization where Argo profiles are missing.

25 | **3.2 Correction of precipitations**

26 | Many studies (e.g. Janowiak et al., 1998; Janowiak et al., 2010; Kidd et al., 2013) have
27 | compared reanalysis and atmospheric model precipitation fields with observation-based
28 | datasets, and have shown that atmospheric model products always bring significant and
29 | systematic errors, and are not able to close the global average freshwater budget. For instance,
30 | Janowiak et al. (2010) found that the IFS operational model and ERA-Interim reanalysis (Dee
31 | et al., 2011) from ECMWF perform well for temporal variability with respect to observational
32 | datasets, but they globally overestimate the daily precipitations. Although progresses have

1 been made in the ECMWF forecast model, substantial errors still occur in the tropics (Kidd et
2 al., 2013). The correction of atmospheric forcing within ocean applications has already been
3 successfully explored by adjusting atmospheric fluxes via observational datasets in global
4 applications (Large and Yeager, 2009; Brodeau et al., 2010). Other studies only focused on
5 precipitation correction (Troccoli and Kallberg, 2004; Storto et al., 2012).

6 The proposed method in this paper consists of correcting the daily precipitation fluxes by
7 means of a monthly climatological coefficient, inferred from the comparison between the
8 Remote Sensing Systems (RSS) Passive Microwave Water Cycle (PMWC) product (Hilburn,
9 2009) and the IFS ECMWF precipitations. We use remote PMWC product because of its
10 relative high $1/4^\circ$ resolution able to represent more accurately narrow permanent features such
11 as the Intertropical Convergence Zone. The use of spatially varying monthly climatological
12 coefficient is justified by the fact that the inter-annual variability is well captured by the
13 ECMWF forecast model and allows us to apply the correction outside the special sensor
14 microwave/imager era. This latter assertion is a limitation of the method as it assumes the
15 operational ECMWF forecast model has a constant bias. In order to avoid discontinuities
16 when either PMWC or ECMWF products exhibit zero precipitation, e.g. in arid areas, we do
17 not apply any correction in monthly mean values less than 1 mm of rainfalls fluxes. Also, in
18 order to keep the more accurate small-scale signal from the high resolution forcing, the
19 correction is only applied to large-scale component obtained by a low-pass Shapiro filter.

20 Hilburn et al. (2014) provided accuracy of RSS over ocean rain retrievals validated against
21 well established long-term in situ datasets such as observations from Pacific Marine
22 Environment Laboratory rain gauges on moored buoys in the tropics. They found that on
23 monthly averages, the standard deviation between satellite and buoy is 15.5 %. The
24 differences are greatest in the Indian Ocean and Western Pacific. We then arbitrarily capped
25 the correction beyond 20 % in order to take into account these satellite-based retrievals errors.

26 Lastly, we did not apply the correction poleward 65° N and 60° S because of lack and
27 important biases of satellite-based precipitations estimate (Lagerloef et al., 2010) at high
28 latitudes.

29 Figure 6 represents the difference between the IFS precipitations coming from ECMWF and
30 the PMWC product using satellite data, before and after large scale correction. As already
31 pointed out by Stephens et al. (2010), original IFS forcings exhibit a systematic over-
32 estimation of precipitation within the inter-tropical convergence zones (up to 3 mm day^{-1}) and
33 under-estimation at mid- and high-latitudes (up to -4 mm day^{-1}). After correction, the mean
34 bias compared with PMWC is reduced from 0.47 to 0.19 mm day^{-1} .

1 To validate this correction, two global ocean hindcast simulations of several years, using only
2 the 3D-VAR large-scale biases correction in temperature and salinity, have been performed,
3 one with IFS correction and the other without. Figure 7 represents the mean surface salinity
4 innovation (difference between the assimilated observation and the model) on the year 2011.

5 ~~At the global scale, the bias reduction is not very significant, but t~~These maps demonstrate
6 that the IFS correction is beneficial in many local areas. The strongest benefice concerns the
7 Tropics where the IFS correction allows to ,–reducing the magnitude of the near-surface
8 salinity fresh mean bias ~~in the Tropics~~ down to 0.5 psu. The fresh bias reduction in the
9 Tropics reaches 0.15 psu in average.

10 **3.3 Assimilation of climatological temperature and salinity climatology in the** 11 **deep ocean**

12 ~~Due to unresolved processes (internal waves, spurious mixing in overflow regions, tidal~~
13 ~~mixing) and inaccurate atmospheric forcing (bulk formulas), the model may drift at depth. The~~
14 ~~model may exhibit significant drift at depth that can be related to the misrepresentation of~~
15 ~~several processes for which an exhaustive list would be hard to give here. Difficulties~~
16 ~~encountered by ocean model using z-coordinates in overflow regions are likely to be largely~~
17 ~~responsible for this. In addition, Eulerian vertical coordinates (vs lagrangian, isopycnal~~
18 ~~coordinates) may add a spurious diapycnal component in the interior where mixing is~~
19 ~~essentially in the isopycnal direction. Lastly, the model lacks of an accurate interior mixing~~
20 ~~scheme such as the one of De Lavergne et al. (2016) that does take into account internal tidal~~
21 ~~wave mixing (tides are not explicitly resolved in PSY4V3). Interior mixing is indeed crudely~~
22 ~~represented by spatially constant background diffusivity in the model.~~

23 ~~For systems which assimilate observations in a multivariate way, the problem can be more~~
24 ~~critical because of the deficiencies of the background error covariances that may contain~~
25 ~~spurious correlations for extrapolated and/or poorly observed variables.~~ Unfortunately, there
26 are very few temperature and salinity profiles below 2000 m to constrain the model drift.
27 Hence, the climatology is currently the only source of information at depth to prevent the
28 model from drifting. Virtual vertical profiles of temperature and salinity below 2000 m are
29 built from the monthly WOA13v2 climatology. These virtual observations are geographically
30 positioned on the model horizontal grid with a coarse resolution ($1^\circ \times 1^\circ$) and on the model
31 vertical levels from 2200 m to the bottom.

1 As in Greiner et al. (2006), we define empirically the standard deviations (departures from the
 2 climatology) σ_T for temperature and σ_S for salinity, as a simple linear vertical profile:

$$3 \quad \begin{cases} \sigma_T = \text{MAX} \left(\left(\frac{0.6-z/10^4}{3} \right); 0.05 \right) \\ \sigma_S = \sigma_T / 8 \end{cases} \quad (4)$$

4 where z is the depth (in meters).

5 We define then σ_{TS} the density departure from the climatology:

$$6 \quad \sigma_{TS} = \alpha \sigma_T + \beta \sigma_S \quad (5)$$

7 where α represents the thermal expansion coefficient and β the saline contraction coefficient.

8 Following Jackett and Mcdougall (1995), these coefficients are assumed to depend only on
 9 latitude and depth of the ocean as illustrated by Fig. 8.

10 If we note d_{TS} the density innovation, d the temperature or the salinity innovation and σ the
 11 temperature or the salinity departure from the climatology, the value of the climatological
 12 error e is prescribed as:

$$13 \quad \begin{cases} \text{If } |d_{TS}| \leq 2 \sigma_{TS} \text{ then } e = \infty \text{ (observation rejected)} \\ \text{If } |d_{TS}| > 2 \sigma_{TS} \text{ then } \begin{cases} \text{if } 2\sigma < |d| < 3\sigma \text{ then } e = \text{MIN} \left(\frac{2\sigma}{3} \left(\frac{|d|}{|d|-2\sigma} \right); 20\sigma \right) \\ \text{if } |d| \geq 3\sigma \text{ then } e = 2\sigma \\ \text{if } |d| \leq 2\sigma \text{ then } e = 20\sigma \end{cases} \end{cases} \quad (6)$$

14
 15 A non-Gaussian error is used to impose a weak constraint on the model at depth (Fig. 9). That
 16 way, we correct the model drift without constraining a slow moderate variability or trend.
 17 Basically, the hypothesis is that small to medium departures from the climatology (2σ or less)
 18 has an even probability. For instance, a 0.2 °C model warming at 2000 m due to a positive
 19 North Atlantic Oscillation pattern must not be corrected as zero. Indeed, a 0.2 °C cooling is as
 20 likely as the warming, since the climatology is the time average of those anomalies. So, only
 21 large departures from climatology (3σ or more) should be corrected. It corresponds to highly
 22 unlikely events that are typical of model drifts. An interesting point is that model drift is often
 23 corrected locally, downstream the outflow, before it spreads out (see Fig. 10). Ideally, it gives
 24 a little regional correction instead of a large basin scale bias.

25 To validate this kind of assimilation, two global ocean simulations of several years, using
 26 only the 3D-VAR large-scale biases correction in temperature and salinity, have been

1 performed. Due to the high computational cost of the system PSY4V3, the assimilation of
2 WOA13v2 below 2000 m has been tested with a global intermediate-resolution system at $\frac{1}{4}^\circ$,
3 which is, in all other aspects, very close to the high resolution system PSY4V3. All in situ
4 observations have been used as well.

5 In practice, the assimilation of WOA13v2 climatological profiles below 2000 m in the system
6 concerns mostly some regions where the steep bathymetry might be an issue for the model
7 (Kerguelen Plateau, Zapiola Ridge, and Atlantic ridge). Figure 10 shows mean temperature
8 (left) and salinity (right) innovations (WOA13v2 climatological profiles minus model) in
9 2013 at 2865 m. The assimilation of these climatological profiles occurs more or less at the
10 same locations over the time period 2007-2016. Since the conditions of the system of
11 equations (6) relate to the density innovation, we have a perfect symmetry of the temperature
12 and salinity data which are assimilated. This has the effect of not disturbing the density
13 gradients too much.

14 If we focus on latitudes between 30° S and 60° S, Fig. 11 represents temperature (top panels)
15 and salinity (low panels) annual anomalies over depth (500 - 5000 m) and time (2007-2014).
16 The simulation on the left does not assimilate climatological vertical profiles while the
17 simulation on the right assimilates some. These maps demonstrate that the assimilation of
18 WOA13v2 below 2000 m is beneficial, reducing drifts below 2000 m. In the Antarctic
19 Circumpolar Current (ACC), the assimilation of these profiles makes it possible to maintain,
20 for instance, the Antarctic Bottom Water (see Gasparin et al., 2018 – In revision in Journal of
21 Marine Systems). This also impacts the vertical repartition of the steric height, without
22 degrading the quality of the results comparing with profiles from the Argo network.

23 **3.4 Construction of the backgroundforecast error covariance**

24 The seasonally varying backgroundforecast error covariance is based on the statistics of a
25 collection of three-dimensional3D ocean state anomalies. This approach is based on the
26 concept of statistical ensembles in which an ensemble of anomalies is representative of the
27 error covariance. In this way, truncation no longer occurs and all that is needed is to generate
28 the appropriate number of anomalies. The way in which these anomalies are computed from a
29 long numerical experiment is described in Lellouche et al. (2013).

30 In this section, we detail two features of the system PSY4V3 compared to the previous system
31 PSY4V2, regarding the construction of the background error covariance. First, we evaluate
32 the impact of anomaly filtering on analysis increment. Second, we evaluate the potential

1 added value on the quality of the analysis increments of the choice of the simulation from
2 which to calculate the anomalies. -In the previous system PSY4V2, a free simulation was used
3 to calculate the anomalies. For the system PSY4V3, the anomalies are computed from a
4 simulation in which only a 3D-VAR large scale bias correction of T/S has been performed.~~In~~
5 ~~the following section, we evaluate the potential added value of this choice on the quality of~~
6 ~~the analysis increments.~~

7 **3.4.1 Anomaly filtering**

8 The signal at a few horizontal grid “ Δx ” intervals in the model outputs on the native full grid
9 is not physical but only numerical (Grasso, 2000) and should not be taken into account when
10 updating an analysis. This is why several passes of a Shapiro filter have to be applied at the
11 anomalies computation stage in order to remove the very short scales that in practice
12 correspond to numerical noise. This can also help to filter out the noise from the covariance
13 matrix due to the sampling error (Raynaud et al., 2009).

14 To illustrate the impact of the anomaly filtering, we set up some experiments with different
15 levels of filtering. Each experiment consists in the assimilation of a single altimeter track over
16 one assimilation cycle. These experiments have been performed with a Mercator Ocean
17 regional system at $1/36^\circ$ using the SAM data assimilation scheme, in order to reduce the high
18 computing cost of the global system PSY4V3 as well as the time consuming to build different
19 sets of anomalies at the global scale. Figure 12 shows SLA increments obtained with these
20 different levels of anomaly filtering. It should be noted that the anomaly filtering has a direct
21 effect on the analysis increment, since the latter is a linear combination of the anomalies.

22 Figure 12a represents SLA innovation along the single assimilated track. Figure 12b,c,d
23 represents the SLA increments obtained respectively with 10, 100 and 300 Shapiro passes as
24 the anomaly filtering mentioned above (corresponding approximately to a 3, 10 and 15
25 horizontal grid “ Δx ” intervals filter). We can see that the correction under the track remains
26 more or less the same. The strongest differences occur outside the track where the innovation
27 information is extrapolated.

28 Other experiments, closer to real time integration set up have been performed, assimilating all
29 the altimeter tracks available on a 7-day assimilation window, instead of one single track.
30 Figure 13 shows the difference of SLA increments using 10 and 300 Shapiro passes as
31 anomaly filtering (corresponding approximately to 20 km and 80 km). The conclusions are
32 the same as those concerning the experiments with a single assimilated track. The corrections

under the tracks remain almost the same for the two levels of filtering. Both analyses are close to the data under the tracks. The strongest differences occur outside the tracks where the innovation information is extrapolated to fill the gaps. Low filtered increments (10 Shapiro passes) have small-scale structures that are statistical artifacts. Small structures can cascade in the model, and stay trapped between the repetitive tracks, without correction by the assimilation. This happens less when more filtering (300 Shapiro passes) is performed on the anomalies beyond the effective resolution of the model.

3.4.13.4.2 Choice of the simulation from which to calculate the anomalies

The system PSY4V3 was run over the October 2006 – October 2016 period to catch-up the real-time (“OPER” simulation), starting from ~~three-dimensional~~^{3D} temperature and salinity initial conditions based on the EN4 climatology. This simulation benefited from the full data assimilation system, including the 3D-VAR biases correction and the SAM filter. Two other simulations over the same period have been performed. The first one is a “FREE” simulation (without any data assimilation) and the second one has exactly the same model tunings but only benefits from the temperature and salinity 3D-VAR large-scale biases correction (“BIAS” simulation).

Figure 14 and Figure 15 show comparisons between this triplet of PSY4 simulations and two observational products. The first product is the CMEMS/DUACS (Data Unification and Altimeter Combination System) Merged-Gridded Sea Level Anomalies heights in delayed time on a $\frac{1}{4}^\circ$ regular horizontal grid with a 1-day temporal resolution (Pujol et al., 2016). The second one is the Roemmich-Gilson Argo monthly climatology on a 1° regular horizontal grid (Roemmich and Gilson, 2009) which is commonly used in the oceanographic community.

Figure 14a,b,c shows the 2007-2015 SSH variability for the three simulations (subsamped in a similar way to DUACS). SSH variability difference is defined as the difference of SSH standard deviations from PSY4 simulations and the DUACS product (Fig. 14d,e,f). Comparing to the variability of the DUACS product, the fronts in high mesoscale variability regions such as the Gulf Stream, the Kuroshio, the Agulhas current or the Zapiola eddy are misplaced in the FREE simulation. In the BIAS simulation, these fronts are better positioned due to the large-scale correction of temperature and salinity. However, this simulation presents more energy compared to DUACS, apart of the main fronts. This corresponds to a leakage of vorticity from the fronts due to the mean advection. Note that the gridded DUACS product also underestimates the variability as wavelengths smaller than 200 km are barely resolved in the gridded fields. The effective resolution of DUACS product ranges from almost

1 500 km at the Equator to 150 km at high latitude. For OPER simulation, the effective
2 resolution is relatively similar or slightly larger in the inter-tropical band and almost 100 km
3 at high latitude. The mesoscale features are well constrained in the OPER simulation with the
4 information coming from satellite data.

5 Time-averaged density differences along the equatorial Pacific between two ENSO events
6 (“Oct-Dec 2008 minus Oct-Dec 2009”), computed from the PSY4 simulations and from the
7 Roemmich-Gilson Argo monthly Climatology, are shown in Fig. 15. The SCRIPPS Argo
8 product presents a higher density difference in the eastern part of the equatorial Pacific. It
9 corresponds to the change from moderate La Niña conditions early 2008 to moderate El Niño
10 conditions in 2009. The FREE simulation is not dense enough in the east compared to
11 observations particularly at the pycnocline depth (1025 kg/m^3 isopycn). The BIAS simulation
12 intensifies the density difference. The OPER simulation gets even closer to the SCRIPPS
13 Argo product. There is also an upward tilt of the density difference maximum in agreement
14 with the observations.

15 In summary, the BIAS simulation better represents the density fronts on the horizontal (Gulf
16 Stream) and on the vertical (Pacific pycnocline). The covariance matrix deduced from this
17 simulation has information on the density gradients that is well placed. This is valuable off the
18 equator through geostrophy, and at the equator to control the zonal pressure gradient. The
19 variance in sea level is stronger than the DUACS one (see Fig. 14e) but the most important
20 point for the construction of the anomalies is to have well-placed density gradients. In the
21 OPER simulation and as mentioned in Lellouche et al. (2013) in the description of the data
22 assimilation system SAM, an adaptive scheme will correct the variance and will give an
23 optimal background model error variance based on a statistical test formulated by Talagrand
24 (1998).

25 **3.5 Adaptive tuning of observation errors**

26 In order to refine the prescription of observation errors (instrumental and representativenessity
27 errors), adaptive tuning of ~~observation~~ errors for the SLA and SST has been implemented in
28 PSY4V3. We let “Talagrand method” (Talagrand, 1998) to adjust the background error.
29 Instrumental error doesn’t change with time. On the contrary, the representativeness error is
30 really flow-dependent. Taking into account the representativeness error is particularly
31 important for assimilated OSTIA SST because the sky is clear only 30% of the time in
32 average. The method has not been used for temperature and salinity vertical profiles because

1 of the reduced number of in situ data compared with satellite data. ~~T~~Then, ~~hree-~~
2 ~~dimensional~~3D fixed observation errors are then used for the assimilation of in situ
3 temperature and salinity vertical profiles.

4 The method consists in the computation of a ratio, which is a function of observation errors,
5 innovations and residuals (Desroziers et al., 2005). It helps correcting inconsistencies on the
6 specified observation errors. This ratio can be expressed as:

$$7 \quad \mathbf{ratio} = \frac{\mathbf{residual}(\mathbf{innovation})^T}{\mathbf{observation\ error}} \quad (7)$$

8
9 Ideally, *ratio* is equal to ~~+~~one. When the ratio is less (respectively larger) than one~~+~~, it means
10 that the observation error is overestimated (respectively underestimated). The objective of this
11 diagnostic is to improve the error specification by tuning an adaptive weight coefficient acting
12 on the error of each assimilated observation. As a first guess of the method, the initial
13 prescribed observation error matches the one used in the previous system (Lellouche et al.,
14 2013) where the observation error variance was increased near the coast and on the shelves
15 for the assimilation of SLA, and increased only near the coast (within 50 km of the coast) for
16 the assimilation of SST.

17 Figure 16 represents the temporal evolution of the ratio defined in Eq. (7) for Envisat satellite.
18 At the beginning of the simulation, the observation error is overestimated (ratio less than
19 one~~+~~). The ratio tends to 1 after only a few weeks of simulation.

20 For SLA (Fig. 17), the a priori prescribed observation error is globally significantly reduced.
21 The median value of the error changed from 5 cm to 2.5 cm in a few assimilation cycles and
22 allows for better results. This method allows us to have more realistic and evolutive
23 observation error maps which can provide valuable information for the space agencies.

24 The realism of tropical oceans is crucial for seasonal forecasting applications. Tropical
25 Instability Waves (TIWs) can be diagnosed from SST (Chelton et al., 2000). These Kelvin
26 Helmholtz waves initiate at the interface between areas of warm and cold sea surface
27 temperatures near the Equator and form a regular pattern of westward-propagating waves.
28 Figure 18 gives an example of adjustment of the observation error to the model physics and
29 atmospheric variability. The SST anomalies in the equatorial Pacific clearly show the
30 propagation westwards of TIWs in the second half of the year. This is more pronounced
31 during episodes of La Niña (mid-2007 and mid-2010). The observation error anomalies

1 estimated by “Desroziers method” show that the error increases when these TIWs are more
2 marked. This can be explained two ways. First, the representativeness error increases because
3 the data is not corresponding exactly at the right time and the right position to the model
4 counterpart. In case of clouds, SST value can result from OSTIA time or space interpolation.
5 This would be detrimental with the fast propagation of TIWs. Second, large errors can result
6 of a ~~by uncertainties in SST observations (clouds) and~~ model shift of the TIWs structures. The
7 error decreases in the reverse case.

8 We have also performed an Empirical Orthogonal Function (EOF) analysis to assess the
9 variability of the SST observation error (Fig. 19). Mode 1 is associated to the seasonal cycle
10 and mode 2 (not shown) corresponds to the migration of the seasonal signal. Mode 3 is
11 associated to the inter-annual signal with for instance the transition La Niña / El Niño,
12 showing that the SST error is able to adapt both to the seasonal and inter-annual fluctuations.

14 **4 Scientific assessment**

15 This section describes the PSY4V3 system’s quality assessment with diagnostics over
16 particular years, together with time series over multiyear periods. To evaluate the quality of
17 the system, the departure from the assimilated observations (SST, SLA, T/S vertical profiles
18 and sea ice concentration) is measured. Moreover, the analyses are also compared with
19 observations that have not been assimilated by the system such as tide gauges, velocity
20 measurements from drifting buoys, NOAA SST and AMSR sea ice concentration. NOAA
21 SST and AMSR sea ice analyses are not fully independent, since the upstream observations
22 are the same than for assimilated CMEMS OSTIA SST and OSI Sea Ice concentrations, but
23 comparisons to a variety of estimates using different algorithms and protocols provides a
24 useful consistency analysis.

25 **4.1 SST**

26 **4.1.1 Assimilated SST**

27 The OSTIA product is assimilated in the system PSY4V3. Compared to the previous system
28 PSY4V2, some large scale cold biases with respect to OSTIA are reduced in the Indian,
29 Eastern South Pacific, and western North Pacific (not shown). On the other hand, warm biases
30 are not reduced, especially in regions of strong inter-annual warm events such as the Eastern
31 Tropical Pacific where strong El Niño took place in 2015/2016, but also in the ACC, the Gulf

1 Stream and the Greenland Current (Fig. 20a). Some inconsistencies can be found between
2 OSTIA SST and in situ near surface temperature, particularly in the North Pacific where the
3 system PSY4V3 presents a cold bias compared to in situ near surface temperature but a warm
4 bias compared to OSTIA SST (Fig. 20b). Figure 20c shows the difference between drifting
5 buoys SST and the system PSY4V3 over the year 2015. The drifting buoys SST data are
6 present in the CMEMS in situ database used by Mercator but they have not been assimilated
7 in the system because the depth of these data is a nominal value and we chose to assimilate
8 only data with a measured depth value. Although we plan to assimilate these data in the future
9 system, we use currently this data as independent information. This allows us to see that SST
10 from in situ vertical profiles and SST from drifting buoys are coherent with each other. We
11 thus find again the cold bias highlighted by the comparison with -SST from in situ vertical
12 profiles in the North Pacific. It is a lack of stratification in the model, which causes mid-
13 latitude cold surface biases during (boreal) summer and a warm bias between 50 m and 100
14 m.

15 We checked also the time series of the mean and the RMS of the misfit (innovation) between
16 the observed SSTs and the model. For OSTIA SST, which is the gridded SST assimilated in
17 PSY4V3, we obtain a mean warm bias of -0.1 °C and a RMS error of 0.45 °C (Fig. 21). Time
18 series of the differences between the model and NOAA AVHRR SST, which was assimilated
19 in the previous PSY4V2 system, are also shown on Fig. 21. This allows to compare both
20 gridded SST products. Seasonal fluctuations of the SST biases on global average can be seen
21 as a lack of stratification in the model, which causes stronger mid-latitude warm biases during
22 (boreal) summer (and a warm bias between 50 m and 100 m). For in situ SST, the bias is
23 smaller, suggesting that OSTIA and AVHRR might be colder than in situ near surface
24 observations on global average. We can notice a drop in the RMS of in situ surface data in
25 January 2014, which is due to the use of near real time observations, where most of the
26 surface observations do not have sufficient quality flag.

27 **4.1.2 Comparison with an independent high resolution SST external product**

28 CLS (Collecte Localisation satellites) operates since 2002 a near real time oceanography data
29 service named CATSAT, for scientific, institutional or private users (support to fishery
30 management or to the offshore oil and gas industry). These data include satellite observations
31 such as chlorophyll-a, SST and altimetry. Maps of SST are computed from Aqua/MODIS, S-
32 NPP/VIIRS and Metop/AVHRR infra-red sensors at 2 km resolution, using nighttime data

1 only to avoid diurnal warming effects. We can then evaluate the system ability to produce the
2 mesoscale by comparing with the CATSAT daily SST product. On Fig. 22, the CATSAT
3 daily snapshot can be considered as an independent dataset since the OSTIA SST assimilated
4 in the system has mostly seen microwave measurements during two weeks, as it was very
5 cloudy in the Gulf of Mexico. 31st of March 2016 is the first clear day showing well, from
6 infrared measurements, the Loop Current and other structures in the western part of the Gulf
7 of Mexico. The Loop Current is almost forming a closed meander. This is reproduced by the
8 system PSY4V3, as well as secondary structures like the filament in the North (Fig. 22).
9 Visible limitations of this 1/12° system concern the fine sub-mesoscale that can not be
10 resolved, and the lack of tidal mixing along Yucatan coasts (Kjerfve, 1981).

11 4.2 Temperature and salinity vertical profiles

12 For the T/S vertical profiles, we checked time series of the RMS of the difference between the
13 model analysis and the observations, for temperature on the left and for salinity on the right
14 (Fig. 23) in the whole water column. We compare observation and – climatology (red line),
15 the previous system PSY4V2 (blue line), and the new system PSY4V3 (black line).

16 On global average, and compared to the previous system PSY4V2, the system PSY4V3
17 slightly degrades the temperature statistics (-0.03 °C) but it significantly greatly improves the
18 salinity statistics by decreasing the 0-5000 m RMS salinity by 0.1 psu. This allows-enables us
19 to get a more accurate description of the water masses. This better balance arises from the
20 new in situ errors that give more weight to the salinity data (not shown). We can also notice
21 that the systems are always better than the climatology. The comparison to climatology is a
22 minimum performance indicator that the system must achieve. The differences with the
23 climatology are worset from the beginning of the year 2013. It can be explained by the fact
24 that six different decades of WOA13v2 monthly climatology can be found on the NODC
25 website from 1955 to 2012. We chose the available 2005-2012 “truncated decade” (near of
26 our time period simulation) even if it is biased to cold, given the strong La Niña event on
27 2010-2011. Previous decades (before 2005) are even colder and can no longer be used for
28 recent dates. Moreover, 2005-2012 “truncated decade” doesn’t contain the period of transition
29 towards El Niño events and in particular the strong one occurring in 2015. So, in situ
30 temperature and salinity vertical profiles we assimilated in the system and which see this
31 transition are coherent with this WOA13v2 product until the end of year 2012 and this is no
32 longer the case afterward.

1 Moreover, the system PSY4V3 experiences a slight warm bias (negative observation minus
2 forecast difference) in subsurface (25 - 500 m) on global average (not shown). For the year
3 2015, part of this signal comes from the strong inter-annual ENSO signals in the Tropical
4 Pacific where the near surface bias is also warm, as well as in the ACC and the Gulf Stream.
5 Seasonal cold surface biases appear in the mid latitudes, linked with a lack of stratification
6 during summer. Summer warming is injected too deep ~~and-which~~ results in subsurface
7 spurious warming and ~~a too-shallow~~ mixed layer that is too shallow. However, these biases
8 remain small on global average.

9 **4.3 Sea Level**

10 **4.3.1 Assimilated SLA**

11 The system PSY4V3 is closer to altimetric observations than the previous one with a global
12 forecast RMS difference of around 6 cm instead of 7 cm for the system PSY4V2 (not shown).
13 This RMS difference is consistent with the prescribed a priori observations errors (about 2 cm
14 for altimeters instrumental error and 4 cm for MDT error in average). The statistics come
15 from the data assimilation innovations computed from the forecast used as the background
16 model trajectory, and give an estimate of the skill of the optimal model forecast. These scores
17 are averaged over all seven days of the data assimilation window, which means the results are
18 indicative of the average performance over the seven days, with a lead time equal to 3.5 days.

19 More precisely, on the year 2015, the SLA mean and RMS errors are considerably reduced in
20 the new system PSY4V3 compared to the previous one (Fig. 24). The mean bias is reduced by
21 0.3 cm (from -0.8 cm to 0.5 cm) and the RMS is reduced by 2.4 cm (from 7.9 cm to 5.5 cm).
22 This is mainly due to the use of the “Desroziers” method to adapt the observations errors
23 online, which yields to more information from the observations being used (see Sect. 3.5).
24 These improvements occur in nearly all regions of the ocean but are more pronounced in
25 some regions (e.g. North Atlantic, Hudson Bay, Labrador Sea). In some others regions (e.g.
26 Indonesian or west tropical Pacific), ~~it-remains~~ some errors in sea level remain and are linked
27 to the uncertainty in the MDT or missing parametrisations in the model (interaction wave-
28 current, tides).

29 **4.3.2 Comparison to tide gauge data**

30 The system PSY4V3 produces hourly outputs at the surface that can be compared with tide
31 gauge measurements. For that, we used the BADOMAR product (Lefevre et al., 2005) which

1 is a specific processed tide gauges database developed and maintained at CLS and consists of
2 filtered tide gauge data from the GLOSS/CLIVAR ([Global sea Level Observing](#)
3 [System/Climate Variability and Predictability](#)) “fast” sea level data tide gauge network
4 ([GLOSS Implementation Plan, 2012](#)). These tide gauge data are corrected from inverse
5 barometer effect and tides. High frequency model SSH compares well with tide gauges in
6 many places, with a slight improvement in PSY4V3 with respect to PSY4V2 (not shown).
7 The best agreement between the system PSY4V3 and tide gauges is found in the tropical
8 band, as can be seen in Fig. 25, while shelf regions and closed seas are less accurate. This
9 confirms the latitude dependence of the correlation between tide gauges and satellite altimetry
10 or modelled SSH discussed in Vinogradov and Ponte (2011) or Williams and Hugues (2013).
11 The improvements related to water masses and SLA lead to a correct Global Mean Sea Level
12 (GMSL) trend. We checked the system GMSL by comparing the results with recent estimated
13 trend from the paper of Chambers et al. (2017). We found for the model a trend of 3.2 mm yr^{-1}
14 ¹ over the PSY4V3 simulation time period which is coherent with DUACS value (3.17 ± 0.67
15 mm yr^{-1}). Moreover, the temporal evolution of the global mean model SSH is coherent and
16 phased with the observations.

17 **4.4 Sea ice concentration**

18 **4.4.1 Assimilated sea ice concentration**

19 The system PSY4V3 assimilates OSI SAF sea ice concentration in both hemispheres with a
20 monovariate/monodata scheme. As expected, PSY4V3 is closer to the observations than the
21 previous system PSY4V2 (not shown), in which no sea ice observations had been assimilated.
22 As illustrated by Fig. 26, the system PSY4V3 has a slight overestimation of ice during the
23 melting season in summer (up to 3 % on average in both hemispheres). Conversely, the mean
24 error is stronger on average during winter (10 to 20 % underestimation, depending on the
25 year). RMS errors are also larger during summer (up to 20 % in the Arctic and 30 % in the
26 Antarctic with respect to OSI SAF observations), and [they](#) drop to less than 10 % in winter.
27 These RMS errors quantify the capacity of the system to capture weekly time changes in the
28 ice cover.

29 We have also checked the evolution of the sea ice volume diagnosed by the system PSY4V3
30 ~~which assimilates observations of sea ice concentration with a monovariate/monodata scheme.~~
31 The data assimilation scheme SAM produces increment of sea ice concentration which is the

1 unique sea ice correction applied in the model using the Incremental Analysis Update (IAU)
2 method described in Lellouche et al. (2013). The sea ice volume then adjusts to this correction
3 considering a constant sea ice thickness. No sea ice thickness observations are assimilated in
4 the system. The risk is therefore to obtain unrealistic drifts or trends of the unconstrained sea
5 ice volume. Presently, sea ice volume retrievals from satellites are associated with large
6 uncertainties (Zygmuntowska et al., 2014). Consequently, modelled sea ice volume is difficult
7 to validate and one of the solutions is to compare modelled sea ice volume from several
8 systems.

9 Figure 27 shows the 2007-2016 evolution of sea ice volume for the system PSY4V3, the
10 PIOMAS modelled product (Schweiger et al., 2011) and the CMEMS GREP (Global
11 Reanalysis Ensemble Product, [http://marine.copernicus.eu/documents/QUID/CMEMS-GLO-](http://marine.copernicus.eu/documents/QUID/CMEMS-GLO-QUID-001-026.pdf)
12 [QUID-001-026.pdf](http://marine.copernicus.eu/documents/QUID/CMEMS-GLO-QUID-001-026.pdf)) composed by four global $\frac{1}{4}^\circ$ reanalyses and the ensemble mean with the
13 associated spread from the four members. All the modelled sea ice volumes present the same
14 2007-2016 inter-annual variability. PSY4V3 and PIOMAS are included in the spread whose
15 range ~~is reduced~~ ~~decreases~~ over time from 4,000 km³ in 2007 to 3,000 km³ ~~from the year in~~
16 2012 ~~and remains almost constant afterward~~. The GLORYS2V4 reanalysis is known to have a
17 large sea ice volume compared to other reanalyses (Chevallier et al., 2017). Although we use
18 the same method for the assimilation of sea ice concentration in GLORYS2V4 and PSY4V3,
19 the sea ice volume diagnosed by PSY4V3 lies in values ranging between 13,000 and 15,800
20 km³, in a better accordance with GREP and PIOMAS products.

21 4.4.2 Contingency table analysis

22 The contingency table analysis approach described in Smith et al. (2016) has been applied to
23 evaluate sea ice extent as compared to observation. Satellite ice concentration coming from
24 AMSR2 (L1B brightness with a NASA team 2 algorithm to compute sea ice concentration)
25 has been used as independent observation to provide a general assessment in the detection of
26 false alarms if ice coverage. Although this type of evaluation is usually done on forecasts, we
27 used hindcasts. For the computation of the statistics we have used a stereo-polar grid at a 20
28 km resolution. In each cell of that grid we have then computed binary values corresponding to
29 ice/open water conditions for the model and the sea ice observations by using a 40 %
30 concentration threshold. We have also restricted our study to the Proportion Correct Total
31 (PCT), following the conclusion of Smith et al. (2016), saying that it was more insightful to
32 refer to the PCT rather than others proportions. The PCT quantity is defined as $PCT = (\text{Hit ice}$

1 + Hit water)/n (see Table 3), where n is the total number of observations with a sea ice
2 concentration greater than 15 %. A value of one corresponds to a perfect score.

3 Figure 28 shows times series of PCT for PSY4V2 and PSY4V3 systems. The lower PCT
4 values are due mostly to an excessive melt in spring and summer for both Arctic and
5 Antarctic. However, the assimilation of sea ice concentration improves significantly the total
6 hit rate during these periods.

7 **4.5 Currents**

8 The aim of this section is to use velocity observations which were not assimilated in the
9 system to assess the level of performance of PSY4V3 compared to the previous PSY4V2
10 system. The mean currents are checked by comparing the model to velocity observations
11 coming from Argo floats when they drift at the surface and in situ Atlantic Oceanographic and
12 Meteorological Laboratory (AOML) surface drifters. A paper by Grodsky et al. (2011)
13 revealed that an anomaly in the drogue loss detection system of the Surface Velocity Program
14 buoy had led to the presence of undetected undrogued data in the “drogued-only” dataset
15 distributed by the Surface Drifter Data Assembly Center. Rio (2012) applied a simple
16 procedure using altimeter and wind data to produce an updated dataset, including a drogue
17 presence flag as well as a wind slippage correction. ~~Therefore, We therefore we~~ used this new
18 “drogued-only” surface drifter dataset coming from CMEMS in situ TAC ([Rio and Etienne,
19 2017http://marine.eoernicus.eu/documents/QUID/CMEMS-INS-QUID-013-044.pdf](http://marine.eoernicus.eu/documents/QUID/CMEMS-INS-QUID-013-044.pdf)) to
20 check mean model currents.

21 Figure 29 represents zonal drift innovation for PSY4V2 and PSY4V3 systems. Although
22 some biases persist, mostly in the western tropical basins, significant improvements are
23 obtained almost everywhere with the new system PSY4V3, and more particularly in the
24 equatorial Pacific. The mean bias is reduced (from 0.1 m s^{-1} to 0.08 m s^{-1}), the South
25 Equatorial Current is slower and there is also less noise in PSY4V3. Improvements are also
26 obtained, to a lesser extent, for meridional drift (not shown). The velocities have been slightly
27 improved in terms of velocity values but also in terms of currents direction (angle between
28 observed and modelled velocities). The mean angle difference is reduced from 9.1 degrees to
29 7.2 degrees. These improvements can be attributed to the new MDT used and the more
30 adapted filtering of anomalies. However, large biases persist in the western tropical Pacific
31 (very strong in 2015 because of the strong El Niño event) with a spurious extension of the

1 northern branch of the South Equatorial Current. This is probably linked to the uncertainty
2 still present in the MDT and unresolved or missed parameterized physical processes.

3 More locally, a comparison of the 2007-2015 averaged drifts from the system PSY4V3 and
4 the observations over the Indonesian region has been performed (not shown). Currents in this
5 region are very difficult to resolve because of the many narrow straits and the strong tidal
6 mixing. The retroflection of the westward South and North Equatorial Currents (along Papua
7 and near 12° N) into the eastward North Equatorial Counter Current (near 4° N) are well
8 reproduced structures in the Pacific. The system South Equatorial Current is a little too strong
9 at the edge of the warm pool but it is about the only weakness. The complex flow in the
10 Sulawesi Sea, the Makassar Strait and the South China Sea is also well reproduced by the
11 system. The correlation is 0.70 (respectively 0.64) for the zonal (respectively meridional)
12 velocity.

13 **5 Summary and ways for improvement of the future system**

14 The Mercator Ocean system PSY4V3, in an operational mode since October 19, 2016,
15 benefits of many important updates. PSY4V3 has a quite good statistical behaviour with an
16 accurate representation of the water masses, the surface fields and the mesoscale activity.
17 Most of the components of the system PSY4V3 have been improved compared to the
18 previous version: global mass balance, three-dimensional~~3D~~ water masses, sea level, sea ice
19 and currents. Major variables like sea level and surface temperature are hard to distinguish
20 from the data.

21 In this paper, the updates showing the highest impact on the products quality and that don't
22 result from routine system improvements, have been illustrated and evaluated separately. A
23 particular focus was therefore made on the initialization, the correction of precipitation, the
24 assimilation of climatological temperature and salinity in the deep ocean, the construction of
25 the background~~forecast~~ error covariance and the adaptive tuning of observations error.

26 Initial climatological condition has been improved in order to be more consistent with the
27 vertical profiles of temperature and salinity which has been assimilated thereafter. Rather than
28 taking directly the climatological temperature and salinity of the month corresponding to the
29 start of the simulation, we performed a pointwise linear regression, allowing to obtain an
30 initial condition at the appropriate time and based only on real observations. One-year free
31 simulations have been performed and show that biases are globally reduced.

1 Uncertainties inherent to atmospheric analyses and forecasts can induce large errors in the
2 ocean surface fluxes. For instance a slight shift in the position of a storm can induce local
3 errors in salinity, temperature and currents. In the tropical band, precipitations are
4 systematically overestimated. Moreover, large scale salinity biases can appear because the
5 global average freshwater budget is not closed. For this reason, IFS ECMWF atmospheric
6 analysed and forecasted precipitations have been corrected at large scale using satellite-based
7 PMWC product. This correction is beneficial in many areas, reducing the magnitude of the
8 near-surface salinity fresh mean bias in the Tropics down to 0.5 psu. This surface fresh bias
9 reduction in the Tropics reaches 0.15 psu in average.

10 Due to ~~misun~~resolved processes ~~es and inaccurate atmospheric forcing~~, the model may also drift
11 at depth. To keep some water mass properties, the DRAKKAR group used restoring of
12 temperature and salinity toward annual climatology of Gouretski and Koltermann (2004) in
13 specific areas. This choice was driven by the Antarctic Bottom Water restoring zone where
14 this climatology is recognized as the more suitable. For Mercator systems which assimilate
15 observations in a multivariate way, the problem can be more critical because of the
16 deficiencies of the background errors for extrapolated and/or poorly observed variables. To
17 overcome these deficiencies, vertical climatological T/S profiles have been assimilated below
18 2000 m using a non-Gaussian error at depth, allowing the system to capture a potential
19 climate drift in the deep ocean. In practice, the assimilation of climatological profiles below
20 2000 m in the system PSY4V3 concerns mostly some regions where the steep bathymetry
21 might be an issue for the model (Kerguelen Plateau, Zapiola Ridge, and Atlantic ridge). This
22 kind of assimilation reduces drifts below 2000 m and impacts the vertical repartition of the
23 steric height, without degrading the quality of the results comparing with the profiles from the
24 Argo network.

25 We have also proposed solutions to reduce some problems related to linearity and stationarity
26 hypotheses in the assimilation schemes. The first one concerns the construction of the
27 ~~background~~~~forecast~~ error covariance. Rather than calculating the anomalies from a free
28 simulation, we chose to calculate them from a simulation benefiting only of the 3D-VAR
29 large-scale biases correction in temperature and salinity and representing better the density
30 fronts on the horizontal and on the vertical. Moreover, anomalies have been filtered in order
31 to remove the scales beyond the effective resolution of the model. The second one concerns
32 the tuning of the observations errors. Adaptive tuning of SLA and SST errors has been

1 successfully implemented. It allows us to have more realistic and evolutive SLA and SST
2 error maps.

3 All these scientific and technical choices have been validated and integrated in the system
4 PSY4V3 which has been evaluated for the period 2007-2016 by means of a thorough
5 procedure involving statistics of model departures from observations. The system PSY4V3 is
6 close to SLA along track observations with a forecast (range 1 to 7 days) RMS difference
7 below 6 cm. Moreover, the correlation of the system PSY4V3 with tide gauges is significant
8 at all frequencies, however many high frequency fluctuations of the SSH might not be
9 captured by the system because tides or pressure effects are not yet included. The description
10 of the ocean water masses is very accurate on average and departures from in situ
11 observations rarely exceed 0.5 °C and 0.1 psu. In the thermocline, RMS errors reach 1 °C and
12 0.2 psu. In high variability regions like the Gulf Stream, the Agulhas Current or the Eastern
13 Tropical Pacific, RMS errors reach more than 2 °C and 0.5 psu locally. A warm bias persists
14 in subsurface, with peaks in high variability regions such as the Eastern Tropical Pacific, Gulf
15 Stream or Zapiola. Most departures from observed SST products do not exceed the intrinsic
16 error of these products (around 0.6 °C).

17 A global comparison with independent velocity measurements (surface drifters) shows that
18 the location of the main currents is very well represented, as well as their variability.
19 However, surface currents of the mid latitudes are underestimated on average. The
20 underestimation ranges from 20 % in strong currents to 60 % in weak currents. Some
21 equatorial currents are overestimated, and the western tropical Pacific still suffer from biases
22 in surface currents related to MDT biases. On the contrary the orientation of the current
23 vectors is better represented.

24 Lastly, the system reproduces the sea ice seasonal cycle in a realistic manner. However,
25 ~~compared to assimilated data, the~~ sea ice concentrations ~~is slightly~~are overestimated in ~~the~~
26 ~~Arctic mainly during winter seasons (due to atmospheric forcing errors and too much sea ice~~
27 ~~accumulation) and in the Antarctic during austral winter. They are and~~ underestimated during
28 ~~austral~~ summer ~~seasons(too much sea ice melt and errors caused by the rheology~~
29 ~~parameterization of the sea ice model).~~ A contingency table analysis approach has been also
30 used to evaluate sea ice extent as compared to observations. This approach shows clear
31 improvements due to the assimilation of sea ice concentration in the system PSY4V3.

32 Remarkable improvements have been achieved with the system PSY4V3 compared to the
33 previous version. However, some biases have been highlighted in the ocean surface features

1 as well as the three-dimensional~~3D~~ ocean structure at basin, sub-basin and local scales. The
2 simulation biases may be due to the initial state (especially in the deep layer where historical
3 observation data are rare), the atmospheric forcing uncertainties, the river runoff
4 approximations, the efficiency of the assimilation scheme, and the model errors induced by
5 unresolved or parameterized physical processes. Numerous projects have already been set up
6 at Mercator Ocean to propose innovative solutions. The integration of the ingredients from
7 these projects into the future CMEMS global high resolution system is planned for 2019. The
8 improvement of numerical simulations could thus be carried out, based on sensitivity ~~tests~~
9 experiments on some model parameters (e.g. coastal runoffs, atmospheric forcing, high
10 frequency phenomena including tides, ~~more sophisticated~~multi-category sea ice model,
11 interaction and retroaction between ocean currents and waves, vertical mixing and advection
12 scheme). Better algorithms and more sophisticated parameterizations already available in the
13 version 3.6 of the NEMO code should help in the future to resolve issues related to important
14 ocean processes and to reduce model biases. It is also planned to assimilate new types of
15 observations in the system (drifting buoys SST, higher resolution SST (L3 products), satellite
16 sea surface salinity, velocity observations from AOML surface drifters, and deep-ocean
17 observations from Argo surface floats) to better constrain the modeled variables and to
18 overcome the deficiencies of the background errors in particular for extrapolated and/or
19 poorly observed variables. Another important issue is to use a shorter assimilation time
20 window and a 4D analysis in the assimilation scheme to better correct the fast evolving
21 processes. The next version of the global high resolution system will also include seasonal
22 errors for in situ vertical profiles already used in the CMEMS eddy-resolving 1992-2016
23 reanalysis GLORYS at 1/12° horizontal resolution, which is based on the system PSY4V3
24 and ~~will~~appeared on CMEMS catalogue in April 2018.

25 26 Acknowledgements

27 This study has been conducted using E.U. Copernicus Marine Service Information. The
28 authors thank Luc Vandenbulcke and the anonymous reviewer for their careful reading and
29 for providing very constructive comments which improved the manuscript. Special thanks to
30 our Mercator Océan colleague Jérôme Chanut for his help to answer to the questions
31 regarding the specifics of the NEMO code.

1 **References**

- 2 Amante, C. and Eakins, B. W.: ETOPO1 1 Arc-minute global relief model: procedures, data
3 sources and analysis, NOAA Technical Memorandum NESDIS NGDC-24, 25 pp., 2009.
- 4 Arakawa, A. and Lamb, V. R.: A potential enstrophy and energy conserving scheme for the
5 shallow water equations, *Mon. Weather. Rev.*, 109, 18–36, 1981.
- 6 [Artana, C., Lellouche, J-M., Park, Y-H., Garric, G., Koenig, Z., Sennéchaël, N., Ferrari, R.,
7 Piola, A.R., Saraceno, M., and Provost, C.: Fronts of the Malvinas Current System: surface
8 and subsurface expressions revealed by satellite altimetry, Argo floats, and Mercator
9 operational model outputs, *J. Geophys. Res. Oceans*, doi: 10.1029/2018JC013887, 2018.](#)
- 10
- 11 Barnier, B., Madec, G., Penduff, T., Molines, J. M., Treguier, A. M., Le Sommer, J.,
12 Beckmann, A., Biastoch, A., Böning, C., Dengg, J., Derval, C., Durand, E., Gulev, S., Remy,
13 E., Talandier, C., Theetten, S., Maltrud, M., McClean, J., and De Cuevas, B.: Impact of partial
14 steps and momentum advection schemes in a global circulation model at eddy permitting
15 resolution, *Ocean Dynam.*, 56, 543-567, 2006.
- 16 Becker, J. J., Sandwell, D. T., Smith, W. H. F., Braud, J., Binder, B., Depner, J., Fabre, D.,
17 Factor, J., Ingalls, S., Kim, S.H., Ladner, R., Marks, K., Nelson, S., Pharaoh, A., Trimmer, R.,
18 Von Rosenberg, J., Wallace, G., and Weatherall, P.: Global Bathymetry and Elevation Data at
19 30 Arc Seconds Resolution: SRTM30_PLUS, *Mar. Geod.*, 32, 355-371, doi:
20 10.1080/01490410903297766, 2009.
- 21 [Benkiran, M. and Greiner, E.: Impact of the Incremental Analysis Updates on a Real-Time
22 System of the North Atlantic Ocean, *J. Atmos. Ocean. Tech.*, 25, 2055-2073, 2008.](#)
- 23 Bidlot, J.-R.: Impact of ocean surface currents on the ECMWF forecasting system for
24 atmosphere circulation and ocean waves, GlobCurrent Preliminary User Consultation
25 Meeting, <http://globcurrent.ifremer.fr/component/k2/itemlist/category/118?Itemid=960>,
26 Brest, 7-9 March 2012.
- 27 Blanke, B. and Delecluse, P.: Variability of the tropical Atlantic-Ocean simulated by a
28 general-circulation model with 2 different mixed-layer physics, *J. Phys. Oceanogr.*, 23, 1363-
29 1388, 1993.

1 Brodeau, L., Barnier, B., Treguier, A.M., Penduff, T., and Gulev S.: An ERA40-based
2 atmospheric forcing for global ocean circulation models, *Ocean Modelling*, 31, issues 3-4, 88-
3 104, doi: 10.1016/j.ocemod.2009.10.005, 2010.

4 Bruinsma, S., Lemoine, J.-M., Biancale, R., and Vales, N.: CNES/GRGS 10-day gravity field
5 models (release 02) and their evaluation, *Adv. Space Res.*, 45, 4, 587-601, doi:
6 10.1016/j.asr.2009.10.012, 2010.

7 Chambers, D. P., Cazenave, A., Champollion, N., Dieng, H., Llovel, W., Forsberg, R., von
8 Schuckmann, K., and Wada, Y.: Evaluation of the global mean sea level budget between 1993
9 and 2014, *Surv. Geophys.*, 38, no. 1, 309-327, doi:10.1007/s10712-016-9381-3, 2017.

10 Chelton, D. B., Wentz, F. J., Gentemann, C. L., De Szoeki, R. A., and Schlax, M. G.:
11 Satellite microwave SST observations of transequatorial tropical instability waves, *Geophys.*
12 *Res. Lett.*, 27, 1239-1242, 2000.

13 Chen, J. L., Wilson, C. R., Tapley, B. D., Famiglietti, J. S., and Rodell, M.: Seasonal global
14 mean sea level change from satellite altimeter, GRACE, and geophysical models, *J. Geodesy*,
15 79, 532-539, doi:10.1007/s00190-005-0005-9, 2005.

16 Chevallier, M., G.C. Smith, J.-F. Lemieux, F. Dupont, G. Forget, Y. Fujii, F. Hernandez, R.
17 Msadek, K. A. Peterson, A. Storto, T. Toyoda, M. Valdivieso, G. Vernieres, H. Zuo, M.
18 Balmaseda, Y.-S. Chang, N. Ferry, G. Garric, K. Haines, S. Keeley, R. M. Kovach, T.
19 Kuragano, S. Masina, Y. Tang, H. Tsujino, X. Wang: Intercomparison of the Arctic sea ice
20 cover in global ocean-sea ice reanalyses from the ORA-IP project, *Clim. Dyn.*, 49: 1107,
21 <https://doi.org/10.1007/s00382-016-2985-y>, 2017.

22 Church, J. A., Clark, P. U., Cazenave, A., Gregory, J.-M., Jevrejeva, S., Levermann, A.,
23 Merrifield, M. A., Milne, G. A., Nerem, R. S., Nunn, P. D., Payne, A. J., Pfeffer, W. T.,
24 Stammer, D., and Unnikrishnan, A. S.: Sea Level Change. In: *Climate Change 2013: The*
25 *Physical Science Basis. Contribution of Working Group I to the Fifth Assessment Report of*
26 *the Intergovernmental Panel on Climate Change* [Stocker, T.F., D. Qin, G.-K. Plattner, M.
27 Tignor, S.K. Allen, J. Boschung, A. Nauels, Y. Xia, V. Bex and P.M. Midgley (eds.)].
28 Cambridge University Press, Cambridge, United Kingdom and New York, NY, USA, 2013.

29 Cravatte, S., Madec, G., Izumo, T., Menkes, C., and Bozec, A.: Progress in the 3D circulation
30 of the eastern equatorial Pacific in a climate, *Ocean Model.*, 17, 28-48, 2007.

1 Dai, A. and Trenberth, K. E.: Estimates of freshwater discharge from continents: latitudinal
2 and seasonal variations, *J. Hydrometeorol.*, 3, 660–687, 2002.

3 Dai A., Qian, T., Trenberth, K., and Milliman, J. D.: Changes in Continental Freshwater
4 Discharge from 1948 to 2004, *J. Climate*, vol. 22, p.2773-2792, 2009.

5 Dee, D. P., and Coauthors: The ERA-interim reanalysis: Configuration and performance of
6 the data assimilation system, *Quart. J. Roy. Meteor. Soc.*, 137, 553–597,
7 doi:<https://doi.org/10.1002/qj.828>, 2011.

8 [De Lavergne C., Madec, G., Le Sommer, J., Nurser, A. G., and Naveira-Garabato, A. C.: On](#)
9 [the consumption of Antarctic Bottom Water in the abyssal ocean, *J. Phys. Oceanogr.*, 46,](#)
10 [635–651, doi:10.1175/JPO-D-14-0201.1, 2016.](#)

11 Desroziers, G., Berre, L., Chapnik, B., and Polli, P.: Diagnosis of observation, background
12 and analysis-error statistics in observation space, *Q. J. R. Meteorol. Soc.*, 131, 3385–3396,
13 doi: 10.1256/qj.05.108, 2005.

14 Drevillon, M., Greiner, E., Paradis, D., Payan, C., Lellouche, J.M., Reffray, G., Durand, E.,
15 Law-Chune, S., and Cailleau, S.: A strategy for producing refined currents in the Equatorial
16 Atlantic in the context of the search of the AF447 wreckage. *Ocean Dynamics*, 63, 63-82,
17 DOI 10.1007/s10236-012-0580-2, 2013.

18 Drillet, Y., Lellouche, J.-M., Levier, B., Drevillon, M., Le Galloudec, O., Reffray, G.,
19 Regnier, C., Greiner, E., and Clavier, M.: Forecasting the mixed layer depth in the north east
20 Atlantic: an ensemble approach, with uncertainties based on data from operational oceanic
21 systems *Ocean Sci. Discuss.*, 11, 1435-1472, [http://www.ocean-sci-](http://www.ocean-sci-discuss.net/11/1435/2014/osd-11-1435-2014.html)
22 [discuss.net/11/1435/2014/osd-11-1435-2014.html](http://www.ocean-sci-discuss.net/11/1435/2014/osd-11-1435-2014.html), 2014.

23 Estournel, C., Testor, P., Damien, P., D’ortenzio, F., Marsaleix, P., Conan, P., Kessouri, F.,
24 Durrieu de Madron, X., Coppola, L., Lellouche, J.-M., Belamari, S., Mortier, L., Ulses, C.,
25 Bouin, M.-N., and Prieur, L.: High resolution modeling of dense water formation in the north-
26 western Mediterranean during winter 2012-2013: Processes and budget, *J. Geophys. Res.*,
27 Wiley-Blackwell, 121 (7), 5367-5392, DOI:10.1002/2016JC011935, 2016.

28 Fichet, T. and Maqueda, M. A.: Sensitivity of a global sea ice model to the treatment of ice
29 thermodynamics and dynamics, *J. Geophys. Res.*, 102, 12609-12646, 1997.

1 Good, S.A., Martin, M.J., and Rayner, N.A.: EN4: quality controlled ocean temperature and
2 salinity profiles and monthly objective analyses with uncertainty estimates, *J. Geophys. Res.*,
3 118, 6704-6716, doi:10.1002/2013JC009067, 2013.

4 Grasso, L. D.: The differentiation between grid spacing and resolution and their application to
5 numerical modelling, *B. Am. Meteor. Soc.*, 81, 579-580, 2000.

6 Greiner, E., Benkiran, M., Blayo, E., and Dibarboue, G.: MERA-11 general scientific paper,
7 1992-2002 PSY1V2 reanalysis, reference MOO-MR-431-37-MER Mercator-Ocean,
8 Toulouse, France, 71 pp., 2006.

9 Grodsky, S. A., Lumpkin, R., and Carton, J. A.: Spurious trends in global surface drifter
10 currents, *Geophys. Res. Lett.*, 38, L10606, doi: 10.1029/2011GL047393, 2011.

11 Hilburn, K.: The passive microwave water cycle product, Remote Sensing Systems (REMSS)
12 Technical Report 072409, Santa Rosa (CA), 30 pp., 2009.

13 Hilburn, K., Smith D.K., and Mears C. A.: Annual Validation report: Rain, Remote Sensing
14 Systems, www.remss.com, 2014.

15 Hoaglin D., Mosteller F., and Tukey J. W.: Understanding Robust and Exploratory Data
16 Analysis, Wiley Series in probability and mathematical statistics, New-York, 1983.

17 Janowiak, J. E., Gruber, A., Kondragunta, C. R., Livezey, R.E., and Huffman G.J.: A
18 comparison of the NCEP-NCAR reanalysis precipitation and the GPCP rain gauge-satellite
19 combined dataset with observational error considerations, *J. of Climate*, vol. 11, 2960-2979,
20 1998.

21 Janowiak, J. E., Bauer, P., Wang, W., Arkin, P. A., and Gottschalck, J.: An evaluation of
22 precipitation forecasts from operational models and reanalysis including precipitations
23 variations associated with MJO activity, *Monthly weather Review*, 138, p. 4542-4560, 2010.

24 Juza, M., Mourre, B., Lellouche, J.-M., Tonani, M., and Tintore, J.: From basin to sub-basin
25 scale assessment and intercomparison of numerical simulations in the Western Mediterranean
26 Sea, *Journal of Marine Systems*, 149, 36–49, <http://dx.doi.org/10.1016/j.jmarsys.2015.04.010>,
27 2015.

28 [Gasparin, F., Greiner, E., Lellouche, J.-M., Legalloudec, O., Garric, G., Drillet, Y., Bourdalle-](#)
29 [Badie, R., Le Traon, P.-Y., Remy, E., and Drevillon, M.: A large-scale view of oceanic](#)
30 [variability from 2007 to 2015 in the global high resolution monitoring and forecasting system](#)
31 [at Mercator-Ocean, In revision in Journal of Marine Systems, 2018.](#)

1 [Global Sea-Level Observing System \(GLOSS\) Implementation Plan - 2012, UNESCO/IOC](#)
2 [Technical Series No.100, 41 pp., 2012.](#)

3 Gouretski, V. V. and Koltermann, K. P.: Woce global hydrographic climatology. Technical
4 Report 35/2004, Berichte des Bundesamtes fur Seeschiffahrt und Hydrographie, 2004.

5 Jackett, D. R. and Mcdougall, T. J.: Minimal Adjustment of Hydrographic Profiles to Achieve
6 Static Stability, J. Atmos. Oceanic Technol., 12, 381–389, [https://doi.org/10.1175/1520-](https://doi.org/10.1175/1520-0426(1995)012<0381:MAOHPT>2.0.CO;2)
7 [0426\(1995\)012<0381:MAOHPT>2.0.CO;2](https://doi.org/10.1175/1520-0426(1995)012<0381:MAOHPT>2.0.CO;2), 1995.

8 Kidd, C., Dawkins, E., and Huffman, G.: Comparison of Precipitation Derived from the
9 ECMWF Operational Forecast Model and Satellite Precipitation Datasets, Journal of
10 Hydrometeorology, 14 (5), p. 1463-1482, <https://doi.org/10.1175/JHM-D-12-0182.1>, 2013.

11 Kjerfve, B.: Tides of the Caribbean Sea, J. Geophys. Res., 86(C5), 4243-4247,
12 doi:10.1029/JC086iC05p04243, 1981.

13 Koch-Larrouy, A., Madec, G., Blanke, B., and Molcard, R.: Water mass transformation along
14 the Indonesian throughflow in an OGCM, Ocean Dynam., 58, 289-309, doi:10.1007/s10236-
15 008-0155-4, 2008.

16 Koenig, Z., Provost, C., Villaciers-Robineau, N., Sennechael, N., Meyer, A., Lellouche, J.-
17 M., and Garric, G.: Atlantic waters inflow north of Svalbard: Insights from IAOOS
18 observations and Mercator Ocean global operational system during N-ICE2015, J. Geophys.
19 Res. Oceans, 122, 1254–1273, doi:10.1002/2016JC012424, 2017.

20 Lagerloef, G., Schmitt, R., Schanze, J., and Kao, H. Y.: The Ocean and the global water cycle,
21 Oceanography, 23(4), 82-93, <http://dx.doi.org/10.5670/oceanog.2010.07>, 2010.

22 Large, W. G. and Yeager, S. G.: The global climatology of an interannually varying air–sea
23 flux data set, Clim. Dynam., 33, 341-364, doi:10.1007/s00382-008-0441-3, 2009.

24 [Lefevre, F., Sénant, E., et al. : BaDoMar: a tide gauge database used for altimeter calibration,](#)
25 [Workshop on Sea Level Variations Towards an Operational European Sea Level Service,](#)
26 [page 63, 2005.](#)

27 Lellouche, J.-M., Le Galloudec, O., Drevillon, M., Regnier, C., Greiner, E., Garric, G., Ferry,
28 N., Desportes, C., Testut, C.-E., Bricaud, C., Bourdalle-Badie, R., Tranchant, B., Benkiran,
29 M., Drillet, Y., Daudin, A., and De Nicola, C.: Evaluation of global monitoring and
30 forecasting systems at Mercator Ocean, Ocean Sci., 9, 57-81, doi:10.5194/os-9-57-2013,
31 2013.

1 Lengaigne, M., Menkes, C., Aumont, O., Gorgues, T., Bopp, L., Andre, J.M., and Madec, G.:
2 Influence of the oceanic biology on the tropical Pacific climate in a coupled general
3 circulation model, *Clim. Dyn.*, 28, 503-507, DOI:10.1007/s00382-006-0200-2, 2007.

4 Levy, M., Estublier, A., and Madec, G.: Choice of an advection scheme for biogeochemical
5 models, *Geophys. Res. Lett.*, 28, 3725–3728, doi:10.1029/2001GL012947, 2001.

6 Locarnini, R. A., Mishonov, A. V., Antonov, J. I., Boyer, T. P., Garcia, H. E., Baranova, O.
7 K., Zweng, M. M., Paver, C. R., Reagan, J. R., Johnson, D. R., Hamilton, M., and Seidov,
8 D.: *World Ocean Atlas 2013, Volume 1: Temperature*. S. Levitus, Ed., A. Mishonov
9 Technical Ed.; NOAA Atlas NESDIS 73, 40 pp., 2013.

10 Madec, G. and Imbard M.: A global ocean mesh to overcome the North Pole singularity,
11 *Clim. Dynam.*, 12, 381-388, 1996.

12 Madec, G., and the NEMO team: NEMO ocean engine. Note du Pôle de modélisation, Institut
13 Pierre-Simon Laplace (IPSL), France, No. 27 ISSN, 1288-1619, 2008.

14 [Marchesiello, P., Debreu, L., and Coulevar, X.: Spurious diapycnal mixing in terrain-](#)
15 [following coordinate models: The problem and a solution, *Ocean Modelling*, 26 \(3-4\), 156-](#)
16 [169, 2009.](#)

17

18 Menemenlis, D., Fukumori, I., and Lee, T.: Atlantic to Mediterranean Sea level difference
19 driven by winds near Gibraltar Strait, *J. Phys. Oceanogr.*, 37, 359–376, 2007.

20 Pujol, M.-I., Faugère, Y., Taburet, G., Dupuy, S., Pelloquin, C., Ablain, M., and Picot, N.:
21 DUACS DT2014: the new multi-mission altimeter data set reprocessed over 20 years,
22 *Ocean Sci.*, 12, 1067-1090, doi:10.5194/os-12-1067-2016, 2016.

23 Raynaud, L., Berre, L., and Desroziers, G.: Objective filtering of ensemble-based
24 background-error variances, *Quarterly Journal of the Royal Meteorology Society*, Vol. 135,
25 Issue 642, 1177–1199, 2009.

26 Renault, L., Molemaker, M. J., McWilliams, J. C., Shchepetkin, A. F., Lemarie, F., Chelton,
27 D., Illig, S., and Hall A.: Modulation of wind work by oceanic current interaction with the
28 atmosphere, *Journal of Physical Oceanography*, 46 (6), 1685-1704, ISSN 0022-3670, 2016.

1 Rio, M. H., Guinehut, S., and Larnicol, G.: New CNES-CLS09 global mean dynamic
2 topography computed from the combination of GRACE data, altimetry, and in situ
3 measurements, *J. Geophys. Res.*, 116, C07018, doi:10.1029/2010JC006505, 2011.

4 Rio, M.H.: Use of altimeter and wind data to detect the anomalous loss of SVP-type drifter's
5 drogue, *Journal of Atmospheric and Oceanic Technology*, DOI:10.1175/JTECH-D-12-
6 00008.1, 2012.

7 Rio, M.-H., Mulet, S., and Picot, N.: Beyond GOCE for the ocean circulation estimate:
8 Synergetic use of altimetry, gravimetry, and in situ data provides new insight into geostrophic
9 and Ekman currents, *Geophys. Res. Lett.*, 41, doi:10.1002/2014GL061773, 2014.

10 [Rio M.-H. and Etienne H.: For Global Ocean Delayed Mode in-situ Observations of Ocean](http://doi.org/10.13155/41256)
11 [Surface Currents, Copernicus Quality Information Document CMEMS-INS-QUID-013-044,](http://doi.org/10.13155/41256)
12 [http://doi.org/10.13155/41256, 2017.](http://doi.org/10.13155/41256)

13 Roemmich, D. and Gilson, J.: The 2004–2008 mean and annual cycle of temperature, salinity,
14 and steric height in the global ocean from the Argo Program, *Progress in Oceanography*,
15 Volume 82, Issue 2, 81–100, <https://doi.org/10.1016/j.pocean.2009.03.004>, 2009.

16 Roquet, F., Charrassin, J. B., Marchand, S., Boehme, L., Fedak, M., Reverdin, G., and Guinet,
17 C.: Delayed-mode calibration of hydrographic data obtained from animal-borne satellite relay
18 data loggers, *J. Atmos. Ocean. Tech.*, 28, 787–801, 2011.

19 Roulet, G. and Madec, G.: Salt conservation, free surface, and varying levels: a new
20 formulation for ocean general circulation models, *J. Geophys. Res.*, 105, 23927–23942, 2000.

21 Schweiger, A., Lindsay, R., Zhang, J., Steele, M., and Stern, H.: Uncertainty in modeled
22 arctic sea ice volume, *J. Geophys. Res.*, doi:10.1029/2011JC007084, 2011.

23 Scott, R., Ferry, N., Drevillon, M., Barron, C.N., Jourdain, N.C., Lellouche, J.-M., Metzger,
24 E. J., Rio, M. H., and Smedstad, O. M.: Estimates of surface drifter trajectories in the
25 Equatorial Atlantic: a multi-model ensemble approach. *Ocean Dynamics*, 62, 1091-1109. doi
26 10.1007/s10236-012-0548-2, 2012.

27 Silva, T. A. M., Bigg, G. R., and Nicholls, K. W.: Contribution of giant icebergs to the
28 Southern Ocean freshwater flux, *J. Geophys. Res.*, 111, C03004, doi:10.1029/2004JC002843,
29 2006.

30 Smith, G.C., Roy, F., Reszka, M., Surcel Colan, D., He, Z., Deacu, D., Belanger, J.-M.,
31 Skachko, S., Liu, Y., Dupont, F., Lemieux, J-F., Beaudoin, C., Tranchant, B., Drevillon, M.,

1 Garric, G., Testut, C.-E., Lellouche, J.-M., Pellerin, P., Ritchie, H., Lu, Y., Davidson, F.,
2 Buehner, M., Caya, A., and Lajoie, M.: Sea ice forecast verification in the Canadian Global
3 Ice Ocean Prediction System, Quarterly Journal of the Royal Meteorology Society, Vol.142,
4 Issue 695, Pages 659–671, 2016.

5 Song, Y. T.: Estimation of interbasin transport using ocean bottom pressure: Theory and
6 model for Asian marginal seas, J. Geophys. Res., 111, C11S19, doi:10.1029/2005JC003189,
7 2006.

8 [Stephens, G. L., L'Ecuyer, T., Forbes, R., Gettleman, A., Golaz, J.C., Bodas-Salcedo, A.,](#)
9 [Suzuki, K., Gabriel, P., and J. Haynes, J.: Dreary state of precipitation in global models, J.](#)
10 [Geophys. Res., 115, D24211, doi:10.1029/2010JD014532, 2010.](#)

11

12 Storto, A., Russo, I., and Masina, S.: Interannual response of global ocean hindcasts to a
13 satellite-based correction of precipitation fluxes, Ocean Sci. Discuss.,
14 <https://doi.org/10.5194/osd-9-611-2012>, 2012.

15 Szekely, T., Gourrion, J., Pouliquen, S., and Reverdin, G.: CORA, Coriolis Ocean Dataset for
16 Reanalysis. SEANOE doi:<http://doi.org/10.17882/46219>, 2016.

17 Talagrand, O.: A posteriori evaluation and verification of analysis and assimilation
18 algorithms, Proc. of ECMWF Workshop on Diagnosis of Data Assimilation System
19 (Reading), 17–28, 1998.

20 Tranchant, B., Reffray, G., Greiner, E., Nugroho, D., Koch-Larrouy, A., and Gaspar, P.:
21 Evaluation of an operational ocean model configuration at 1/12° spatial resolution for the
22 Indonesian seas (NEMO2.3/INDO12) – Part 1: Ocean physics, Geosci. Model Dev., 9, 1037-
23 1064, 2016.

24 Troccoli, A. and P. Kallberg, P.: Precipitation correction in the ERA-40 reanalysis, ERA-40
25 Project Report Series N°13, 1-10, 2004.

26 Vinogradov, S.V. and Ponte R.M.: Low frequency variability in coastal sea level from tide
27 gauges and altimetry, J. Geophys. Res., 116, C07006, doi:10.1029/2011JC007034, 2011.

28 Willebrand, J. , Barnier, B. , Böning, C. , Dieterich, C. , Killworth, P. D. , Le Provost, C. , Jia,
29 Y., Molines, J. M., and New, A. L.: Circulation characteristics in three eddy-permitting
30 models of the North Atlantic, Progress in Oceanography, 48(2), 123-161, 2001.

1 Williams, J. and Hughes, C.W.: The coherence of small island sea level with the wider ocean:
2 a model study, *Ocean Sci.*, 9, 111-119, 2013.

3 [Winton, M., Hallberg, R. and A. Gnanadesikan, A.: Simulation of Density-Driven Frictional](#)
4 [Downslope Flow in Z-Coordinate Ocean Models, *J. Phys. Oceanogr.*, 28, 2163-2174, 1998.](#)

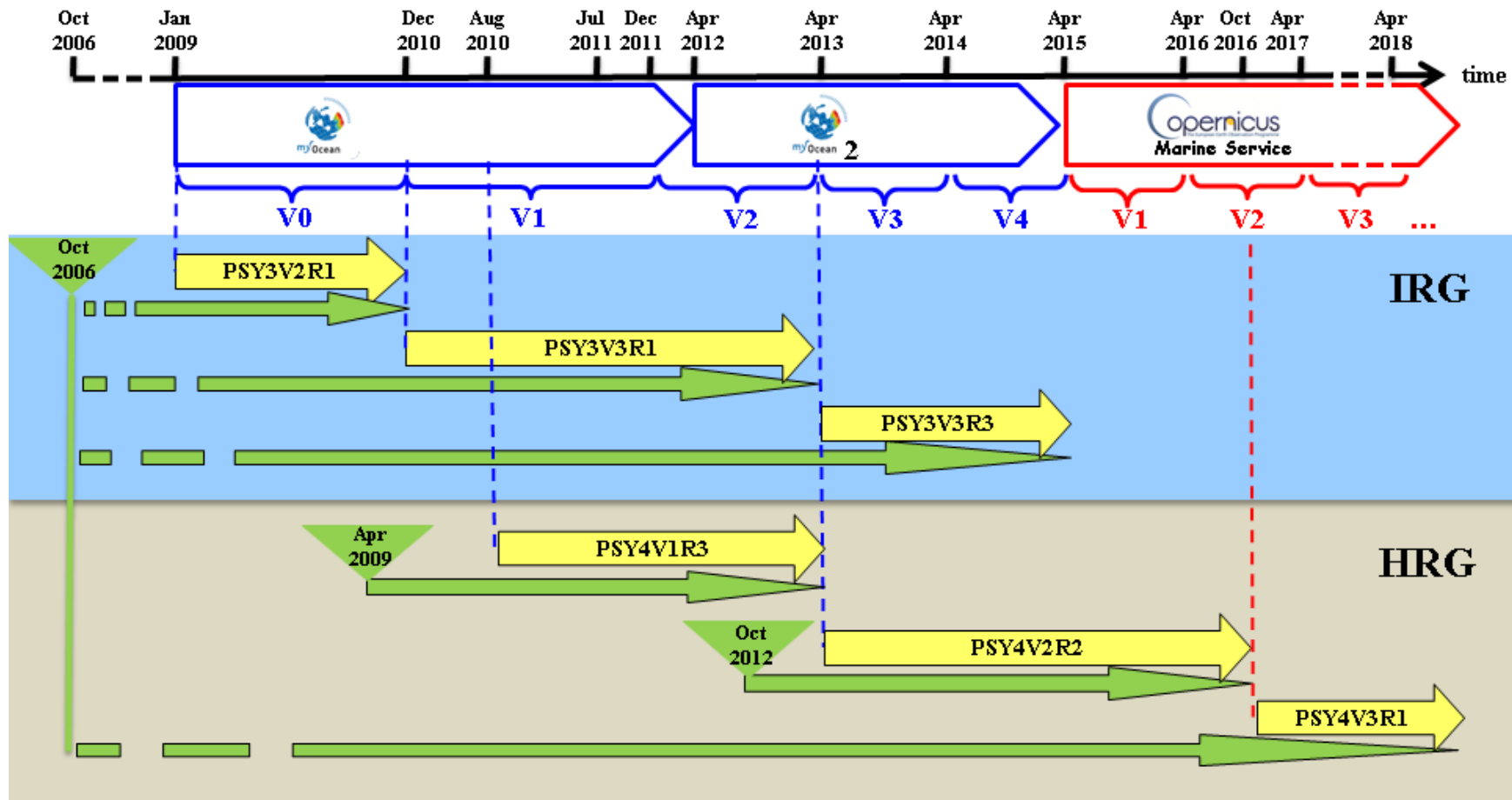
5

6 Zweng, M. M., Reagan, J. R., Antonov, J. I., Locarnini, R. A., Mishonov, A., Boyer, T. P.,
7 Garcia, H. E., Baranova, O. K., Paver, C. R., Johnson, D. R., Seidov, D., and Biddle, M.:
8 World Ocean Atlas 2013, Volume 2: Salinity. S. Levitus, Ed., A. Mishonov, Technical
9 Ed.; NOAA Atlas NESDIS 74, 40 pp., 2013.

10 Zyguntowska, M., Rampal, P., Ivanova, N., and Smedsrud, L. H.: Uncertainties in Arctic sea
11 ice thickness and volume: new estimates and implications for trends, *The Cryosphere*, 8, 705-
12 720, <https://doi.org/10.5194/tc-8-705-2014>, 2014.

13

1



2

3

4

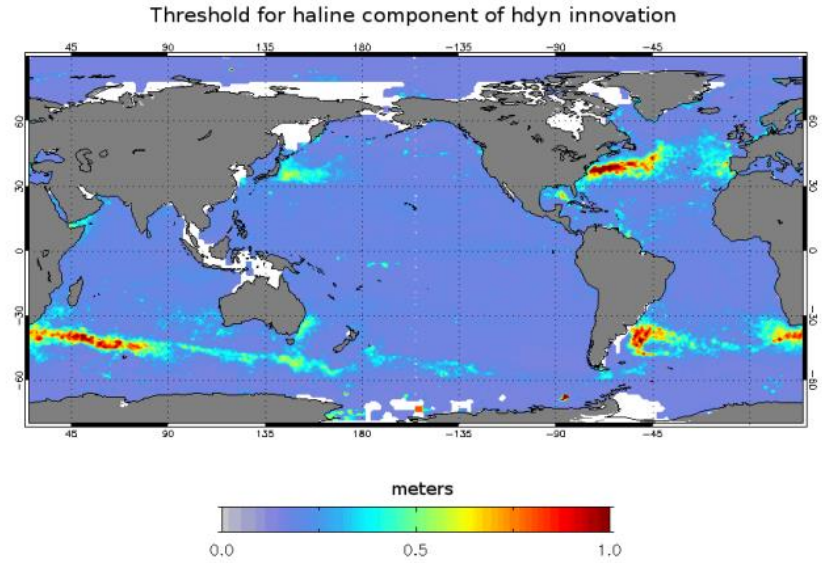
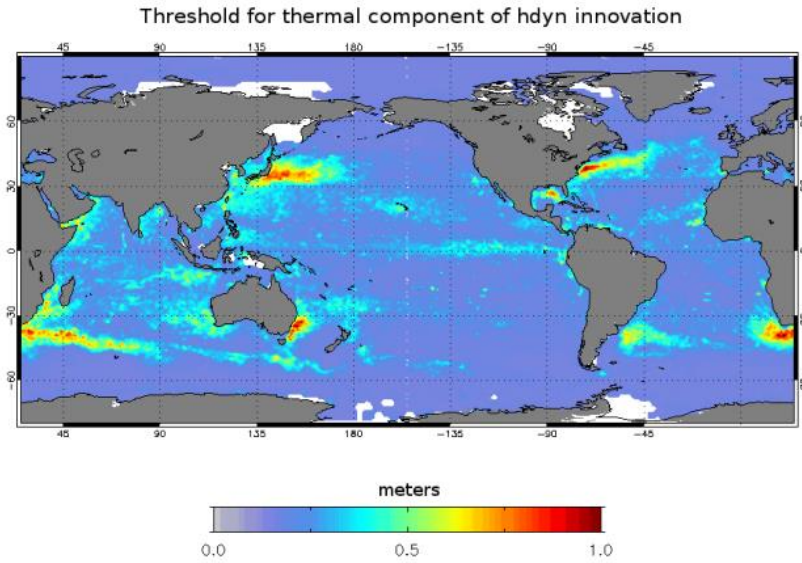
5

6

7

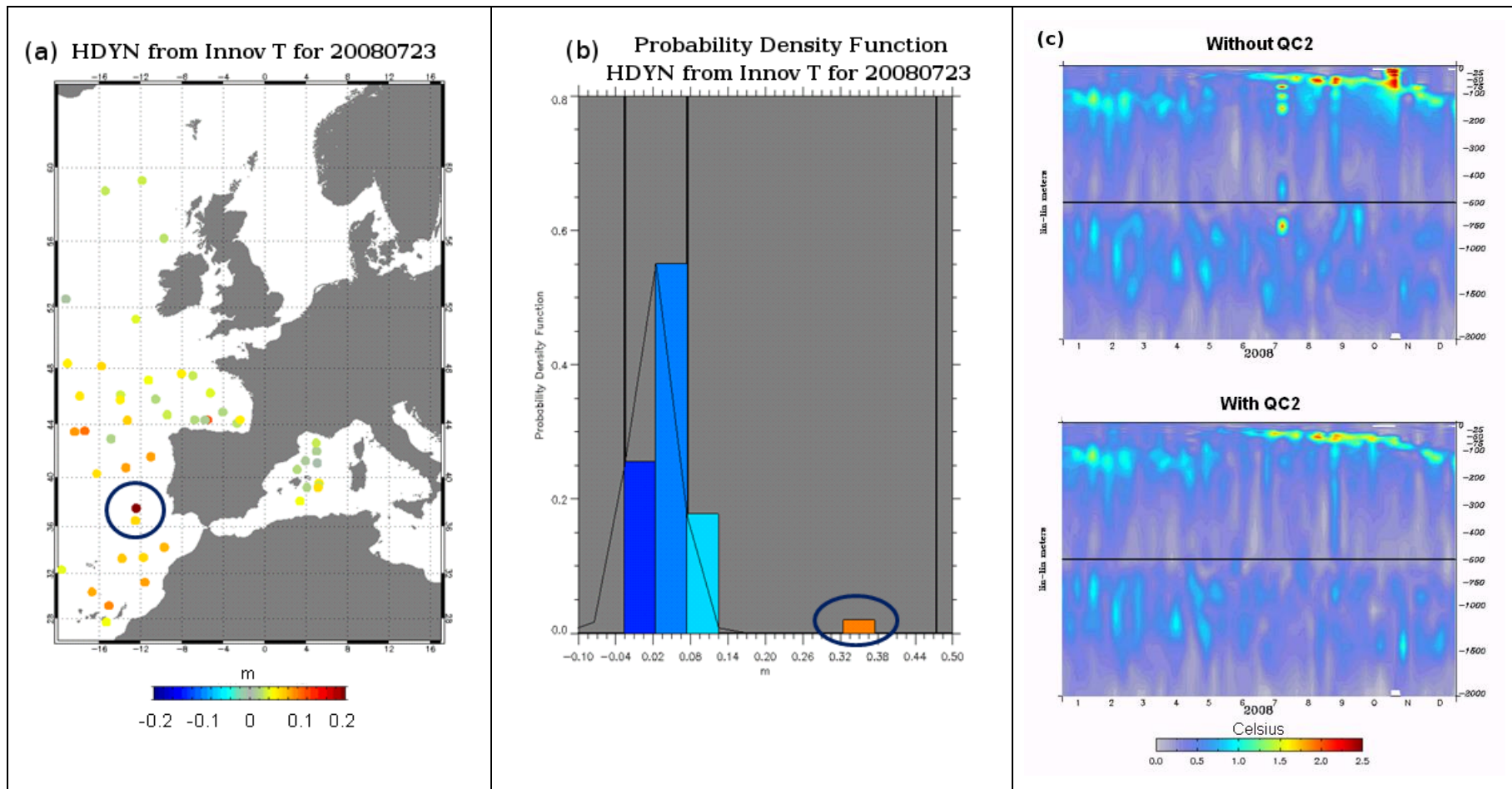
8

Figure 1: Timeline of the Mercator Ocean global analysis and forecasting systems for the various milestones (from V0 to V4) of past MyOcean project and for milestones V1, V2, V3 of the current CMEMS. Real-time productions are in yellow with the reference of the Mercator Ocean system. Available Mercator Ocean simulations are in green including the catch-up to real-time. Global Intermediate Resolution (respectively High Resolution) systems at 1/4° (respectively 1/12°) are referred to as IRG (respectively HRG). Milestones are written in blue for MyOcean project and in red for CMEMS.



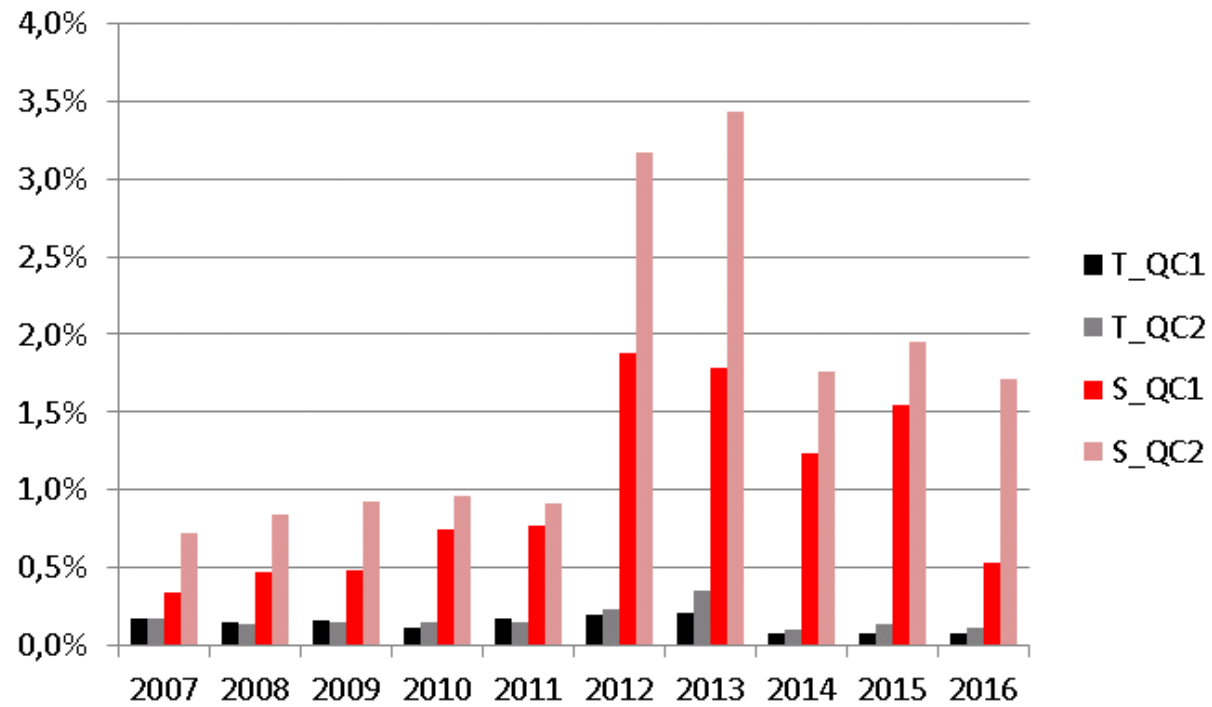
1
2
3
4

Figure 2: Thresholds used for QC2 for thermal component of dynamical height innovation (left panel: $threshold_T$) and for haline component of dynamical height innovation (right panel: $threshold_S$). Units are meters.



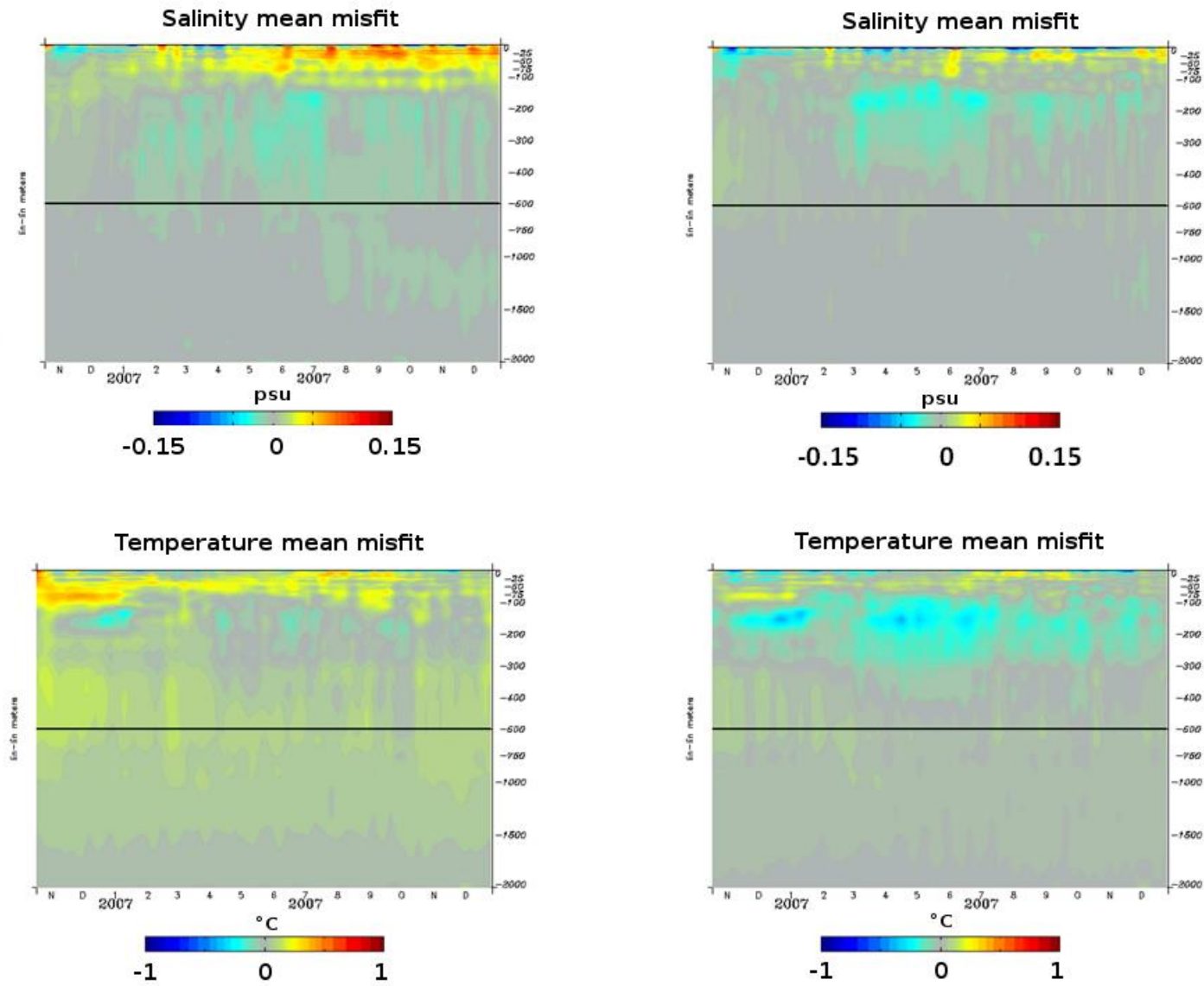
1

2 **Figure 3:** Statistics in the Azores region: a) absolute value of dynamical height innovations (in meters) from temperature innovations for the 7-day assimilation cycle from 16 July 2008 to 23
 3 July 2008, b) PDF of these dynamical height innovations (the value 0.3 m appears in the tail of the PDF), c) RMS innovation with respect to the vertical temperature profiles over the year
 4 2008 for two “twins” simulations (without and with QC2). These last scores are averaged over all seven days of the data assimilation window, with a lead time equal to 3.5 days. Units are °C.



1

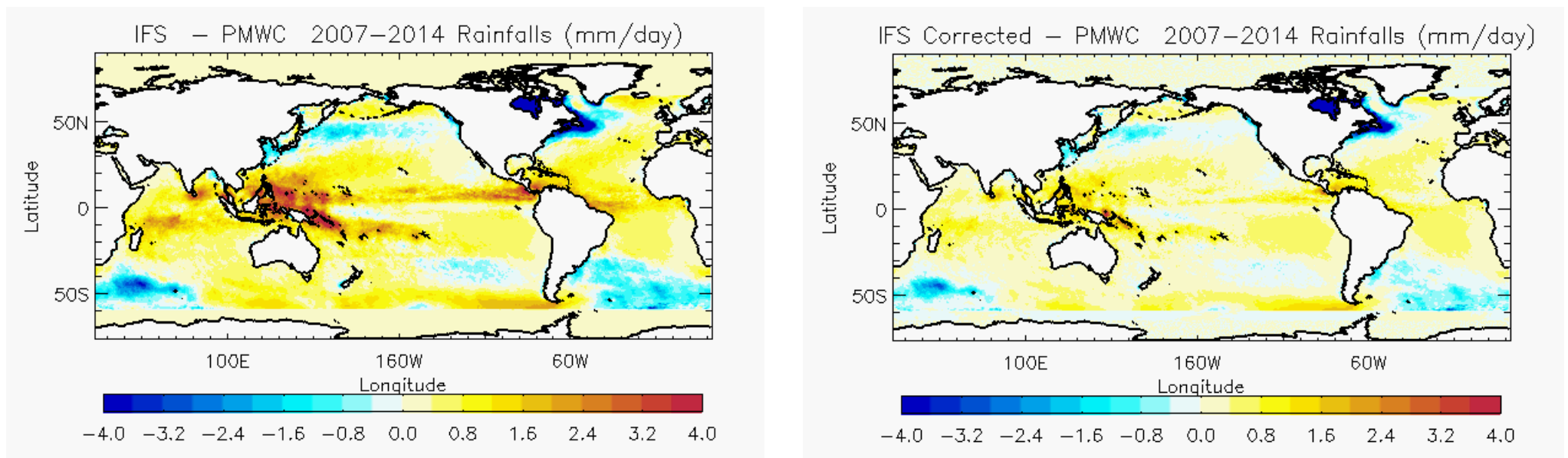
2 **Figure 4:** Statistics of suspicious temperature (T) and salinity (S) detected by QC1 (T_QC1 and S_QC1) and by QC2 (T_QC2 and S_QC2) quality controls as a function of year in the
 3 PSY4V3 2007-2016 simulation time period.



1
2
3
4

Figure 5: Diagnostics (time series) with respect to the vertical temperature and salinity profiles over the October 2006 - December 2007 period. Mean misfit between observations and model for salinity (top panels, units in psu) and for temperature (low panels, units in °C), starting from WOA9 climatology (left panels) and robust EN4 (right panels).

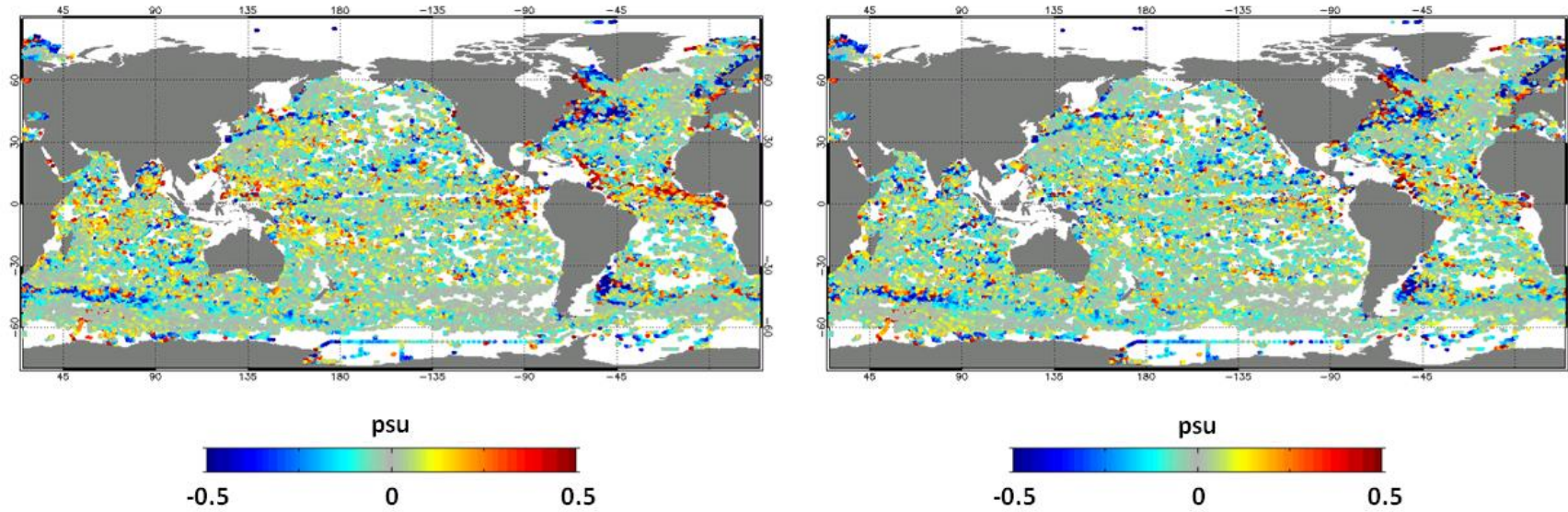
1



2

3 **Figure 6:** Mean 2007-2014 IFS ECMWF atmospheric precipitation bias (units in mm day^{-1}) with respect to PMWC product without (left map) and with (right map) correction.

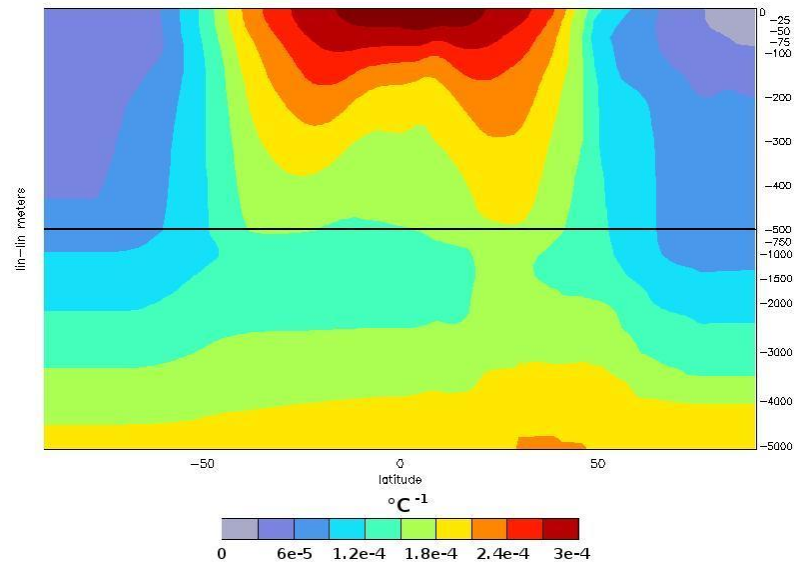
Mean surface salinity innovation (2011)



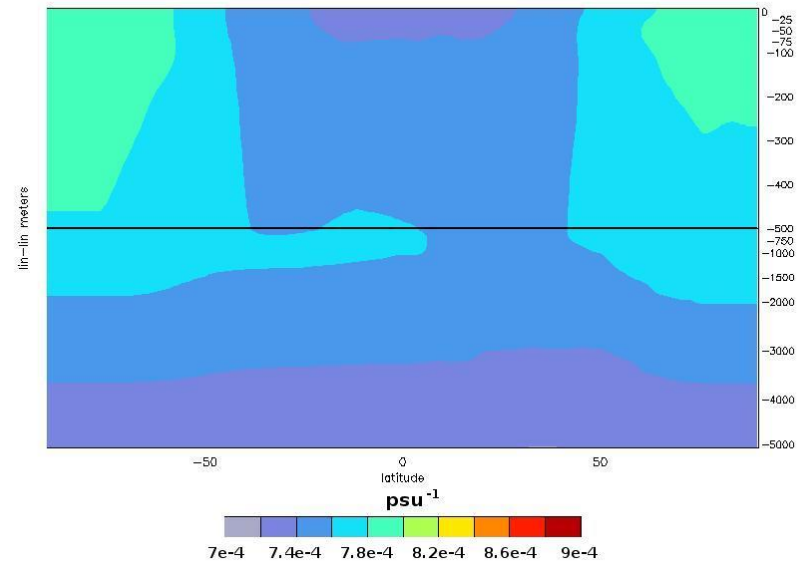
1
2
3
4

Figure 7: Mean surface salinity innovation (difference between the assimilated observation and the model, units in psu) on the year 2011. On the left, the innovation resulting from the use of the original IFS field, and on the right, the innovation resulting from the use of the corrected IFS field.

climatological thermal expansion



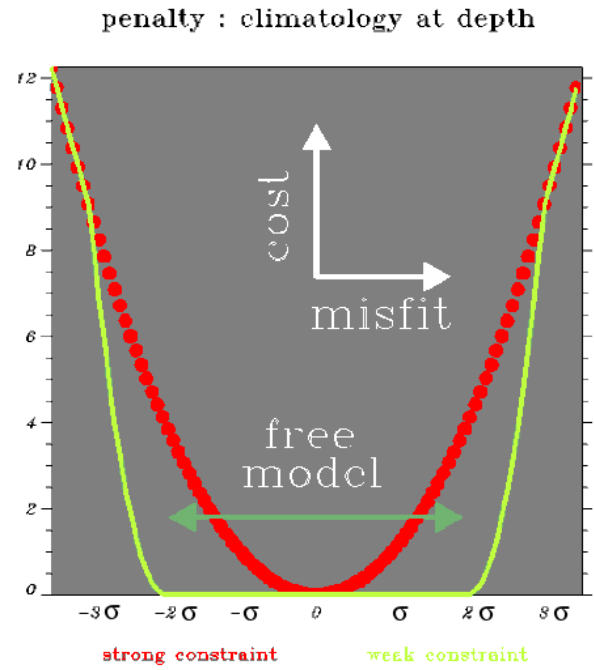
climatological saline contraction



1

2

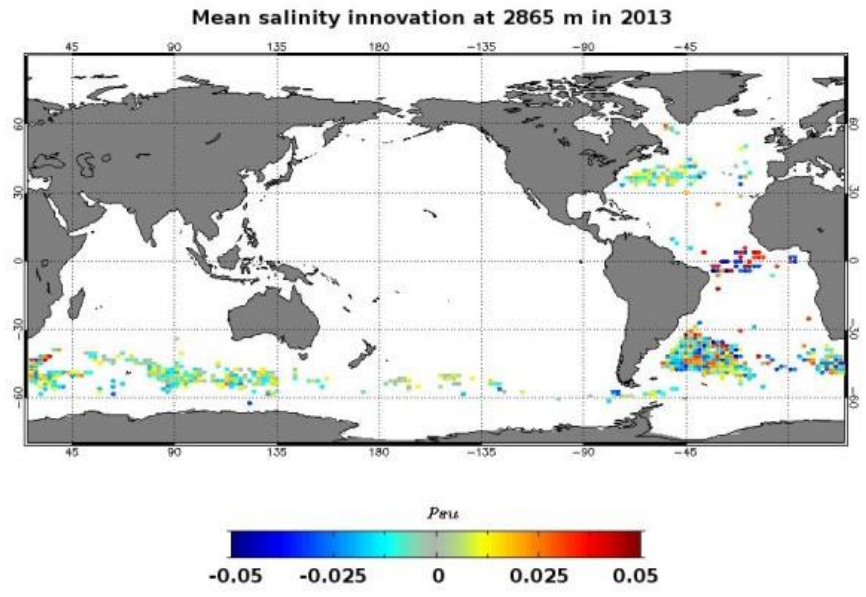
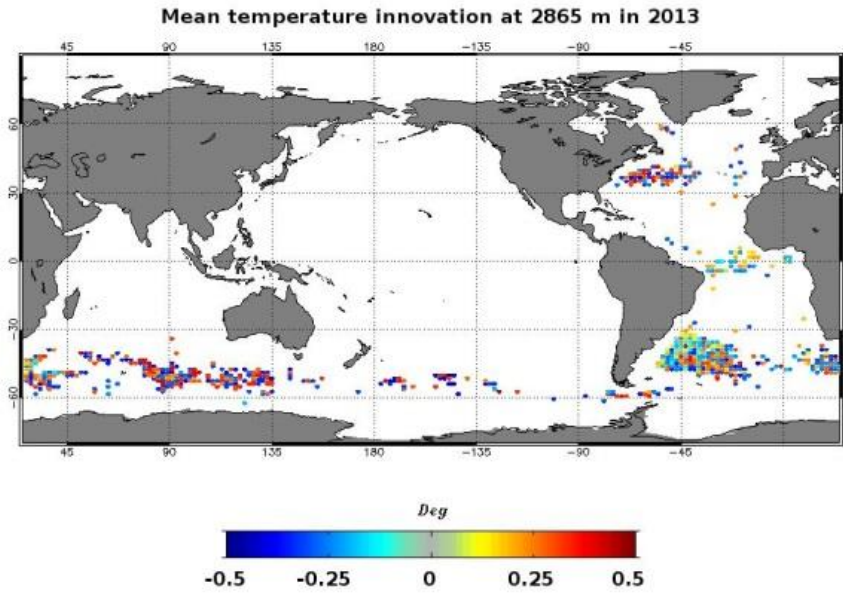
Figure 8: Climatological thermal expansion ($^{\circ}\text{C}^{-1}$) and saline contraction (psu^{-1}) as a function of the latitude and the depth.



1

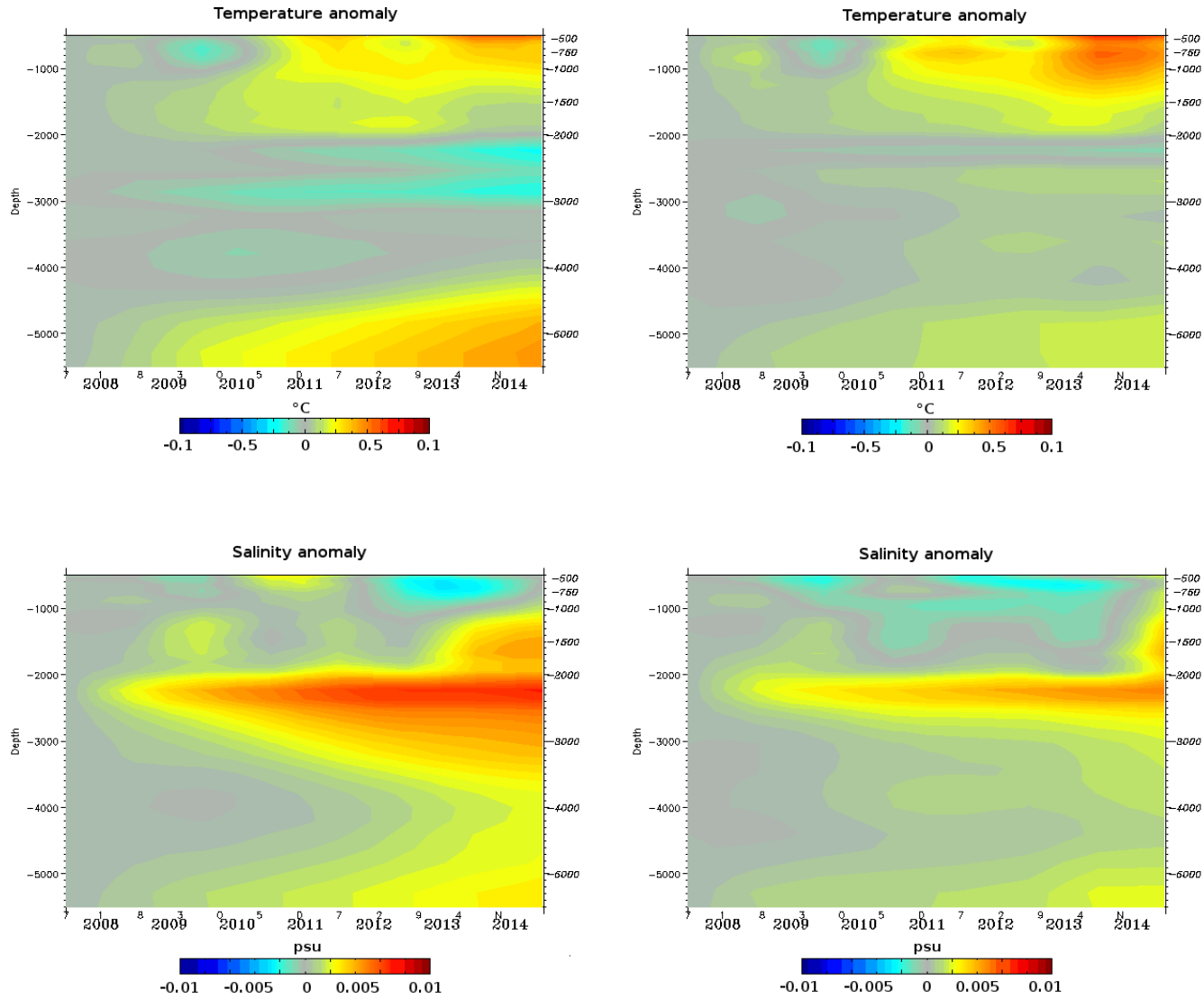
2

3 **Figure 9:** Non-Gaussian error for climatology (corresponding to a weak constrain of the system in green). A cost equal to zero corresponds to an infinite observation error, namely a system
 4 operation in a free mode (without assimilation of climatology).

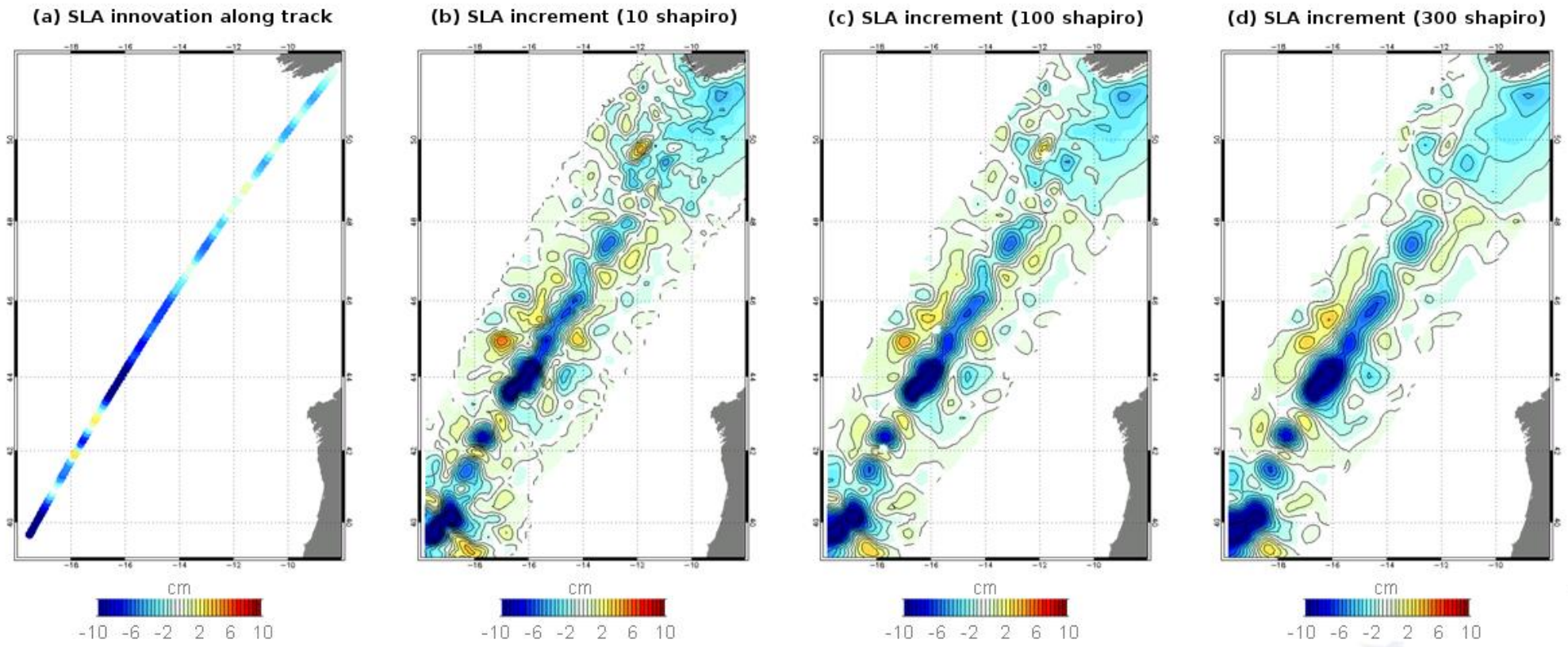


1

2 **Figure 10:** Mean temperature (on the left, units in °C) and salinity (on the right, units in psu) innovations in 2013 at 2865 m for the system PSY4V3.



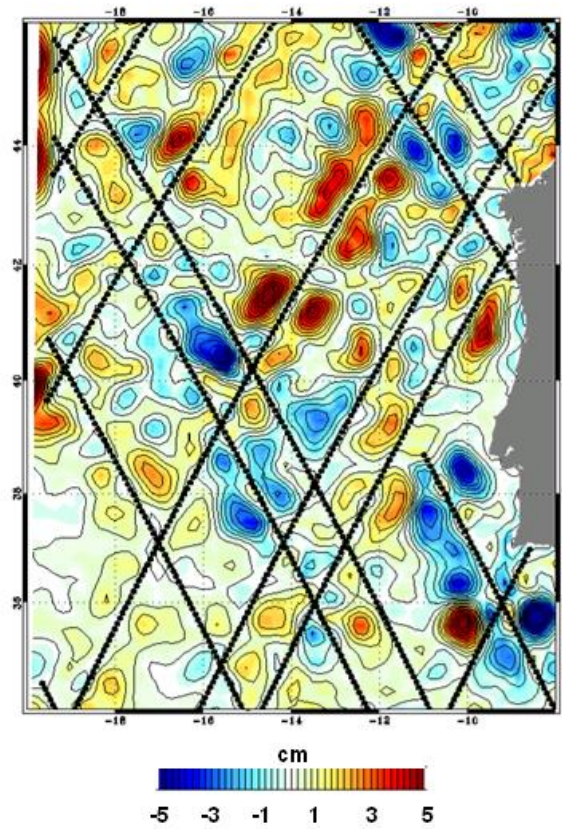
1 **Figure 11** : Temperature (top panels, units in °C) and salinity (low panels, units in psu) annual anomalies over depth (500-5000m) and time (2007-2014) for latitudes between 30° S and 60° S.
 2 The simulation on the left does not assimilate climatological vertical profiles while the simulation on the right assimilates them. Annual anomaly for a specific year is computed as the
 3 difference between the annual mean of this year and the annual mean of the year 2007.



1
2
3
4

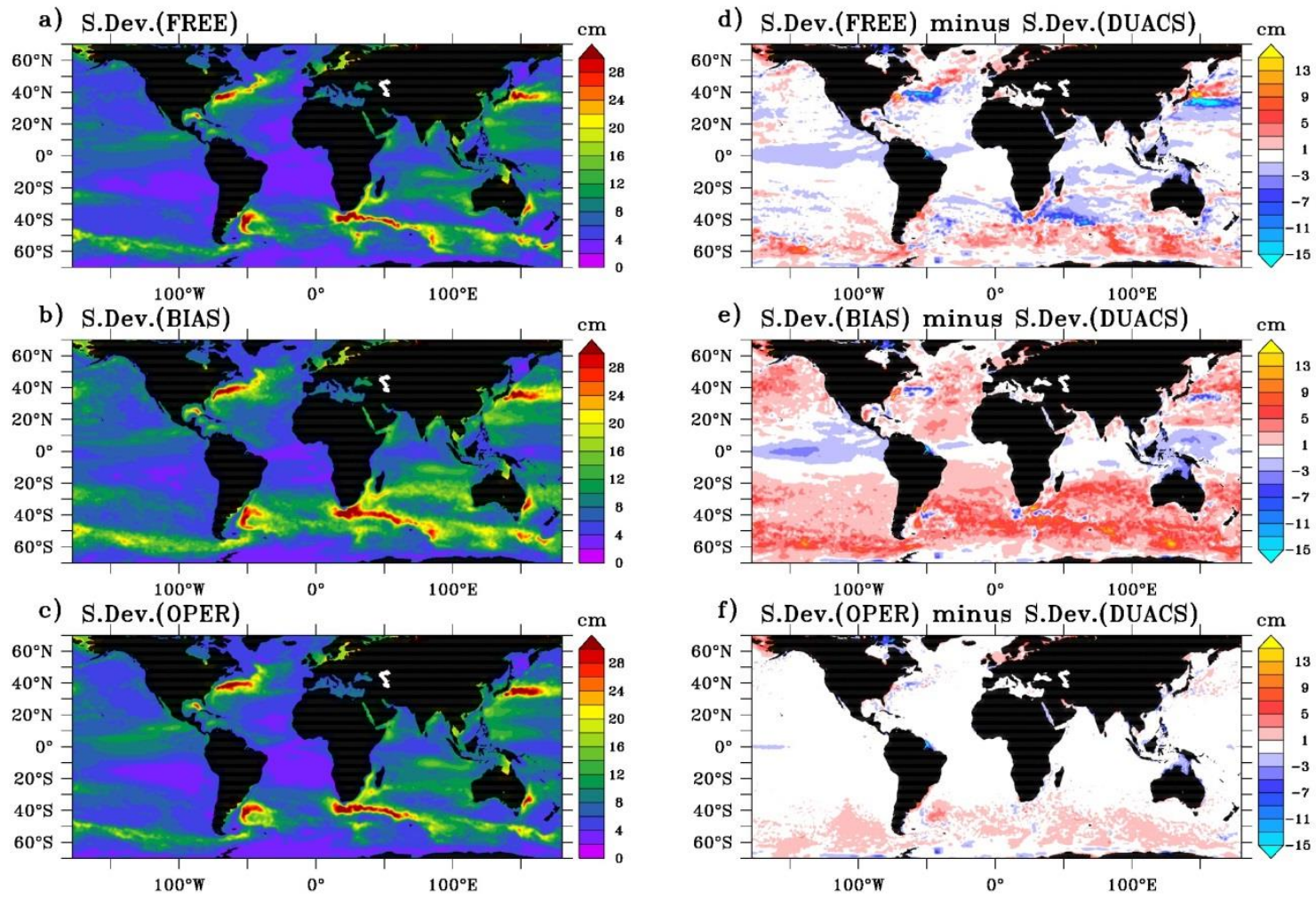
Figure 12: SLA innovation along a single assimilated track altimeter (a). SLA increments respectively with 10 (b), 100 (c) and 300 (d) Shapiro passes as anomaly filtering. These experiments have been performed with a regional system at $1/36^\circ$. Unit is cm.

SLA increment difference



1
2
3
4

Figure 13: SLA increment difference using 10 and 300 Shapiro passes as anomaly filtering in a regional system at $1/36^\circ$. The black lines represent the position of the assimilated altimeter tracks. Unit is cm.

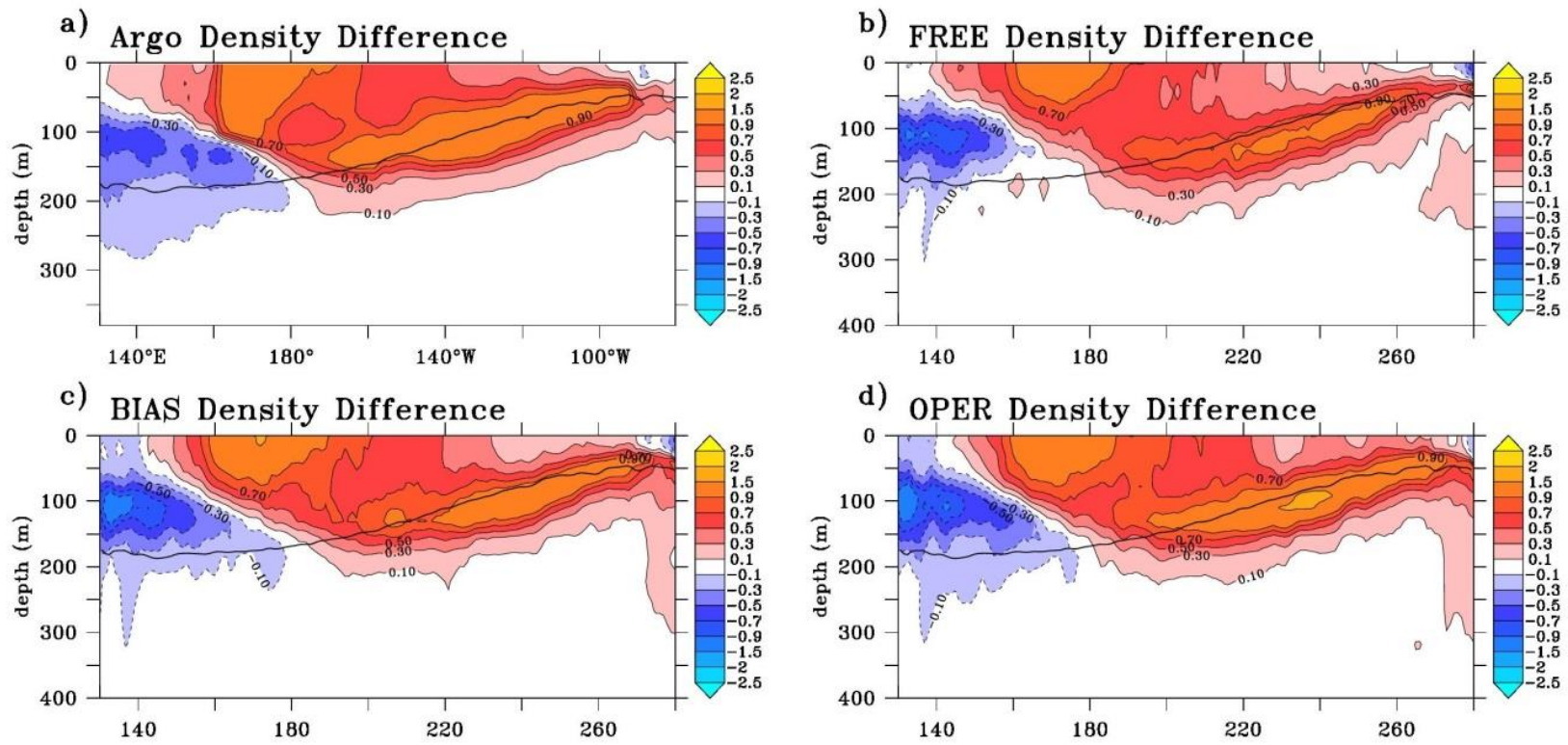


1

2

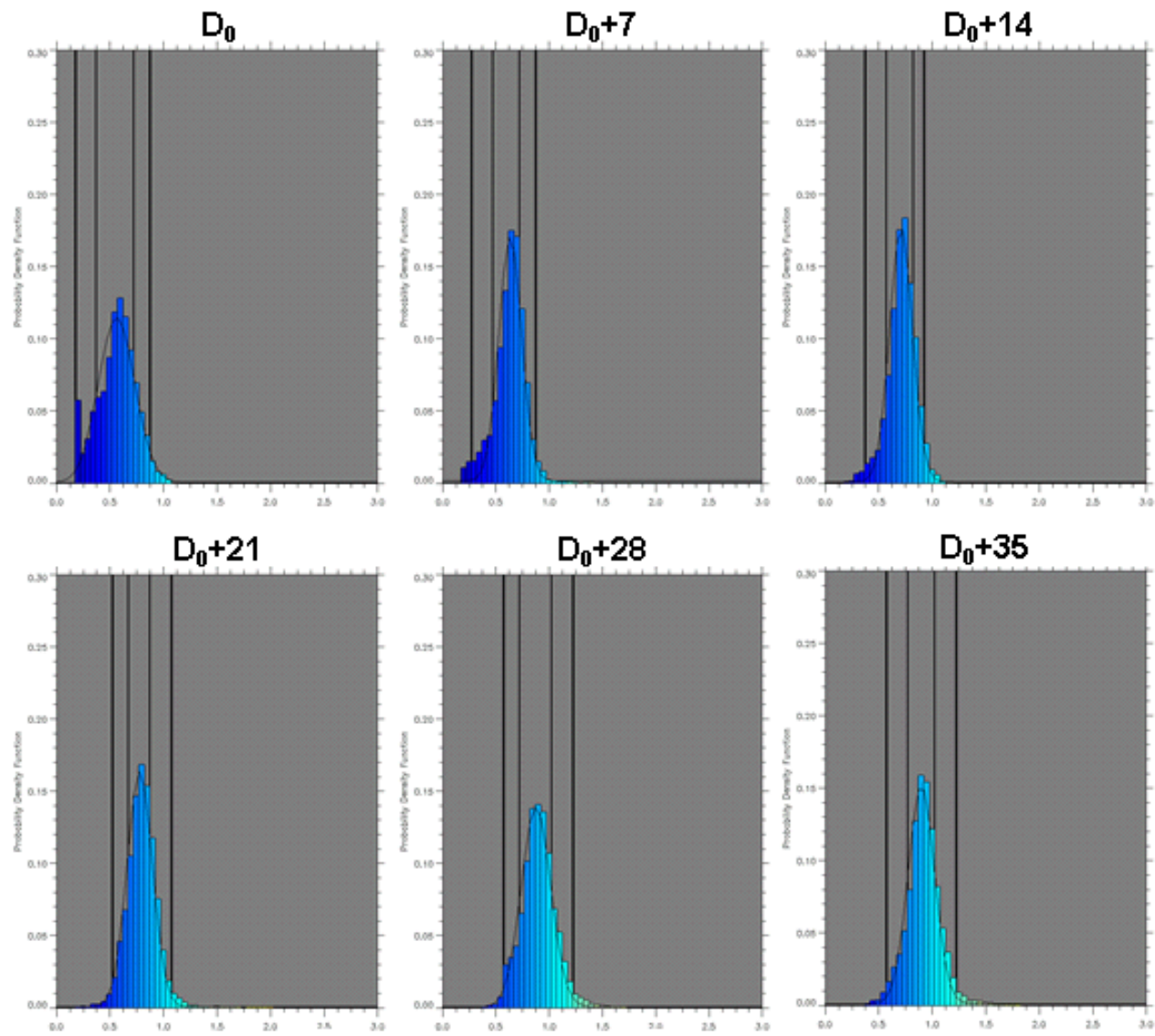
3

Figure 14: 2007-2015 SSH standard deviation (diagnostics made with 1 point every 3 horizontally and 1 day every 5) of the 1/12° PSY4 simulations (a,b,c) and difference of SSH model standard deviation with the one of DUACS gridded product (d,e,f). Units are cm.



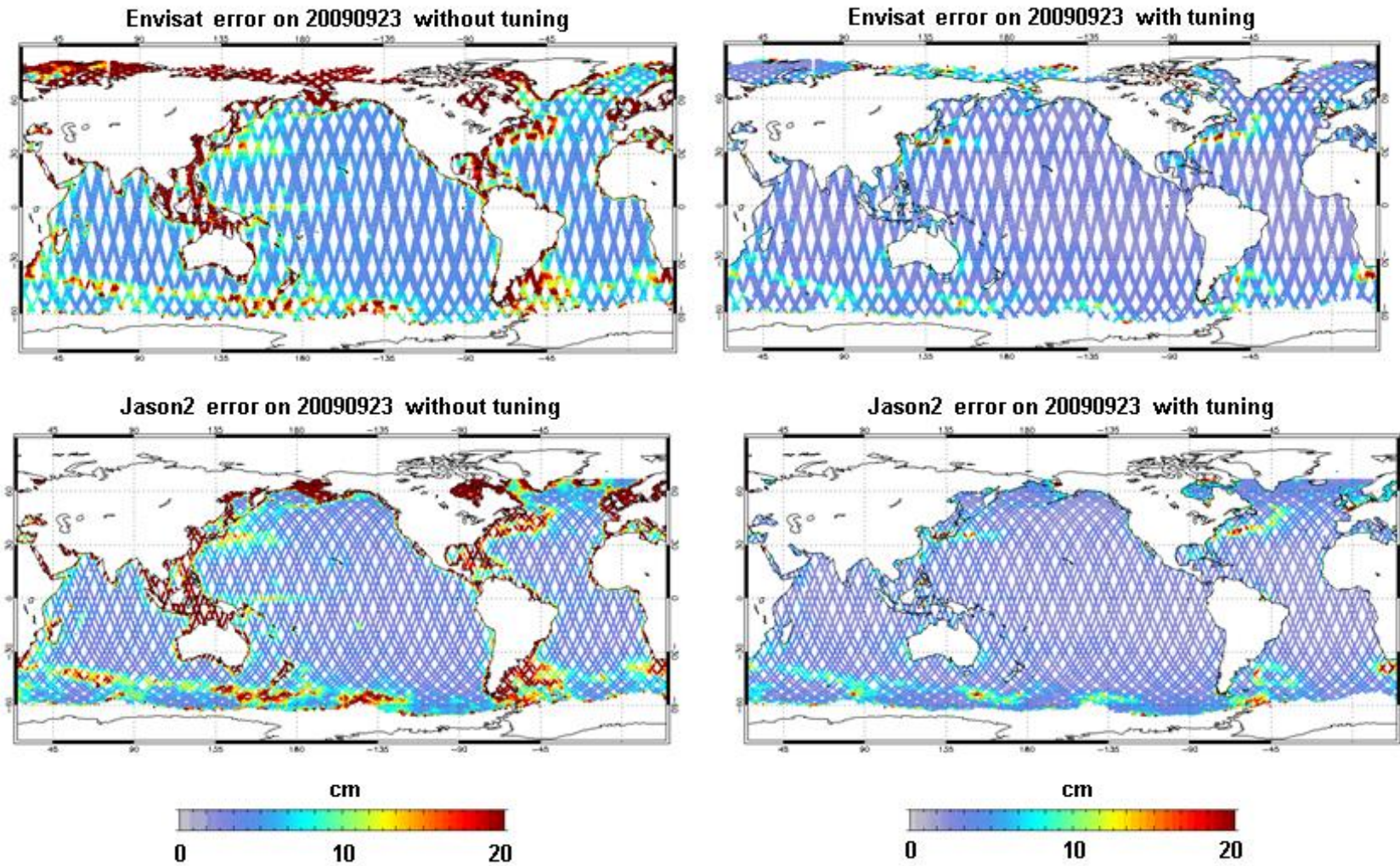
1

2 **Figure 15:** Density difference “OCT-DEC 2008 minus OCT-DEC 2009” in the equatorial Pacific (2° S-2° N) above 400 m depth (a-d) from the SCRIPPS Argo product (a), and the three 1/12°
 3 PSY4 FREE, BIAS and OPER simulations (b-d). The black line indicates the 2007-2015 Argo mean position of the pycnocline depth (isopycn 1025 kg m⁻³).



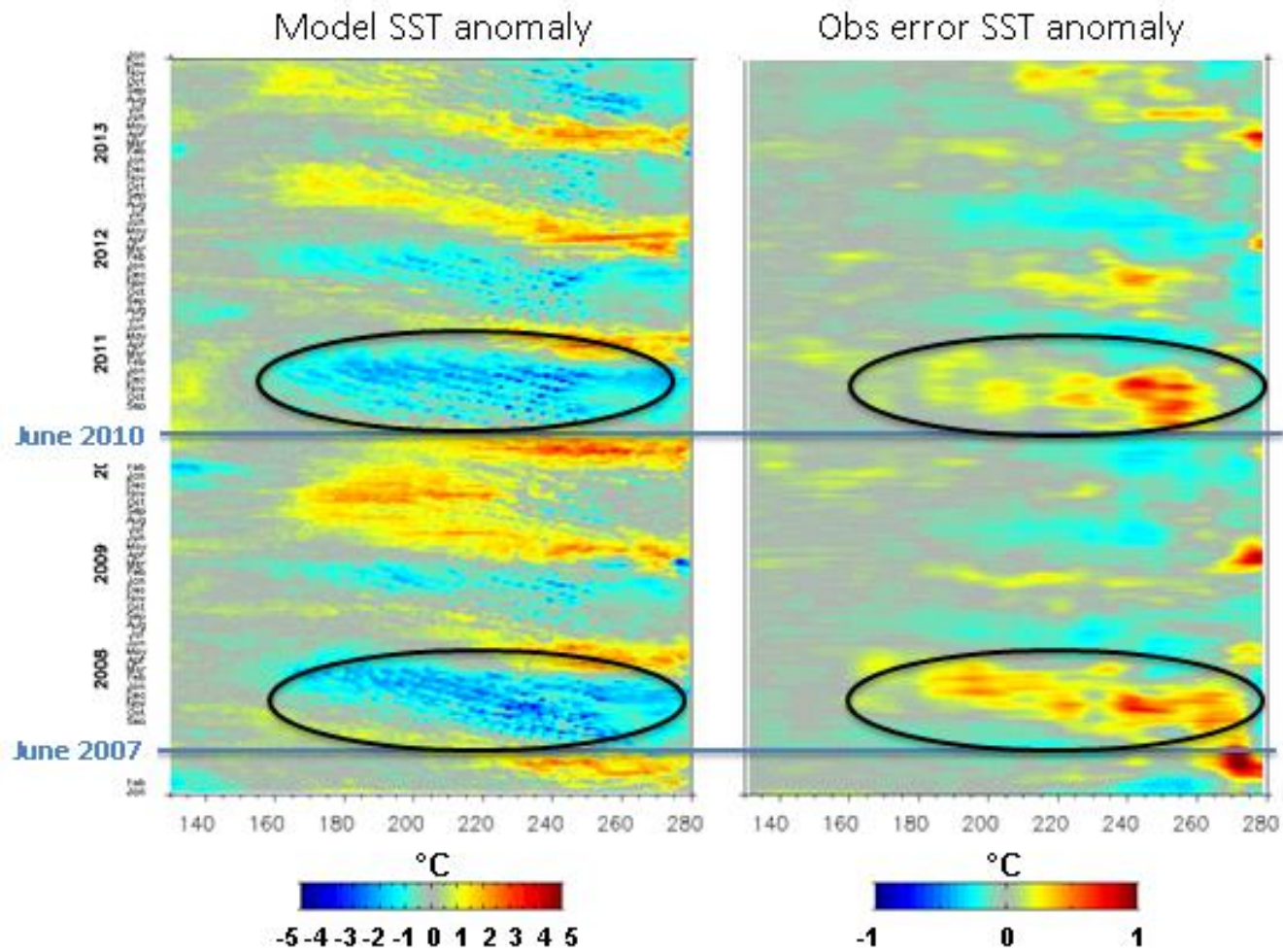
1
2
3

Figure 16: Evolution of the PDF of the ratio for Envisat satellite from D_0 to D_0+35 days. D_0 corresponds to the first day where Envisat is assimilated by the system.

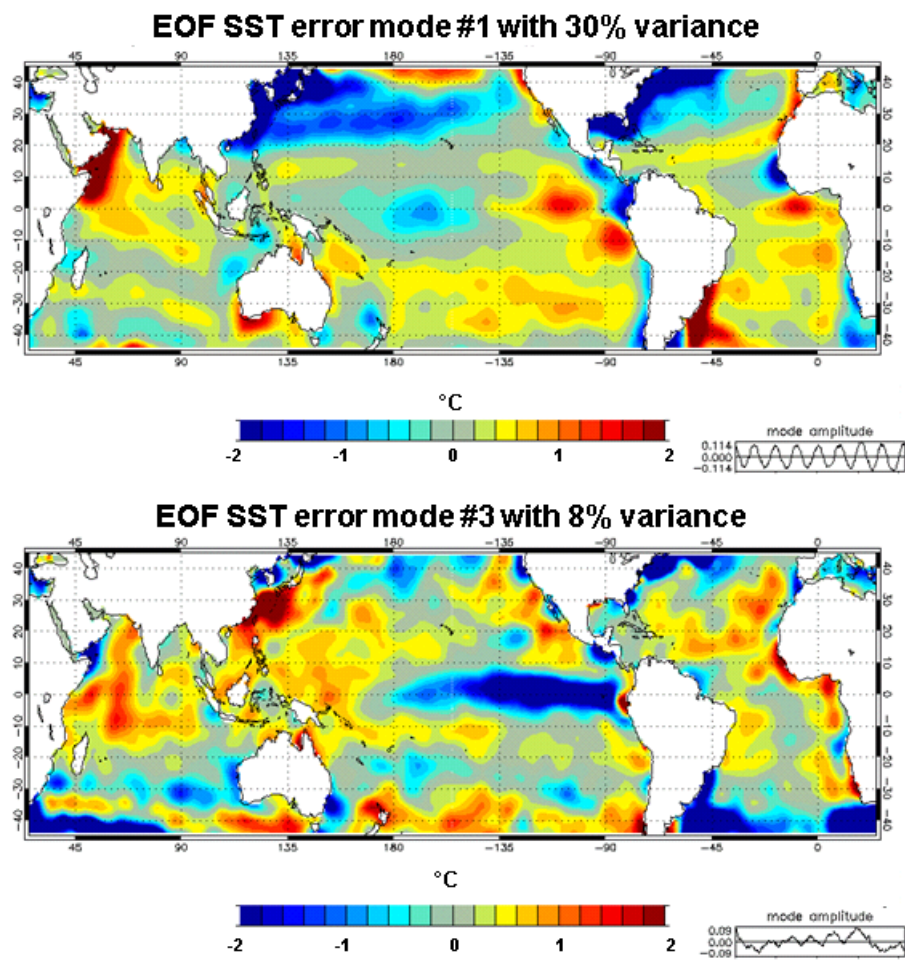


1
2
3
4

Figure 17: Envisat (top panels) and Jason2 (low panels) satellite observation errors used on the 7-day assimilation cycle ending September, 23, 2009 without tuning (left panels) and with tuning (right panels) method. Unit is cm.

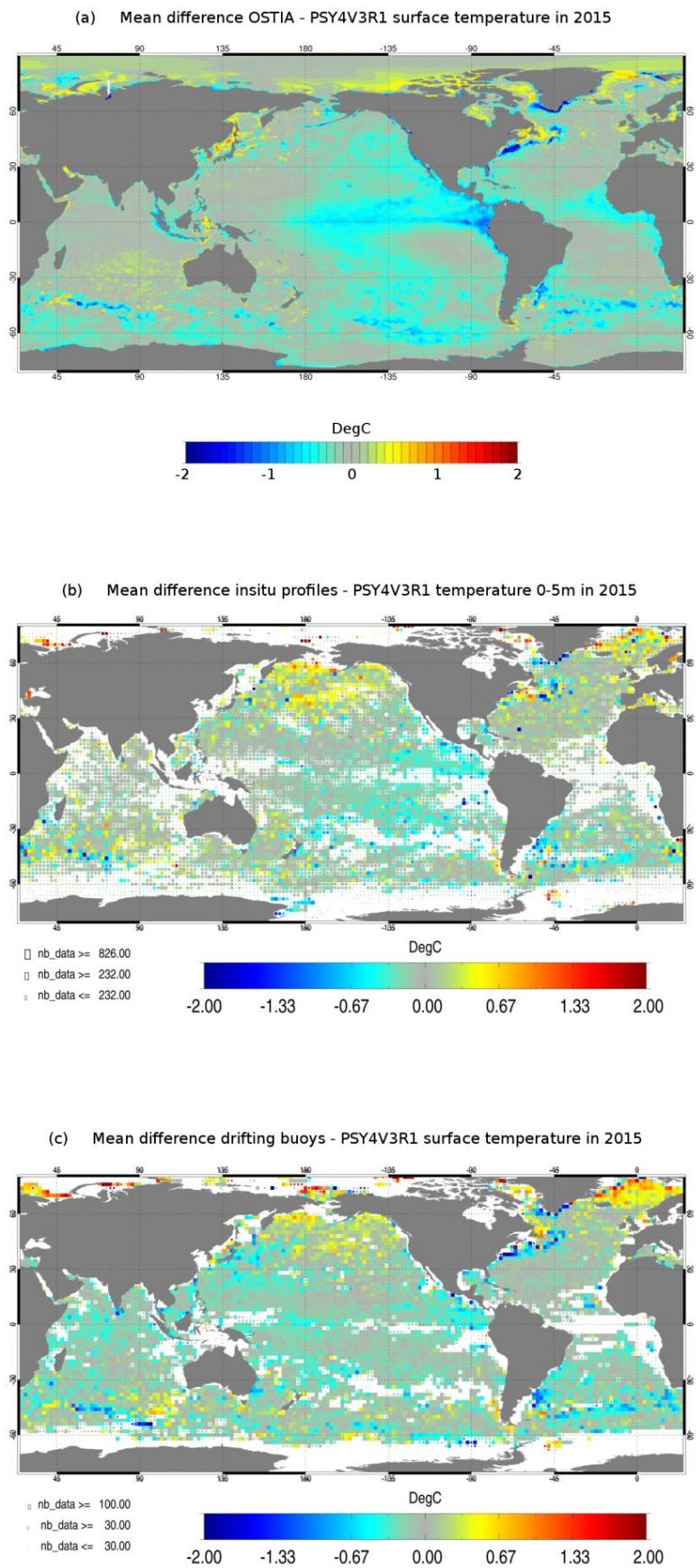


1
2
3 **Figure 18:** Evolution in time of model SST anomaly (on the left) and SST observation error anomaly tuned by “Desroziers” method (on the right) for a section at 3° N. The blue lines represent
4 the beginning of La Niña episodes (mid-2007 and mid-2010). The black ellipses highlight periods when TIWs are more marked. Units are °C.

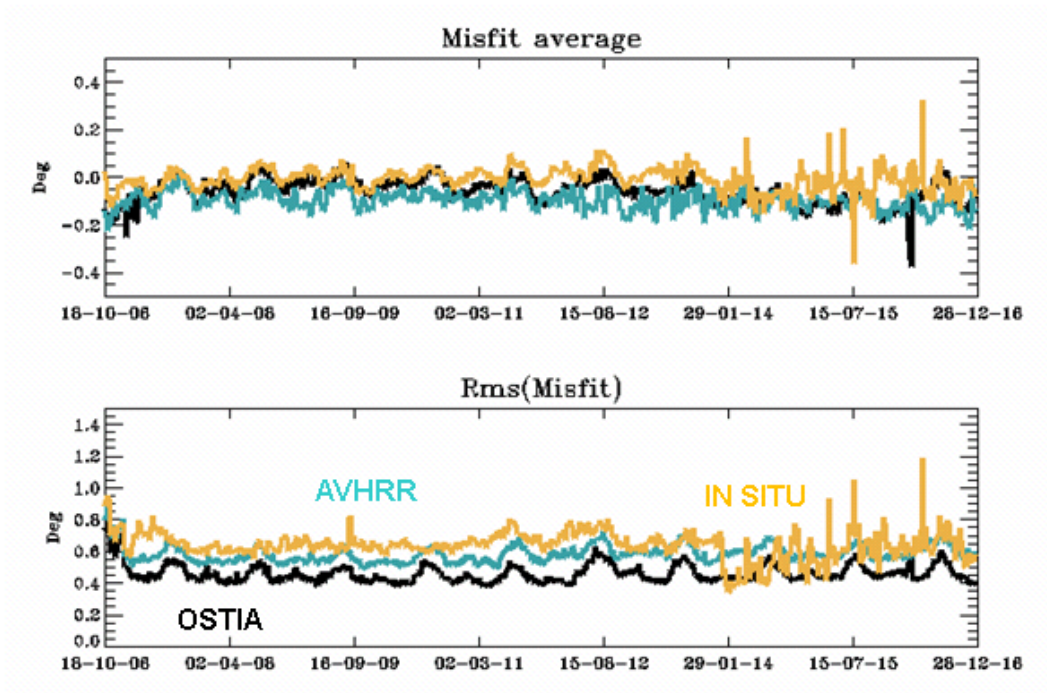


1
2
3
4
5

Figure 19: 1st EOF (top panel) and 3th EOF (bottom panel) of sea surface temperature observation error (°C) over the 2007-2015 time period. The time series at the bottom of each panel correspond to the mode amplitude.

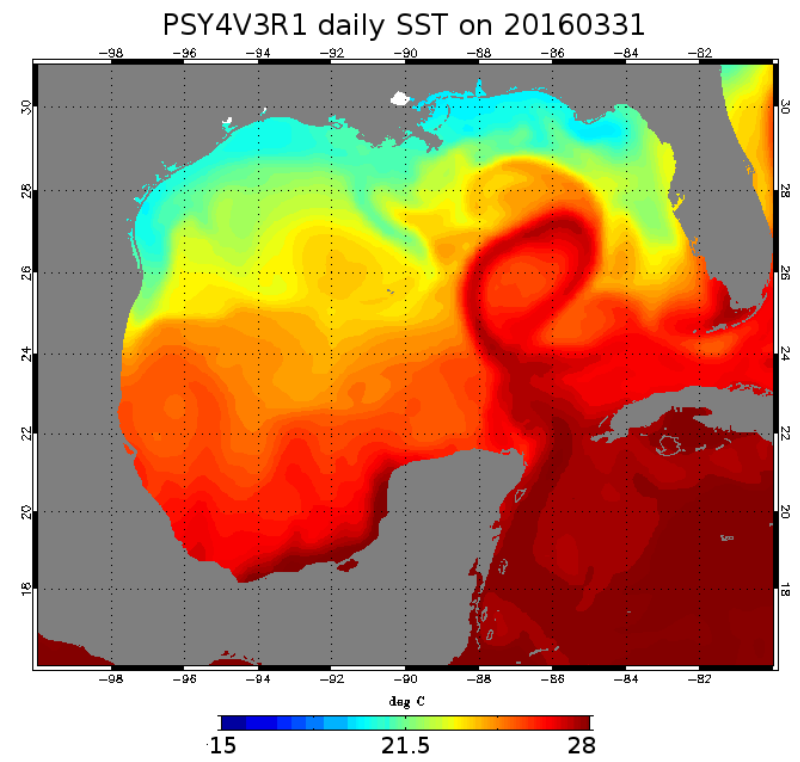
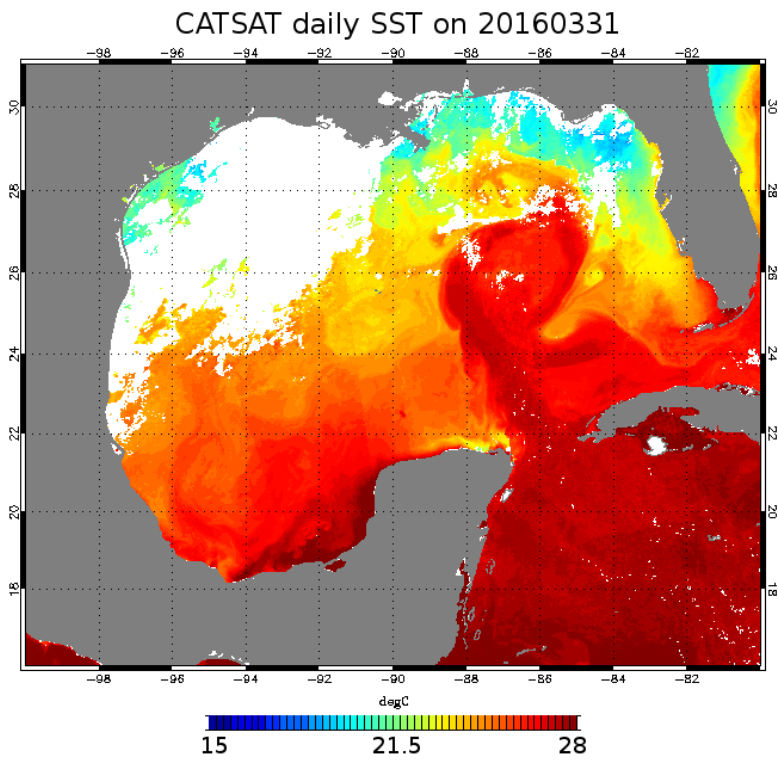


2 **Figure 20:** Mean SST residuals (units in °C) over the year 2015: OSTIA SST minus PSY4V3 (a), in situ SST minus PSY4V3 (b)
3 and drifting buoys SST minus PSY4V3 (c).



1
2
3
4
5

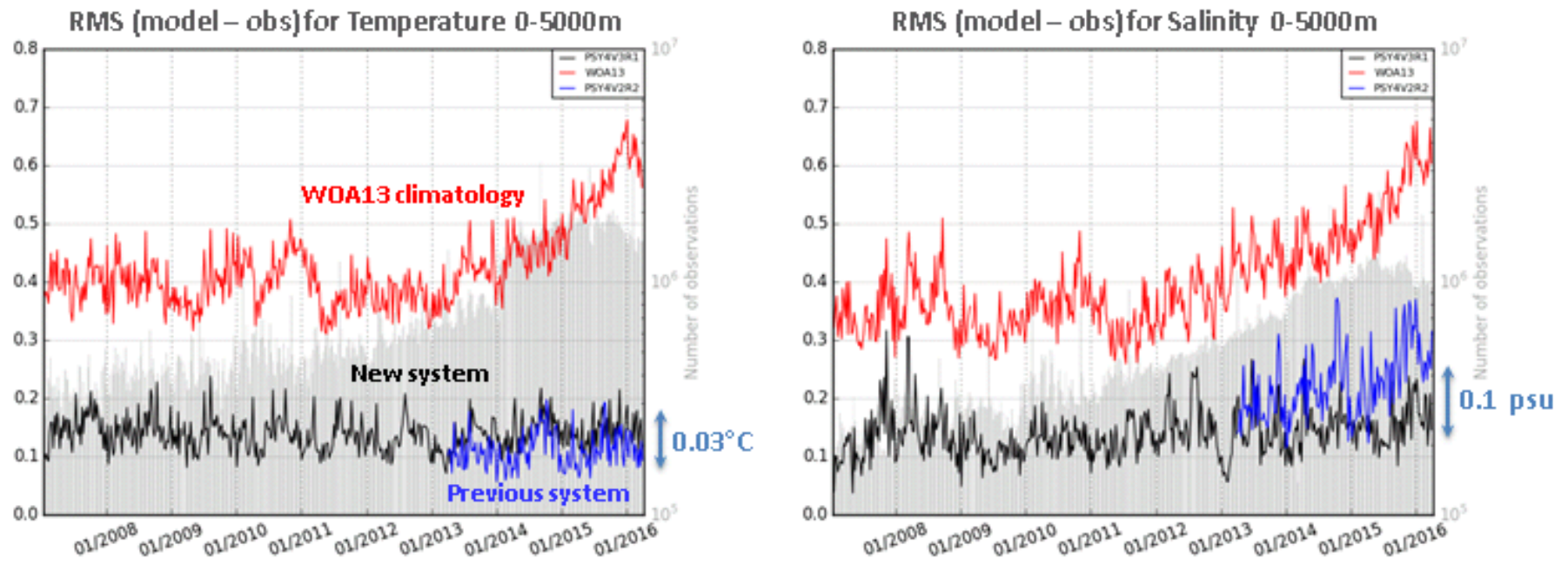
Figure 21: Time series of SST (units in °C) global misfit average (top) and RMS (bottom) for OSTIA observations (black line, assimilated), NOAA AVHRR observations (blue line, not assimilated), and in situ observations (orange line, assimilated), from October 2006 to December 2016.



1

2

Figure 22: High resolution CATSAT SST from CLS (on the left) and PSY4V3 SST (on the right) on March 31, 2016. Unit is °C.

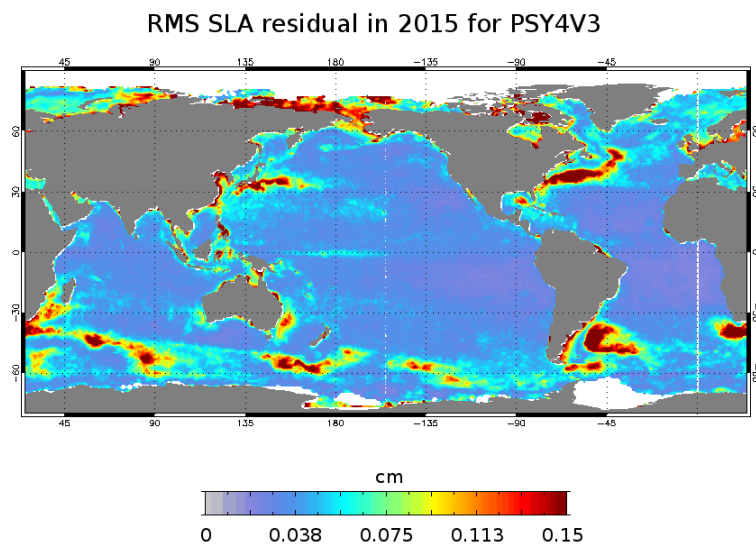
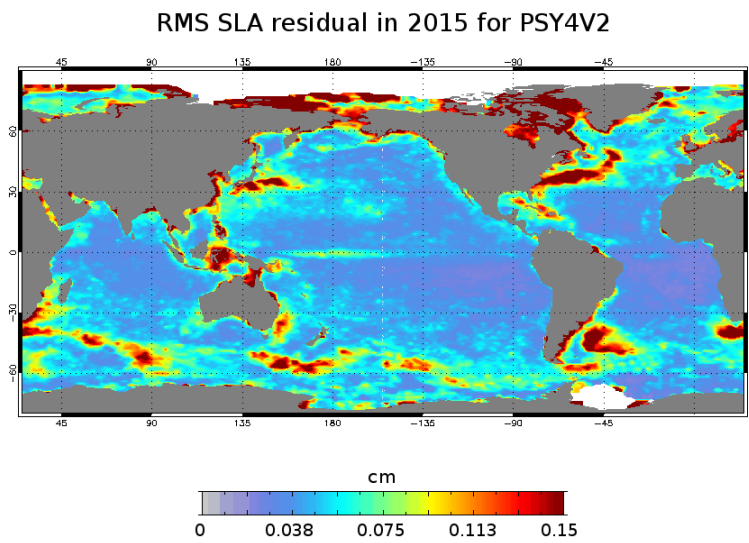
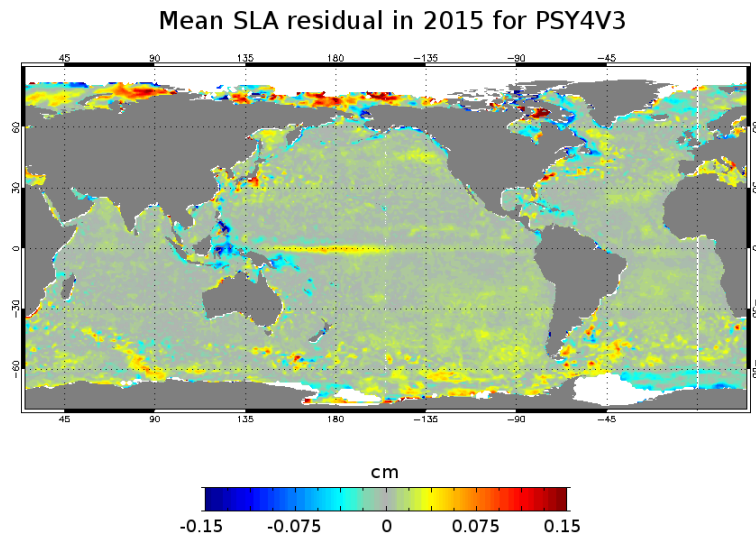
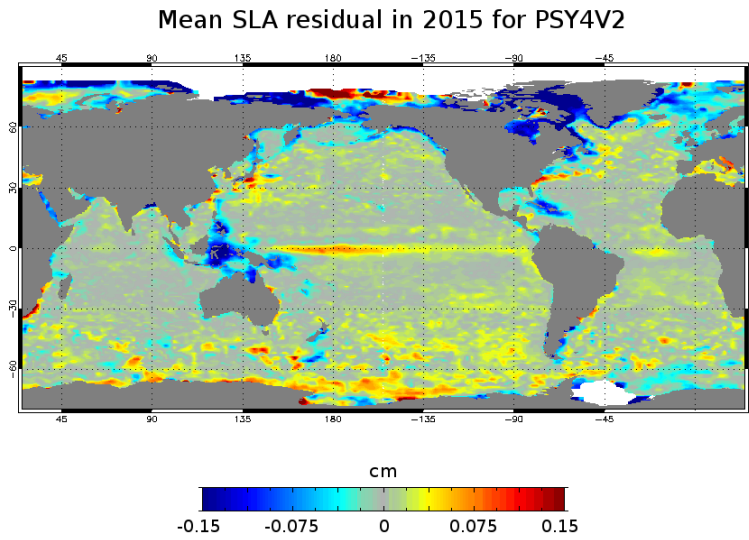


1

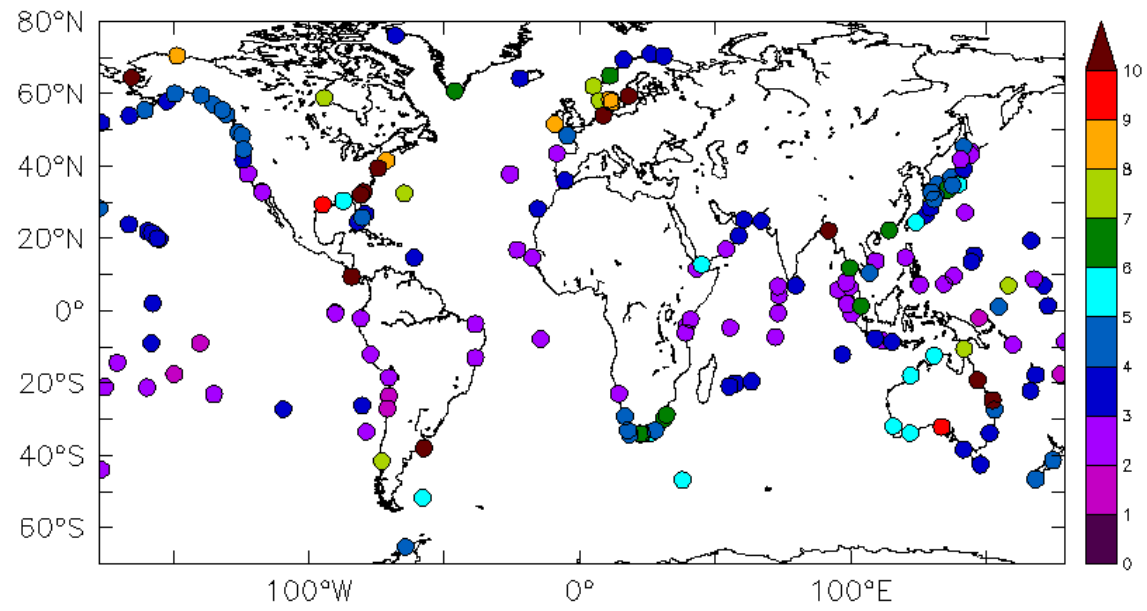
2

3

Figure 23: Time series of the 0-5000m RMS difference between the model analysis and the in situ observations for previous system PSY4V2 (in blue), new system PSY4V3 (in black) and the WOA13v2 climatology (in red). Left panel: temperature (unit in °C), right panel: salinity (unit in psu). Time series of the number of available observations appear in grey.

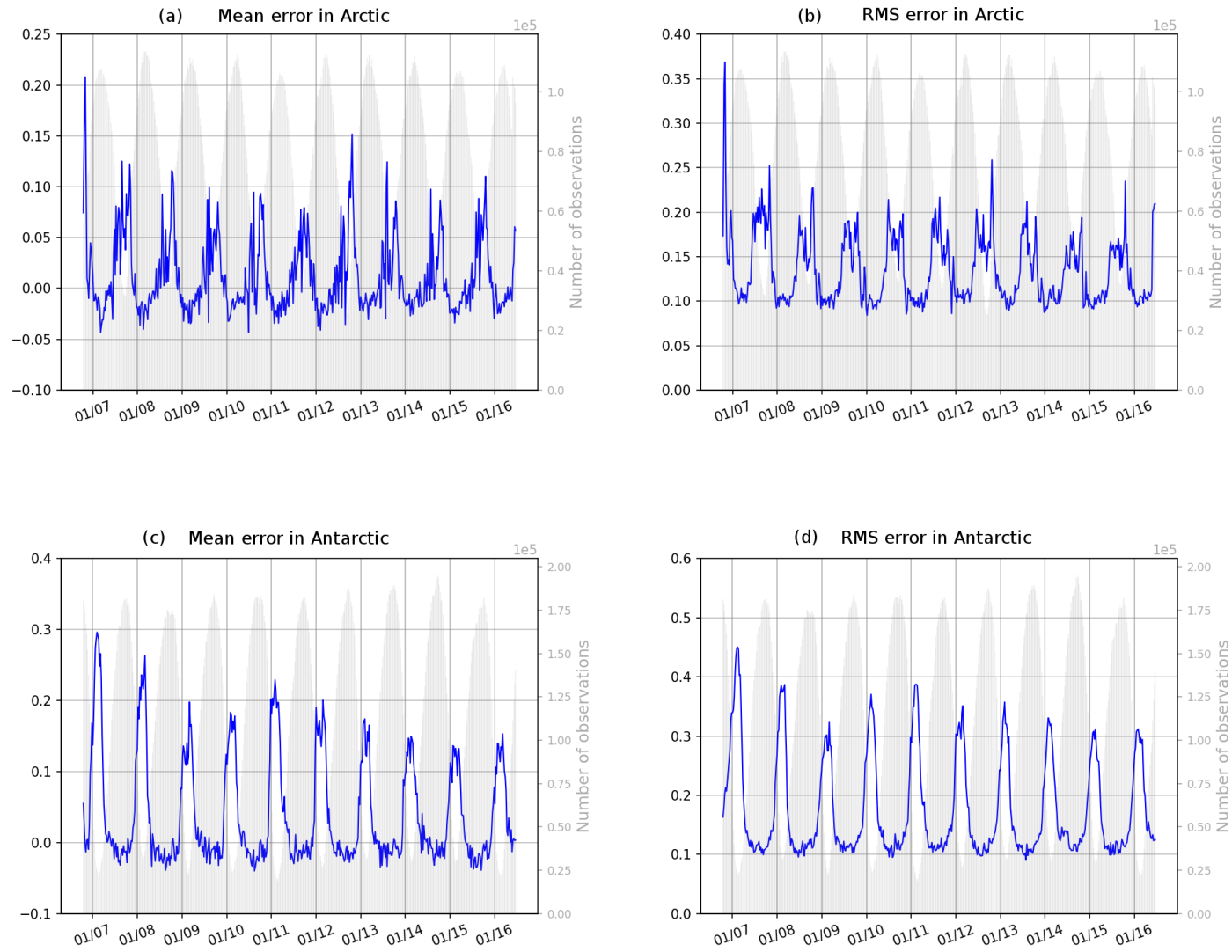


1 **Figure 24:** Mean residual errors (top panels) and RMS residual errors (low panels) of SLA in 2015, for the previous system PSY4V2 (on the left) and the new system PSY4V3 (on the right).
 2 Unit is cm.



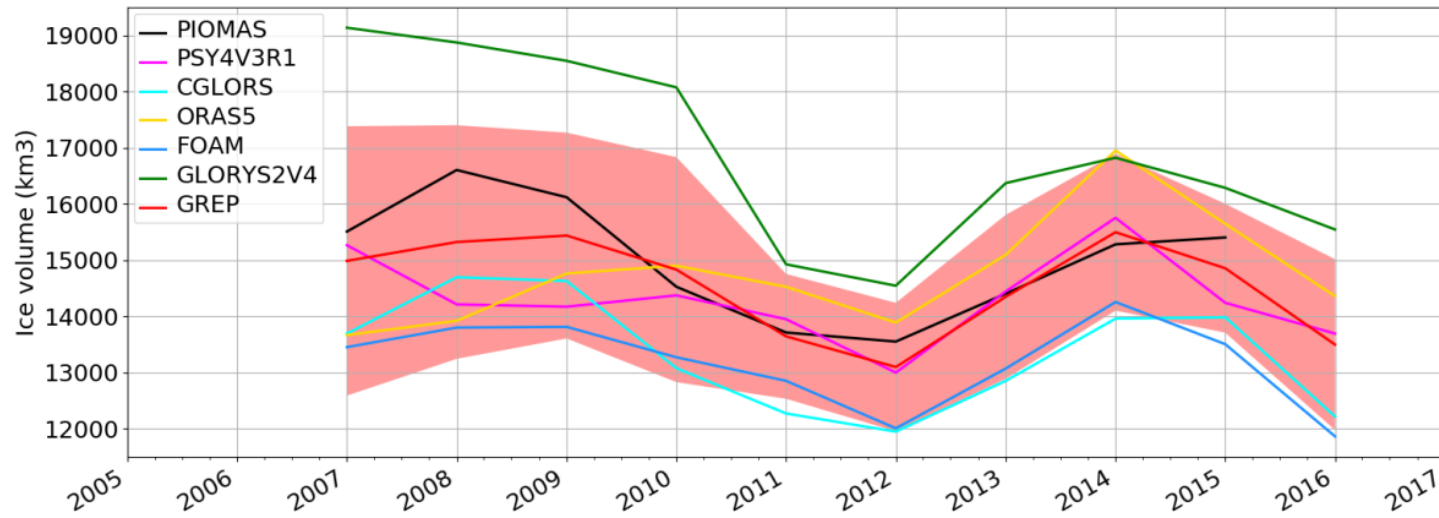
1
2
3

Figure 25: Sea surface height RMS difference between tide gauges observations and the system PSY4V3 for the year 2015. Unit is cm.



1

2 **Figure 26:** Time series of (observation-forecast) mean (a and c) and RMS (b and d) differences of sea ice concentration (0 means no ice, 1 means 100 % ice cover) in the Arctic Ocean (a and
 3 b) and Antarctic Ocean (c and d). The assimilated observations are the sea ice concentrations from OSI TAC. Time series of the number of available observations appear in grey.

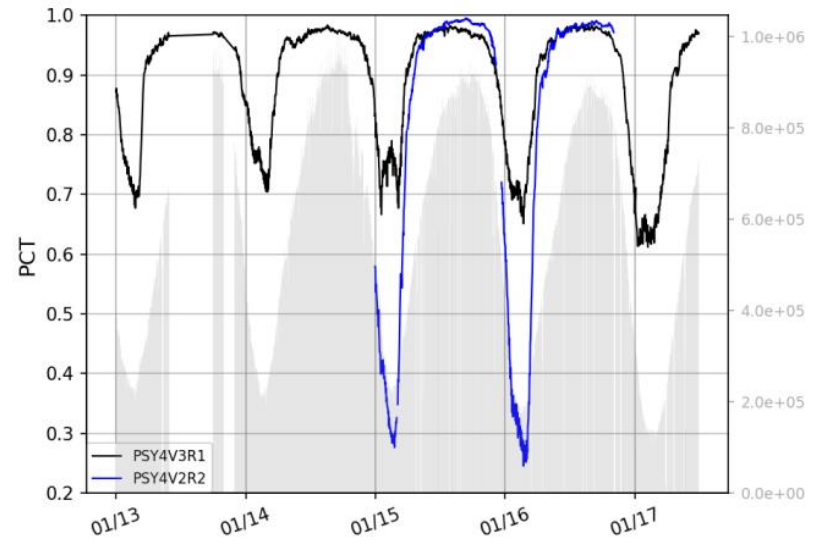
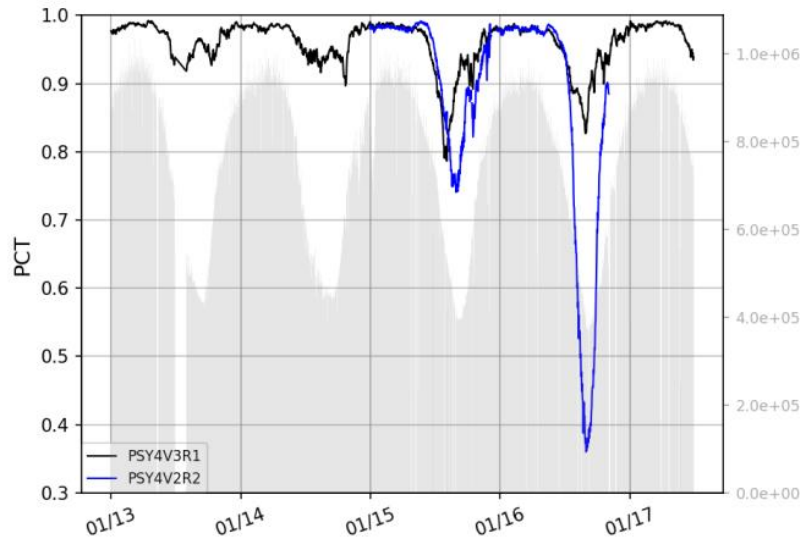


1

2

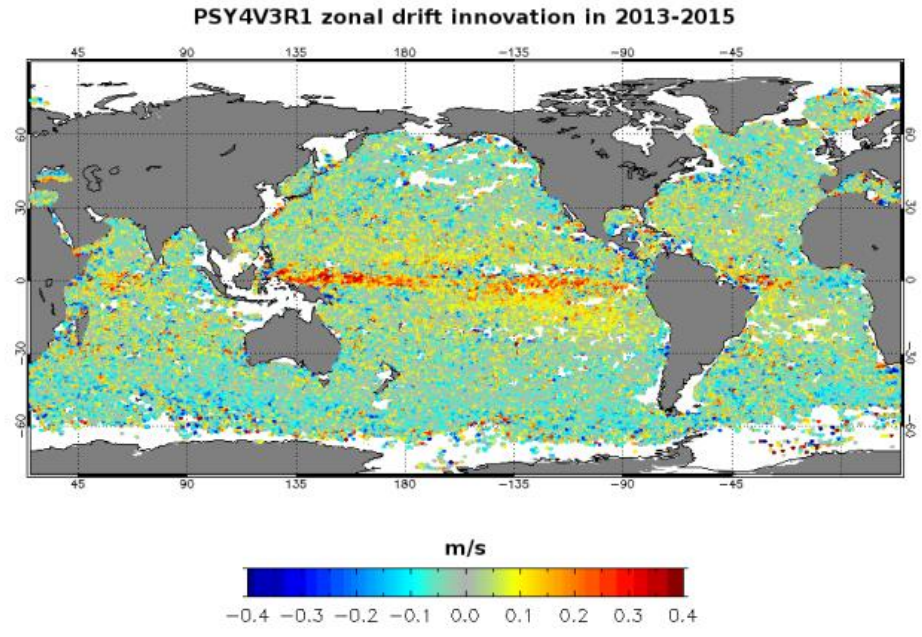
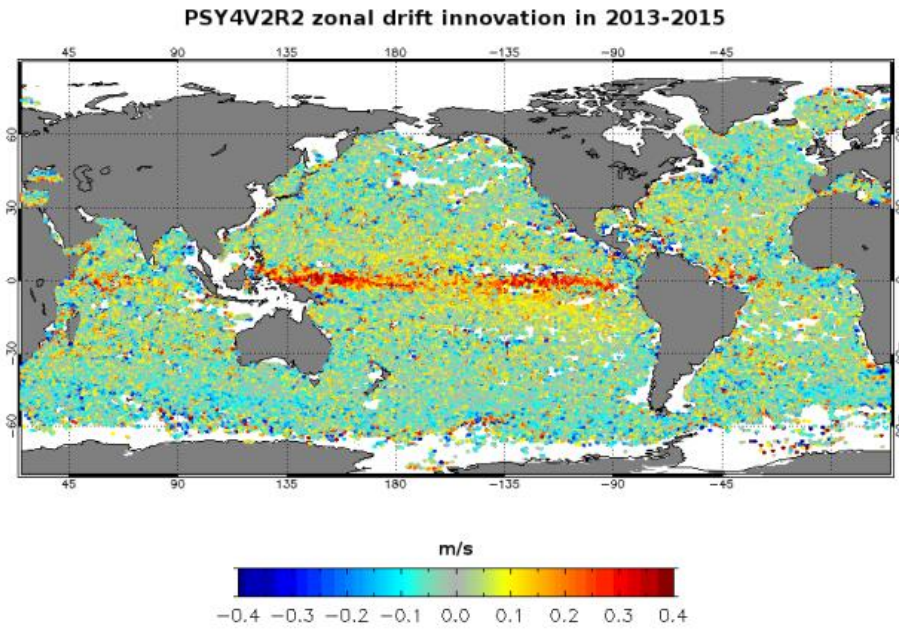
Figure 27: Time series over the 2007-2016 period of the sea ice volume in Arctic for several systems: GREP composed by the four members GLORYS2V4 from Mercator Ocean (France), ORAS5 from ECMWF, FOAM/GloSea from Met Office (UK) and C-GLORS from CMCC (Italy); PSY4V3 from Mercator Ocean (France); PIOMAS product. The spread of GREP product is represented in light red. Unit is km³.

4



1
2
3

Figure 28: Time series of the PCT quantity for PSY4V2 (in blue) and PSY4V3 (in black). The left panel corresponds to Arctic and the right panel to Antarctic. Time series of the number of available observations appear in grey.



1
2
3
4

Figure 29: Mean zonal drift innovation (m s^{-1}) with PSY4V2 (on the left) and PSY4V3 (on the right) over the time period 2013-2015. Observations come from Argo surface floats and a surface drifters corrected dataset (Rio, 2012). Units are m s^{-1} .

Mercator Ocean system reference	Domain	Resolution	Model	Assimilation	Assimilated observations
PSY3V2R1	global	Horizontal: 1/4° Vertical: 50 levels	ORCA025 NEMO 1.09 LIM2, Bulk CLIO 24 h atmospheric forcing	SAM (SEEK)	“RTG” SST SLA T/S vertical profiles
PSY3V3R1	global	Horizontal: 1/4° Vertical: 50 levels	ORCA025 NEMO 3.1 LIM2 EVP, Bulk CORE 3 h atmospheric forcing	SAM (SEEK) IAU 3D-VAR bias correction	“RTG” SST SLA T/S vertical profiles
PSY3V3R3	global	Horizontal: 1/4° Vertical: 50 levels	ORCA025 NEMO 3.1 LIM2 EVP, Bulk CORE 3 h atmospheric forcing New parameterization of vertical mixing Taking into account ocean colour for depth of light extinction Large scale correction to the downward radiative and precipitation fluxes Adding runoff for iceberg melting Adding seasonal cycle for surface mass budget	SAM (SEEK) IAU 3D-VAR bias correction Obs. errors higher near the coast (for SST and SLA) and on shelves (for SLA) MDT error adjusted Increase of Envisat altimeter error QC on T/S profiles New correlation radii	“AVHRR+AMSRE” SST SLA T/S vertical profiles MDT “CNES-CLS09” adjusted Sea Mammals T/S vertical profiles

1 **Table 1:** Specifics of the Mercator Ocean IRG systems. In bold, the major upgrades with respect to the previous version. Available and operational production periods are described in Fig. 1.

Mercator Ocean system reference	Domain	Resolution	Model	Assimilation	Assimilated observations
PSY4V1R3	global	Horizontal: 1/12° Vertical: 50 levels	ORCA12 NEMO 1.09 LIM2, Bulk CLIO 24 h atmospheric forcing	SAM (SEEK) IAU	“RTG” SST SLA T/S vertical profiles
PSY4V2R2	global	Horizontal: 1/12° Vertical: 50 levels	ORCA12 NEMO 3.1 LIM2 EVP, Bulk CORE 3 h atmospheric forcing New parameterization of vertical mixing Taking into account ocean color for depth of light extinction Large scale correction to the downward radiative and precipitation fluxes Adding runoff for iceberg melting Adding seasonal cycle for surface mass budget	SAM (SEEK) IAU 3D-VAR bias correction Obs. errors higher near the coast (for SST and SLA) and on shelves (for SLA) MDT error adjusted Increase of Envisat altimeter error QC on T/S profiles New correlation radii	“AVHRR+AMSRE” SST SLA T/S vertical profiles MDT “CNES-CLS09” adjusted Sea Mammals T/S vertical profiles
PSY4V3R1	global	Horizontal: 1/12° Vertical: 50 levels	ORCA12 NEMO 3.1 LIM2 EVP, Bulk CORE 3 h atmospheric forcing New parameterization of vertical mixing Taking into account ocean colour for depth of light extinction Adding seasonal cycle for surface mass budget 50 % of model surface currents used for surface momentum fluxes Updated runoff from Dai et al., 2009 + runoff fluxes coming from Greenland and Antarctica Addition of a trend (2.2mm yr⁻¹) to the runoff Global steric effect added to the sea level New correction of precipitations using satellite data + no more correction of the downward radiative fluxes Correction of the concentration/dilution water flux term Relaxation toward WOA13v2 at Gibraltar and Bab-el-Mandeb	SAM (SEEK) IAU 3D-VAR bias correction (1 month time window) MDT error adjusted Increase of Envisat altimeter error QC on T/S profiles New correlation radii Addition of a second QC on T/S vertical profiles Adaptive tuning of observation errors for SLA and SST New 3D observation errors files for assimilation of in situ profiles Use of the SSH increment instead of the sum of barotropic and dynamic height increments Global mean increment of the total SSH is set to zero	CMEMS OSTIA SST SLA T/S vertical profiles MDT adjusted based on CNES-CLS13 Sea Mammals T/S vertical profiles CMEMS Sea Ice Concentration WOA13v2 climatology (temperature and salinity) constrain below 2000m (assimilation using a non-Gaussian error at depth)

Table 2: Specifics of the Mercator Ocean HRG systems. In bold, the major upgrades with respect to the previous version. Available and operational production periods are described in Fig. 1.

	AMSR Ice	AMSR Water
Model Ice	Hit ice	False Alarm
Model Water	Miss	Hit water

Table 3: Contingency table entries for sea ice verification of PSY4V3 system as compared to AMSR sea ice concentration observations

1
2
3